1993

Inverse modeling to obtain air permeabilities from multiple well field tests in unsaturated weathered till

Kenneth Brophy Edwards
Iowa State University

Order Number 9321141

Inverse modeling to obtain air permeabilities from multiple well field tests in unsaturated weathered till

Edwards, Kenneth Brophy, Ph.D.

Iowa State University, 1993

U·M·I
300 N. Zeeb Rd.
Ann Arbor, MI 48106

Inverse modeling to obtain air permeabilities from multiple well field tests in unsaturated weathered till

by

Kenneth Brophy Edwards

A Dissertation Submitted to the

Graduate Faculty in Partial Fulfillment of the

Requirements for the Degree of

DOCTOR OF PHILOSOPHY

Department: Civil and Construction Engineering
Major: Civil Engineering (Environmental Engineering)

Approved:

Members of the Committee:

Signature was redacted for privacy.

In Charge of Major Work

Signature was redacted for privacy.

For the Major Department

Signature was redacted for privacy.

Signature was redacted for privacy.

For the Graduate College

Iowa State University
Ames, Iowa

1993

DEDICATION

I would like to dedicate this dissertation to my parents.

TABLE OF CONTENTS

INTRODUCTION 1

LITERATURE REVIEW 4

Contaminant Transport Models 4

Carrier Fluid Models 4

One-dimensional models 5

Air flow models for multiple well field tests 8

Radial unsteady air flow 9

Radial steady air flow 14

Radial and vertical unsteady flow 16

Radial and vertical steady flow 16

Field Tests 19

Influence of water table 19

Air permeability from fitting models to data 19

EXPERIMENTAL SETUP 21

Description of Site 21

Laboratory Test for Well Screen Losses 30

MODEL 33

Selection of Two-Dimensional Model 33

Derivation 34

Boundary Conditions 40

Solution 43

Optimization 44

RESULTS 48
Field Data 48
Parameter conversions 48
Pressure unit conversion 48
Flowrate conversion 53
Data reduction 57
Air Permeability from 1-D Model 58
Air Permeability from 2-D Model 59

DISCUSSION 67
1-D Versus 2-D Modeling 67
2-D Modeling 69
Anisotropy and compressibility 69
Correlations of k with Physical Characteristics 72
Nominal Air Permeabilities for Design in Loam Till 73
Long Term Tests 75
Air Permeability from Other Methods 80
Feasibility of SVE in Till 82

CONCLUSION 85

REFERENCES 87

ACKNOWLEDGMENTS 93

APPENDIX A: CONVERSION FACTORS 94

APPENDIX B:	COMPUTER PROGRAM FOR MODELING AIR TRANSPORT	95
APPENDIX C:	FIELD DATA	108
APPENDIX D:	MODELING SCENARIOS FOR DATA TAKEN 10/7/91	121

LIST OF FIGURES

Figure 1.	Gasometer for determining air permeability in the laboratory	6
Figure 2.	Schematic diagram of radial air flow in unsaturated zone	10
Figure 3.	Schematic diagram of radial and vertical air flow in unsaturated zone	18
Figure 4.	Map of Iowa showing the extent of the Des Moines Lobe of the Wisconsin glacial advance. "x" indicates site location	22
Figure 5.	Location of field site in Story County, Iowa	24
Figure 6.	Typical core where ρ_b=bulk density (g/cm^3). Courtesy of Ressler (1992)	25
Figure 7.	Site plan. Grid interval is 25 cm	26
Figure 8.	Cross-section as if all wells were at same angle from W1	27
Figure 9.	Non-nested monitoring well installation	29
Figure 10.	Air injection scenario; for extraction test, blower is turned around	31
Figure 11.	Boundary conditions	42
Figure 12.	Finite element grid	45
Figure 13.	Pressure averaging over several nodes	47
Figure 14.	Boundary conditions used for modeling scenarios shown in Appendix D	61
Figure 15.	Effect of depth and extraction rate on k. Q in cm^3/s	70

Figure 16.	Vacuum contours from 0 to -0.2 cm of water by 0.01 increments for Q=3600 cm^3/s test on 10/7/91. Four layer compressible fluid model	71
Figure 17.	Depth to water table	74
Figure 18.	Atmospheric pressure on 7/17/92 through 7/19/92 (corrected for site elevation)	76
Figure 19.	Absolute pressure variations with time. Initial extraction rate was 2100 cm^3/s	78
Figure 20.	Gage pressure variations with time. Initial extraction rate was 2100 cm^3/s	79
Figure 21.	Travel times for an extraction rate of 3600 cm^3/s using the 10/7/92 permeabilities	84

LIST OF TABLES

Table 1.	Screen dimensions. Baseline for elevations is 300 cm below ground surface	28
Table 2.	Data and best fit air permeabilities (k in cm^2x10^{-8}, +Q is extraction)	49
Table 3.	Data and fitted pressures for four layer isotropic compressible fluid simulation. All units are cm H_2O except Q	65
Table 4.	Nominal air permeabilities	75

NOMENCLATURE

A = area (cm^2)

b = gasometer sample height (cm)

d = distance from no flow boundary to bottom of well screen (cm)

g = acceleration of gravity (981 cm/s^2)

H = soil thickness (cm)

k = permeability (cm^2)

K = saturated hydraulic conductivity (cm/s)

L = screen length (cm)

m = gage pressure (cm H^2O)

n = porosity

O = order

P = absolute pressure ($g/cm\text{-}s^2$)

P_O = reference air phase (absolute) pressure ($g/cm\text{-}s^2$)

P' = gage pressure ($g/cm\text{-}s^2$)

$\vec{q}$ = specific discharge vector (cm/s)

Q = measured flowrate (cm^3/s)

Q' = apparent flowrate ($g^2/cm^3\text{-}s^4$ if $\Psi = P^2$; $g/cm^2\text{-}s^2$ if $\Psi = P$)

r = radial coordinate (cm)

R = universal gas constant (8.3143×10^7 g-cm^2/s^2-mol-K)

Res = residual (same units as Ψ)

t = time (sec)

T = temperature (K)

W = Theis (1935) well function

x = x-coordinate (cm)

z = vertical coordinate (cm)

Z = objective function, same units as Ψ^2

μ = dynamic viscosity (g/cm-s)

ρ = density (g/cm^3)

ρ' = derivative of density with pressure

ϕ = head (cm)

Ψ = either P or P^2 depending on model (g/cm-s^2 or g^2/cm^2-s^4)

ω = molecular weight (g/mol)

Subscripts

atm = atmosphere

b = bulk

B = boundary

infl = influence (e.g. radius of influence)

j = region

m = mass

o = reference

r = radial

STP = standard temperature and pressure

w = well or water (P_w=well, μ_w= water, ρ_w=water)

z = vertical

INTRODUCTION

There are many hazardous sites contaminated by volatile organic compounds (VOCs) in the United States (Falta et al., 1989). These sites are in the subsurface and reside in or above the ground water. As a spilled liquid (e.g. from a leaking underground storage tank) migrates downward through the vadose zone, some of the liquid is trapped in pore spaces by capillary forces. Known as residual saturation, this liquid can occupy between 2 and 20% of the available pore space (Schwille, 1984). The fate of the trapped liquid depends on its ability to evaporate and move in the gas phase or alternately remain a liquid and move in the aqueous phase. Whether it reaches the water table depends on its ability to move in the aqueous phase as well as on chemical and biological reactions that might take place (Falta et al., 1989).

Several technologies are available for removing spilled liquids from the subsurface. These include excavation, pump and treat, biological treatment, and soil vapor extraction (SVE). Soil vapor extraction is the topic of this paper. SVE is also known as soil venting, vacuum extraction, aeration, and in-situ volatilization. It is an in-situ method for decontaminating soil above the water table involving withdrawal of air from the unsaturated zone using vacuum blowers. The blowers are installed on to wells that are screened in the unsaturated zone. A basic system uses vertical extraction wells; complex systems incorporate trenches, horizontal wells, air injection wells, heating, and surface seals. The contaminated extracted air is treated above ground using carbon adsorption, incineration, or catalytic oxidation (Johnson et al., 1990b) depending on the concentration of the extracted vapor.

Soil venting works because the contaminant is already a vapor and subsequently is extracted with the air, or the VOC vaporizes due to the vacuum supplied by the blower. Upon vaporizing, the contaminant desorbs from the soil

surface and enters the air phase of the soil matrix. There are three major factors which affect performance of a SVE system. They are the chemical composition of the contaminant, induced vapor flow rates through the unsaturated zone, and the flow path of the carrier vapors (usually air) (Johnson et al., 1990b). According to Pedersen and Curtis (1991), SVE is a proven cost-effective method for removing VOCs and motor fuels from contaminated sand and gravel soils. Often, however, systems are installed with little prior knowledge of what to expect in terms of remediation (Hutzler et al., 1988).

The value of this doctoral dissertation lies in the investigation of air movement in loam soils of glacial origin. Though glacial till soils occupy much of the earth's surface in the United States and the world (Press and Siever, 1986), these soils have previously been considered too impermeable for soil venting to be practical. There is a void in the soil venting literature with regards to: (1) obtaining field data, (2) verifying models by using field data, and (3) fitting models to field data to obtain air permeabilities. While there are a few studies of this sort in sands and gravels (Massman, 1989, Baehr and Hult, 1991), reports in till, to my knowledge, have never been reported.

In this dissertation, a literature review describing air phase contaminant transport models will be followed by a review of carrier fluid models. The carrier fluid is air in a soil venting system. It is essential to know how the carrier fluid moves before a contaminant transport model can be used. The model reviews will be followed by reviews of field tests where carrier fluid models are fit to air flow and pressure data for the purpose of determining air permeability. The remainder of the dissertation describes field experiments in unsaturated weathered loam till in Iowa. Air was forced through the soil by either extraction or injection from one vertical well. During an experiment, pressures were recorded at adjacent wells. One-dimensional (radial) and two-

dimensional (radial and vertical) compressible air flow models are fit to data from the field experiments.

LITERATURE REVIEW

The literature review contains several sections. First, contaminant transport models will be discussed as they are ultimately used in predicting air phase contaminant transport. However, before using a contaminant transport model, it is necessary to understand the movement of the carrier fluid - air.

Contaminant Transport Models

Contaminants can move in the vapor phase by advection and diffusion. Most gas phase contaminant transport models incorporate only gas diffusion (Jury et al., 1983; Swallow and Gschwend, 1983; Abriola, 1984; Baehr, 1984; Abriola and Pinder, 1985a,b; Baehr and Corapcioglu, 1987; Baehr, 1987; Silka, 1988; Wilson et al., 1987). A recent model by Sleep and Sykes (1989) included density-driven gas flow in the vadose zone. Density variations are the result of temperature or concentration gradients. Falta et al. (1989) showed that the importance of the density-driven flow mechanism is a function of the air permeability. For air permeabilities greater than 10^{-7} cm^2, density-driven flow is significant.

Carrier Fluid Models

When air (the carrier fluid) movement is studied independently of contaminant movement, the "intrinsic" flow parameters are the air permeability (k) and porosity. Air permeability is a measure of the ability of a soil to transmit a gas due to a pressure gradient. Along with soil moisture content, k is a function of the percentage, size, and continuity of soil pores (Evans, 1965). Freeze and Cherry (1979) list the permeability of various unconsolidated deposits. For glacial till, k varies from 10^{-15} to 10^{-9} cm^2. For sand, k varies from 10^{-9} to 10^{-5} cm^2 and for gravel from 10^{-6} to 10^{-3} cm^2. These values were obtained

from the equation (Freeze and Cherry, 1979):

$$k = \frac{\mu_w K}{\rho_w g} \tag{1}$$

where

k = intrinsic permeability, cm^2

K = saturated hydraulic conductivity, cm/s

g = gravitational acceleration, 981 cm/s^2

μ_w = dynamic viscosity of water, g/cm-s

ρ_w = density of water, g/cm^3

One-dimensional models

In addition to estimating the permeability from the saturated hydraulic conductivity, the permeability can also be found by laboratory measurements on core samples from the field. In the laboratory, a gasometer is used. It is a device that delivers a known rate of air at a known pressure difference through a sample (Evans, 1965; Kirkham, 1946). To find the permeability, Darcy's law is written referring to Fig. 1:

$$Q = -\frac{kA}{\mu_a}\frac{dP}{dx} \tag{2}$$

where

A = cross-sectional area of sample, cm^2

k = air permeability at the soil's moisture content, cm^2

P = absolute pressure, $g/cm\text{-}s^2$

Q = flowrate, cm^3/sec

μ_a = dynamic viscosity of air, g/cm-s

x = distance, cm

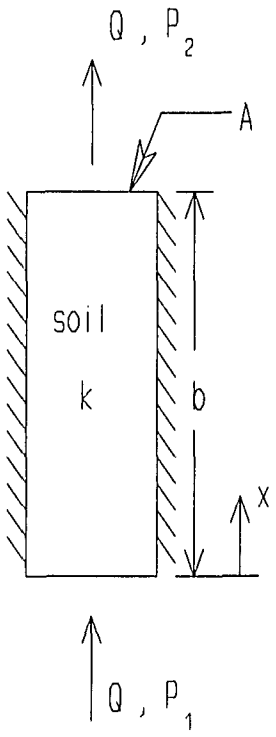

Figure 1. Gasometer for determining air permeability in the laboratory

Equation (2) is valid when viscous forces dominate the air flow (Reynolds Number < 5), flow is steady state, and gravity effects are small (or air flow is horizontal). For vertical samples, ignoring gravity produces an error of less than 1% (Evans, 1965). Equation (2) can be integrated and solved for the air permeability:

$$k = -\frac{Q\mu_a b}{A(P_2-P_1)} \tag{3}$$

where

b = soil thickness, cm

One of the first studies to apply Darcy's law to air flow was by Muskat and Botset (1931) in *Physics'* first issue. They were interested in understanding flow in underground gas reservoirs. All current studies where air flow is slow enough to be dominated by viscous forces assume that Darcy's law (2) is valid.

Equation (3) provides a value for the permeability which is a function of the water content. As the water content increases, there is less room for air to move resulting in a lower permeability. The permeability obtained from tests using air as the fluid will be termed air permeability while the permeability obtained from the hydraulic conductivity as in (1) is the intrinsic permeability. Both permeabilities have units of cm^2. Air permeability has been found to be affected, not only by water content in the soil, but also by trapped air (Poulovassilis, 1970; Stonestrom and Rubin, 1989). Wetting versus drying cycles also affect air permeability (Baehr and Hult, 1991).

Kidder (1957) developed an analytical solution to the one-dimensional transient gas flow equation:

$$\frac{\partial}{\partial x}\left(P\frac{\partial P}{\partial x}\right) = \frac{n\mu_a}{k}\frac{\partial P}{\partial t} \tag{4}$$

with the boundary conditions:

$$P(x,0) = P_i \tag{5}$$

$$P(0,t) = P_1 < P_i \tag{6}$$

$$P(\infty,t) = P_i \tag{7}$$

where

n = vapor-filled porosity

t = time, sec

Equation (4) can be solved to obtain n/k prior to reaching steady state. Since the solution to (4) is $P(x,t)$ and not n/k explicitly, n/k is found by varying n/k until the best fit between the model and the data is found.

Air permeability can also be found from in-situ field tests using air as the fluid. There are various methods. Kirkham (1946) jacked an open-ended cylinder into the ground. Air was injected into the cylinder at a known rate and pressure. The air flowed down through the inside of the cylinder, out the bottom and up to the ground surface. Weeks (1978) described a method for determining the vertical permeability of air based on changes in atmospheric pressure. Piezometers with pressure sensors measured air pressure at various depths under the ground. Changes in atmospheric pressure result in pressure changes under the ground. Unsteady vertical flow equations were used to determine the vertical permeability.

Air flow models for multiple well field tests

Similar to finding hydraulic conductivity from water pumping tests which

has been studied for decades, multiple well air pumping tests (pneumatic tests) can be used to determine air permeability. Since multiple well tests are a large scale field test, they best represent a true soil vapor extraction remediation system. They are a good method for determining air permeability and should result in numbers which truly represent the field situation. The drawback is that modeling the field situation is more difficult than modeling a laboratory experiment. In the laboratory, the experiment can be designed so that the simplest model can be used and the boundary conditions are well known. In the field, the flow may not be one-dimensional and the boundary conditions are more difficult to determine.

Radial unsteady air flow

The simplest models used to analyze vertical, multiple well pneumatic field tests assume that flow is only in the radial direction. Several papers (Johnson et al., 1990, McWhorter, 1990, Massman, 1989) derive the same governing flow equation for radial unsteady air flow; it is the non-linear equation:

$$\frac{1}{r}\frac{\partial}{\partial r}\left(r\frac{\partial P^2}{\partial r}\right) = \left(\frac{2n\mu_a}{k}\right)\frac{\partial P}{\partial t} \qquad (8)$$

where

r = radial coordinate, cm.

To solve (8), each author makes different assumptions yet arrives at the same form of the solution: the Theis (1935) "well function" solution for unsteady radial water flow to a well. Each approach will be described and each approach refers to Fig. 2.

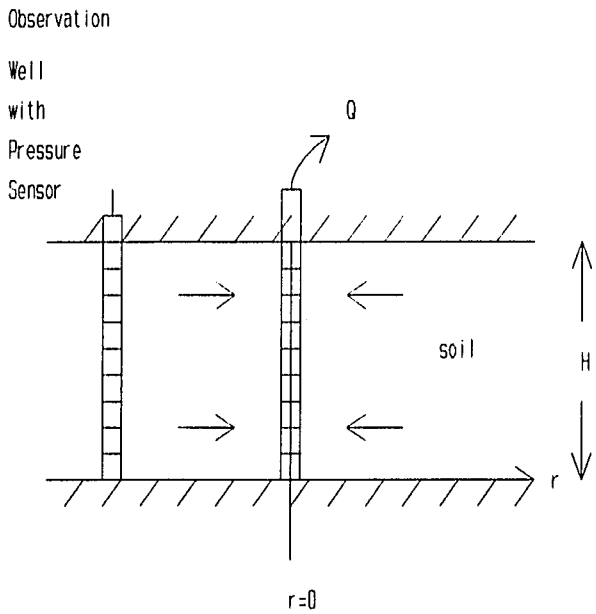

Figure 2. Schematic diagram of radial air flow in unsaturated zone

Johnson et al. (1990a) solved (8) by making the approximation:

$$P^2 = P_{atm} P' \tag{9}$$

where

P'= vacuum measured in the soil, g/cm-s^2

P_{atm} = atmospheric pressure, g/cm-s^2

Equation (9) is valid for low vacuums. Substituting (9) into (8), the following equation is obtained:

$$\frac{1}{r}\frac{\partial}{\partial r}\left(r\frac{\partial P'}{\partial r}\right) = \left(\frac{n\mu_a}{kP_{atm}}\right)\frac{\partial P'}{\partial t} \tag{10}$$

The boundary conditions are:

$$P'(\infty,t) = 0 \tag{11}$$

$$P'(r,0) = 0 \tag{12}$$

$$\lim_{r\to 0}\left(r\frac{\partial P'}{\partial r}\right) = \frac{Q\mu_a}{2\pi Hk} \tag{13}$$

Equation (10) subject to (11) through (13) has a solution similar to the Theis (1935) well function solution:

$$P'(r,t) = \frac{Q\mu_a}{4\pi Hk}\int_{\frac{r^2 n\mu_a}{4kP_{atm}t}}^{\infty}\frac{e^{-x}}{x}dx \tag{14}$$

where

$$W(u) = \int_{\frac{r^2 n\mu_a}{4kP_{atm}t}}^{\infty} \frac{e^{-u}}{u} du \tag{15}$$

The well function, equation (15), has been tabulated in many books, for example Bear (1979), and Huntoon (1980) presented a polynomial approximation.

Massman (1989) also solved (10) but made different assumptions than Johnson et al. (1990a). Massman rewrites (10) as:

$$\frac{1}{r}\frac{\partial}{\partial r}\left(2rP\frac{\partial P}{\partial r}\right) = \left(\frac{2n\mu_a}{k}\right)\frac{\partial P}{\partial t} \tag{16}$$

Then, substituting the Boyle-Mariotte law (Collins, 1961):

$$P = \frac{\rho_a RT}{\omega} \tag{17}$$

where

R = universal gas constant, 8.314×10^7 g-cm^2/s^2-mol-K

T = absolute temperature, K

ω = molecular weight of moist air, g/mol

ρ_a = density of air, g/cm^3

The following is obtained:

$$\frac{1}{r}\frac{\partial}{\partial r}\left(r\frac{\rho_a RT}{\omega}\frac{\partial P}{\partial r}\right) = \left(\frac{n\mu_a}{k}\right)\frac{\partial P}{\partial t} \tag{18}$$

Then, let $\rho_a = \rho_o$ which linearizes the equation allowing an analytical solution to be found. ρ_o is the initial gas (air) density. (18) can be re-written as:

$$\frac{1}{r}\frac{\partial}{\partial r}\left(r\frac{\partial P}{\partial r}\right) = \left(\frac{n\mu_a\,\omega}{k\rho_o RT}\right)\frac{\partial P}{\partial t} \tag{19}$$

which is linear and can be solved easily. In fact, if the substitutions:

$$P = P_{atm} - P' \tag{20}$$

and (17) are made, one arrives at exactly the same expression as Johnson et al. (1990a) in (10) above. The boundary conditions are also the same as Johnson (1990a). Thus, the Massman (1989) and Johnson (1990a) analyses are the same.

Referring again to Fig. 2, McWhorter (1990) began with mass conservation:

$$\frac{\partial Q_m}{\partial r} = -2\pi r H n\frac{\partial \rho}{\partial t} \tag{21}$$

where Q_m = mass flow rate, g/s.

Darcy's law for gas flow can be expressed as:

$$Q_m = -2\pi\frac{Hk}{\mu_a}\rho_a r\frac{\partial P}{\partial r} \tag{22}$$

Combining (21) and (22), one obtains:

$$\frac{Hk}{\mu_a}\frac{1}{r}\frac{\partial}{\partial r}\left(\rho_a r\frac{\partial P}{\partial r}\right) = nH\rho_a'\frac{\partial P}{\partial t} \tag{23}$$

where

$$\rho_a' = \frac{d\rho_a}{dP} \tag{24}$$

or

$$\rho_a' = \frac{\omega}{RT} \tag{25}$$

Equation (23) simplifies to:

$$\frac{1}{r}\frac{\partial}{\partial r}\left(\rho_a r\frac{\partial P}{\partial r}\right) = \frac{n\mu_a}{k}\rho_a'\frac{\partial P}{\partial t} \tag{26}$$

If ρ_a and ρ_a' are constant, then substituting (17) and (25) into (26) provides:

$$\frac{1}{r}\frac{\partial}{\partial r}\left(r\frac{\partial P}{\partial r}\right) = \frac{n\mu_a}{kP}\frac{\partial P}{\partial t} \tag{27}$$

Then, allowing the non-linear P in (27) to be constant at P_{atm} and further substituting (20), one obtains (10) above. So the final equation (27) is identical to Massman (1989) and Johnson (1990a). ρ_a' in (24) can be taken as a constant since according to (25), ρ_a' is only a function of air's molecular weight and temperature. More difficult is to say that ρ_a is constant since we know from (17) that ρ_a varies with pressure. Recognizing that ρ_a and ρ_a' may not be constant, McWhorter (1990) further developed a semi-analytical solution to (23).

Radial steady air flow

Since steady state is usually reached within a week (Johnson et al., 1990a) and venting programs operate for years, a steady state solution better represents the field in most cases.

In light of the observation that steady state is reached soon compared to the duration of a soil venting remediation program, Johnson et al. (1990a) provided a radial steady state solution to (8) where the right hand side equals zero The boundaries are:

$$P(r_w) = P_w \tag{28}$$

$$P(r_{infl}) = P_{atm} \tag{29}$$

The solution is almost trivial and is:

$$P^2(r) = P_w^2 + (P_{atm}^2 - P_w^2)\frac{\ln\left(\frac{r}{r_w}\right)}{\ln\left(\frac{r_{infl}}{r_w}\right)} \tag{30}$$

where

P_w = absolute pressure in extraction well, g/cm-s^2

r_w = radius of extraction well, cm

r_{infl} = radius of influence, cm

A problem with using (30) is that the radius of influence is a difficult number to quantify. One can also use Darcy's law directly. Recognizing that:

$$Q = \frac{Q_m}{\rho_a} \tag{31}$$

equation (22) can be re-written as:

$$Q = -2\pi H \frac{k}{\mu_a} r \frac{\partial P}{\partial r} \tag{32}$$

Integrating between any two radii and pressures, letting $L=H$, and solving for k gives:

$$k = \frac{Q\mu_a}{2\pi L(P_2^2 - P_1^2)} \ln\left(\frac{r_2}{r_1}\right) \tag{33}$$

where L = well screen length, cm

The substitution $L=H$ allows a calculation of k from field data consisting of pressure at two wells and the flowrate as in Fig. 2. The flow must be radial. Withdrawal of air is given a positive Q. For air injection, Q is negative in (33).

Radial and vertical unsteady flow

If a contaminated zone is not bounded by lower permeability or impermeable layers, then two-dimensional models are more appropriate. Often, the contaminated zone is bounded on the top by the ground surface which may be exposed to atmospheric pressure.

Kuo et al. (1990) solved the two-dimensional unsteady compressible gas flow equation:

$$\frac{1}{r}\frac{\partial}{\partial r}\left(r\, k_r(r,z)\frac{\partial P^2}{\partial r}\right) + \frac{\partial}{\partial z}\left(k_z(r,z)\frac{\partial P^2}{\partial z}\right) = \frac{2n\mu_a}{k}\frac{\partial P}{\partial t} \tag{34}$$

where

k_r = air permeability in radial direction, cm^2

k_z = air permeability in vertical direction, cm^2

z = vertical dimension, cm

Equation (34) was solved using a finite difference method where the boundaries could be constant pressure (e.g. atmospheric), zero flow, or variable flow.

Radial and vertical steady flow

As mentioned above, it has been found from field tests that steady state is often reached very quickly. Therefore, steady state air flow equations may be

best. There are two very recent papers that developed analytical solutions for two-dimensional steady state air flow.

Baehr and Hult (1991) derived an expression for steady two-dimensional compressible air flow which has the governing equation (34) except the right hand side is zero. They also developed an analytical solution allowing partially penetrating wells. The solution takes the form of an infinite series. The boundary conditions are as follows and refer to Fig. 3:

$$P^2(r,H) = P^2_{atm} \tag{35}$$

$$\frac{\partial P^2}{\partial z}(r,0) = 0 \tag{36}$$

At $r=r_w$:

$$\frac{\partial P^2}{\partial r} = 0 \quad \text{for } 0<z<d \text{ and } d+L<z<H \tag{37}$$

$$\frac{\partial P^2}{\partial r} = -\frac{\mu_a P_w Q}{\pi k_r r_w L} \quad \text{for } d<z<d+L \tag{38}$$

Shan et al. (1992) solved the very same governing equation (34) as Baehr and Hult (1991) (right hand side equals zero) with the same boundary conditions (35) through (38) but obtained a different form of an analytical solution. Shan et al. (1992) also solved for the stream function analytically. They further discussed theoretical experiments rather than fitting to field data to show behavior of the model.

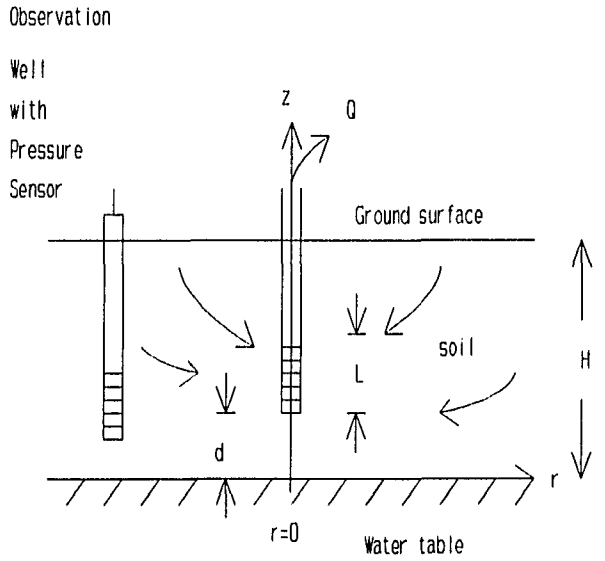

Figure 3. Schematic diagram of radial and vertical air flow in unsaturated zone

Field Tests

Influence of water table

Johnson et al. (1990a) discussed water table upwelling. This refers to the fact that the water table, if sufficiently influenced by applied vacuums, may rise. Ignoring friction, the water table rise is equal to the applied vacuum. McWhorter (1990) stated that water table upwelling will create a larger than expected pressure gradient in the vicinity of the pumped well. In the field studies conducted for the present paper, the rising water table affected the viability of venting significantly by causing turbulence. There was no discrete rise, just bouncing water.

Air permeability from fitting models to data

For certain soil venting applications, the pressure differential may be low enough to assume that the flow of air is incompressible. It was shown above that the Theis (1935) solution for unsteady radial ground water flow can be used for the analysis of air transport. Massman (1989) applied the Theis solution (14) to a field study consisting of pneumatic tests in a methane-contaminated sand and gravel region 24 m thick, overlain by 6 m of glacial till, and underlain by clay in Washington state. The data indicated an excellent match to the Theis solution with a (air) permeability of 10^{-7} cm^2. Based on an extraction rate of 100,000 cm^3/s (200 cubic feet per minute or cfm), a radius of influence of 150 m could be expected in the material.

Baehr and Hult (1990) applied their model to pneumatic tests in a deposit consisting of coarse to medium sands. Various injection and withdrawal rates were used. (The governing equation is the same whether injecting or withdrawing air.) Vertical and horizontal air permeabilities were found based on fitting the model to the field data. For flow rates of 24,000 cm^3/s (50 cfm) up to

71,000 cm^3/s (150 cfm), the radial permeability dropped from $1.5x10^{-6}$ cm2 to $1.3x10^{-6}$. The vertical permeability variation as a function of flow rate was not clear but ranged from $2.5x10^{-7}$ to $1.5x10^{-6}$ cm^2. There are not many reports of fitting models to field data which makes the current research so valuable. There are many case studies, however, two of which follow.

Venting from contaminated sand and gravel proved very effective in an American Petroleum Institute sponsored study (Crow et al., 1987). Vacuums were recorded at various radii and indicated a radius of influence of 30 meters (100 feet) or more at an extraction rate of 19,000 cm^3/s (40 cfm). Measured vacuums appeared to drop off exponentially with distance from the extraction well. Steady state was reached very rapidly. In another study of a controlled spill, an air discharge rate of 2400 cm^3/s (5 cfm) was employed. 57% of the 75 gallons of gasoline that were spilled was removed by venting (Thornton and Wootan, 1982) in an eleven day period.

To my knowledge, there are no published reports of soil venting in glacial till. However, some consulting firms have tried venting in glacial till soils without success (Smith, 1992). Other researchers (currently unpublished) are trying to create fractures in till so that air can more easily move through the soil (Savage, 1992).

EXPERIMENTAL SETUP

The research presented in this thesis consists of obtaining data from field experiments and fitting models to the data. The goal was to obtain the "best fit" air permeability. Several models were tried. The best model was a radial and vertical flow model which split the soil regime into four layers with air permeability estimated for each layer. This chapter describes the field experiment. Modeling and results will be discussed in subsequent chapters.

A number of partially penetrating vertical wells were installed in the vadose zone at a site near Iowa State University. A blower discharged (or injected) air from one of the wells and vacuums (or pressures) were recorded at it and the other wells.

The site can be found on the 7.5 minute United States Geological Survey (USGS) Slater Quadrangle (Iowa) topographic map. The site is in section 19 of Washington Township in Story County at the Iowa State University Experimental Farm (also known as the Curtiss or Woodruff Farm). The location of the site is shown in Fig. 4. From Iowa State University, one should head west on Lincoln Way until reaching South Dakota Avenue. Turn left (south) on South Dakota, then drive two miles until a gravel road is reached and radio towers can be seen off to the right (west). Turn right (west) and travel about half a mile at which point you will be at the radio tower. Turn left (south) and drive until you meet the first road that goes west. Turn right (west) on this road. The site is about a quarter mile down this road on the left. There will be well heads visible from the road.

Description of Site

The site was selected because electrical power was available and the soil is Clarion loam till, a soil similar to other nearby (within 10 km) sites where

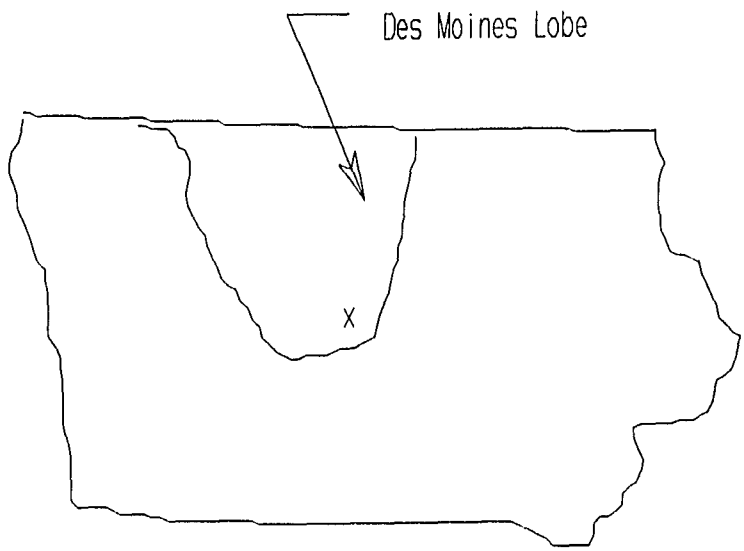

Figure 4. Map of Iowa showing the extent of the Des Moines Lobe of the Wisconsin glacial advance. "x" indicates site location

extensive field work has been done. The site consists primarily of the Des Moines Lobe of the Wisconsin glacial period (Wang, 1990), the extent of which is shown in Fig. 5. Oxidized Wisconsin age till is present to a depth of approximately 320 cm below the ground surface. Unoxidized Wisconsin age till lies underneath the oxidized till.

The following description of the soil at the site was provided by the USDA (1984). At the field site, the 20 cm thick soil surface layer is black loam. The subsurface layer is very dark grayish brown loam and is about 10 cm thick. The subsurface is friable loam. It is about 50 cm thick and is brown in the upper and middle regions and yellowish brown in the lower region. The substratum, to a depth of approximately 150 cm, is light olive brown, mottled loam. There are lenses of silt loam, loamy sand, or sand in the substratum. A diagram of a typical core is shown in Fig. 6 courtesy of Ressler (1992) who analyzed five cores at the site.

The site layout is shown in Figs. 7 and 8 which are a plan (top) view and cross-section, respectively. Seven vertical boreholes were drilled. The holes vary in depth and diameter and are described in Table 1; the distance from W1 is centerline to centerline. Schedule 40 polyvinyl chloride (PVC) screened tubing was inserted in each hole. The PVC screen was surrounded by pea gravel; above the pea gravel, each hole was filled with bentonite powder or pellets up to the ground surface and moistened with water. Boreholes W4 and W5 contain five "nested" wells. A nested well consisted of placement of a screened PVC tube surrounded by gravel. A layer of bentonite (approximately 30 cm) was poured above the gravel and moistened with water to create a barrier between wells; then another PVC screen was installed and so on up to the ground surface. This allowed the vertical flow variation to be monitored at a single radial location. Fig. 9 shows a typical (non-nested) well installation. To monitor the vacuum,

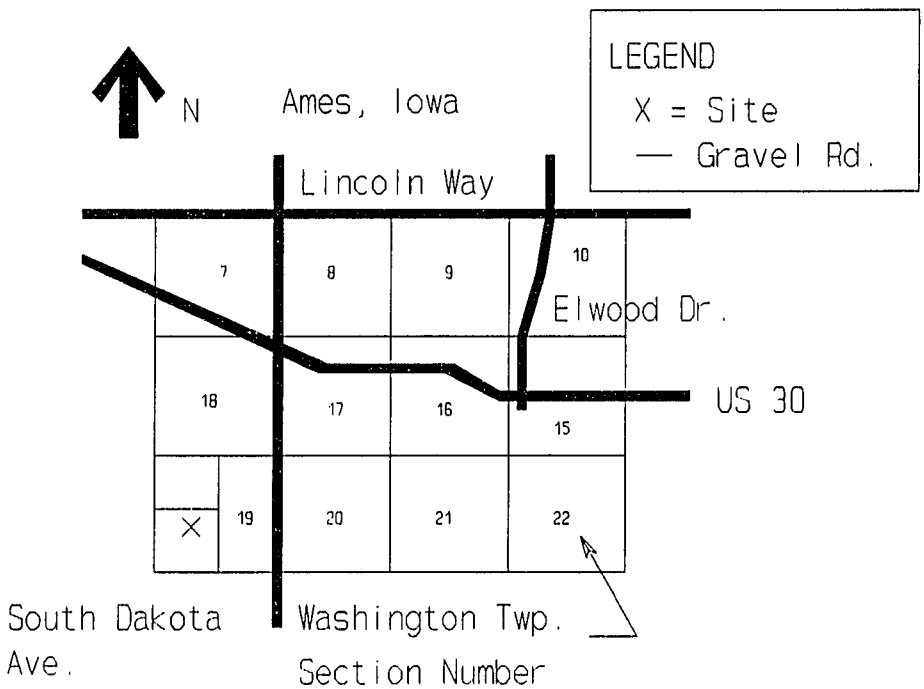

Figure 5. Location of field site in Story County, Iowa

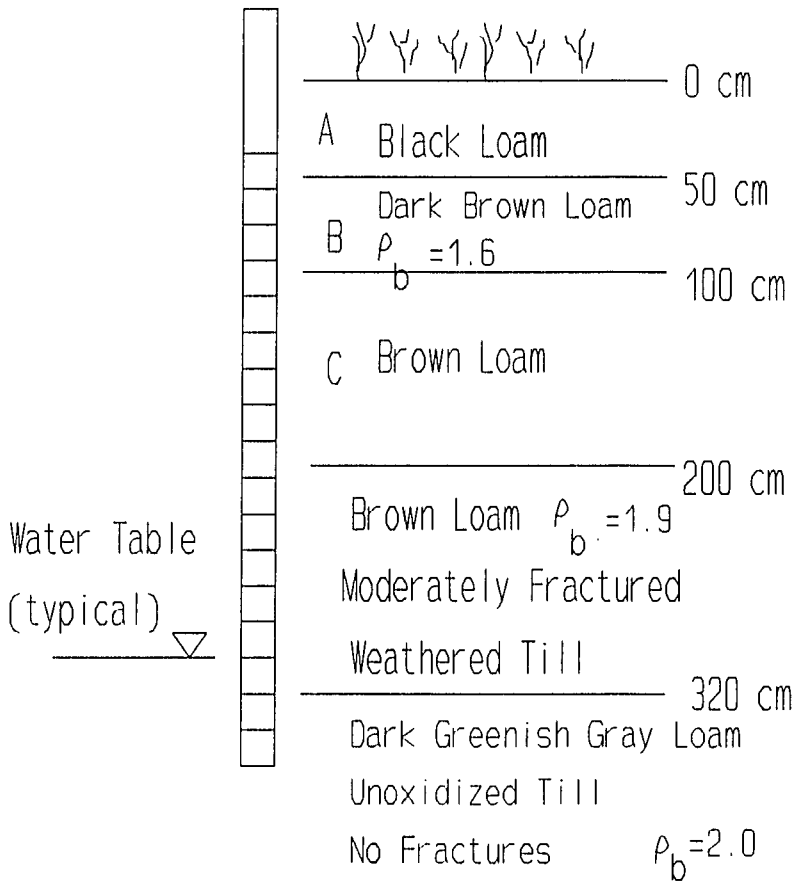

Figure 6. Typical core where ρ_b=bulk density (g/cm^3). Courtesy of Ressler (1992)

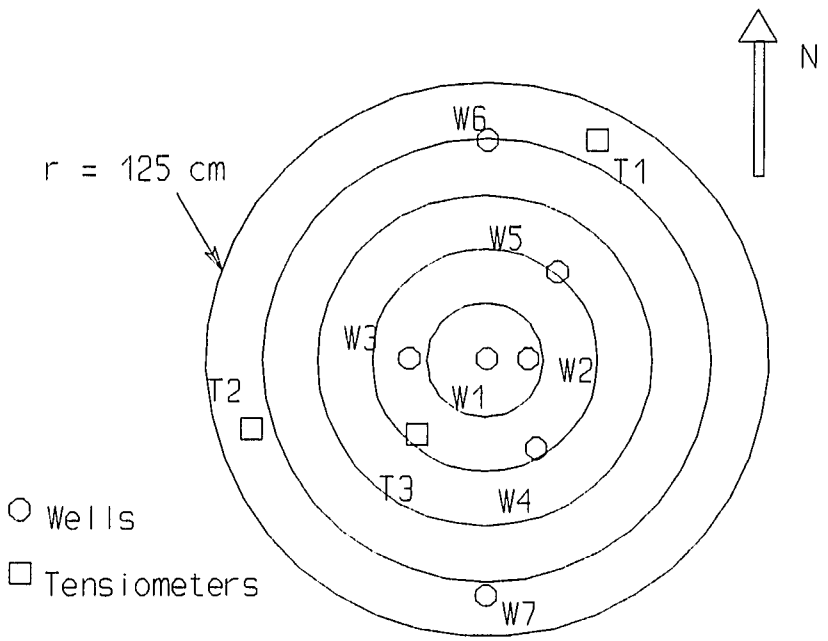

Figure 7. Site plan. Grid interval is 25 cm

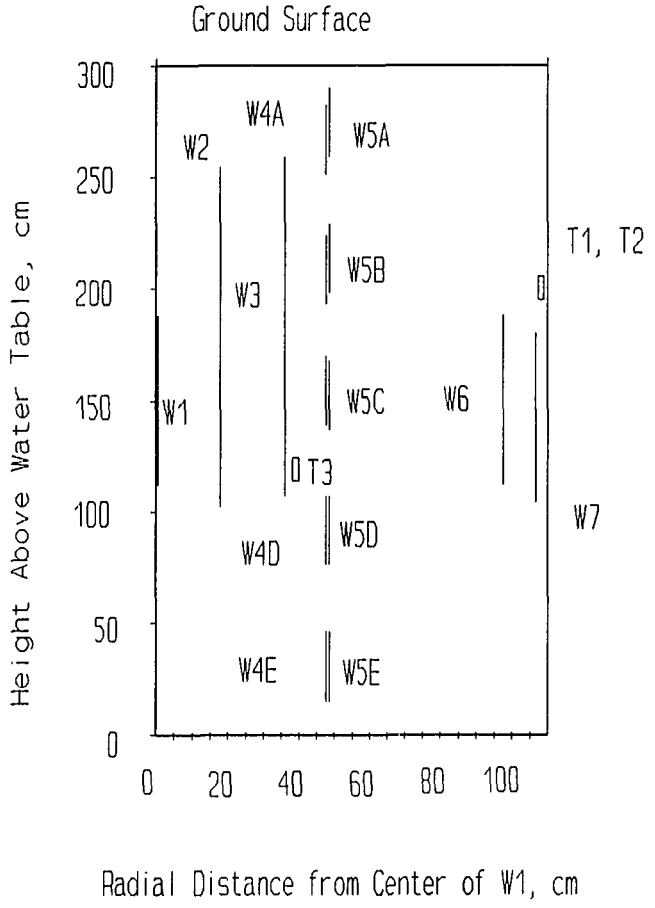

Figure 8. Cross-section as if all wells were at same angle from W1

Table 1. Screen dimensions. Baseline for elevations is 300 cm below ground surface

Well ID	Dist from W1 (cm)	Borehole Diameter (cm)	PVC Dia (cm)	Elev of Bottom of Screen (cm)	Elev of Top of Screen (cm)	Screen Length (cm)
W1	0.0	10.2	5.1	112	188	76
W2	17.8	7.6	2.5	102	254	152
W3	35.9	7.6	2.5	107	259	152
W4A	47.6	10.2	1.9	252	282	30
W4B	47.6	10.2	1.9	194	224	30
W4C	47.6	10.2	1.9	140	170	30
W4D	47.6	10.2	1.9	77	107	30
W4E	47.6	10.2	1.9	16	46	30
W5A	48.6	10.2	1.9	260	290	30
W5B	48.6	10.2	1.9	199	229	30
W5C	48.6	10.2	1.9	138	168	30
W5D	48.6	10.2	1.9	77	107	30
W5E	48.6	10.2	1.9	16	46	30
W6	97.5	10.2	5.1	112	188	76
W7	106.7	10.2	5.1	104	180	76

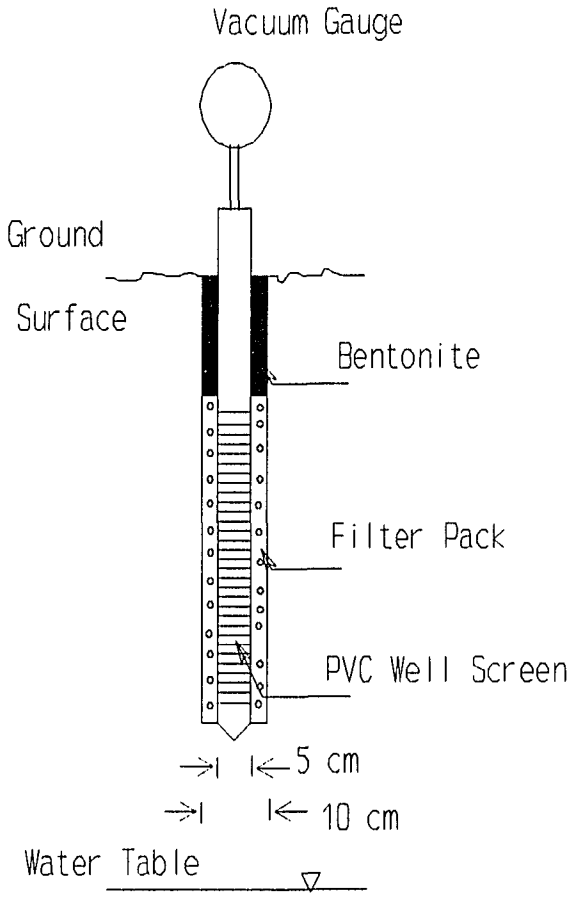

Figure 9. Non-nested monitoring well installation

each well was capped and a tube was connected from a hole in the cap to a manometer calibrated in increments of either 0.01 inch (0.025 cm) or 0.1 inch (0.25 cm) of H_2O. To monitor soil tension, three tensiometers were installed at the locations and depths shown in Figs. 7 and 8.

To increase the radius of influence, an impermeable boundary was created on the ground surface by roto-tilling approximately 10 cm deep in a 200 cm radius around well W1. The tilled area was filled with a 1:1 mixture of powdered bentonite and soil from the site. Water was sprinkled on the surface. A layer of plastic was laid and then covered by a layer of roof shingles with bricks on top in case of strong winds.

Throughout most of the year, all of the wells are above the water table. A 15-amp (120 Volt) blower withdrew or injected air from one of the wells, usually W1. A variac was wired to the blower so that the power to the blower was adjustable. At full power, the blower could deliver 43,000 cm^3/sec (92 cubic feet per minute or cfm) of air when no load was applied and zero flow at 330 cm H_2O (130 inch H_2O) vacuum. A pressure gage and thermometer were mounted in well, W1. A schematic diagram for an injection test is shown in Fig. 10. For an extraction test, the blower is turned around. The pressure gage and thermometer at the flowmeter were used to correct the rotameter flowrate reading for air temperature and pressure; the calculation will be shown in the RESULTS section under "Parameter conversions."

Laboratory Test for Well Screen Losses

There was concern that due to high velocities, there may have been significant pressure losses in the well screen of the pumped well. While such losses are not of consequence in the modeling of the tests since the flowrate, not the pressure, is used as the boundary condition, losses do impact conclusions

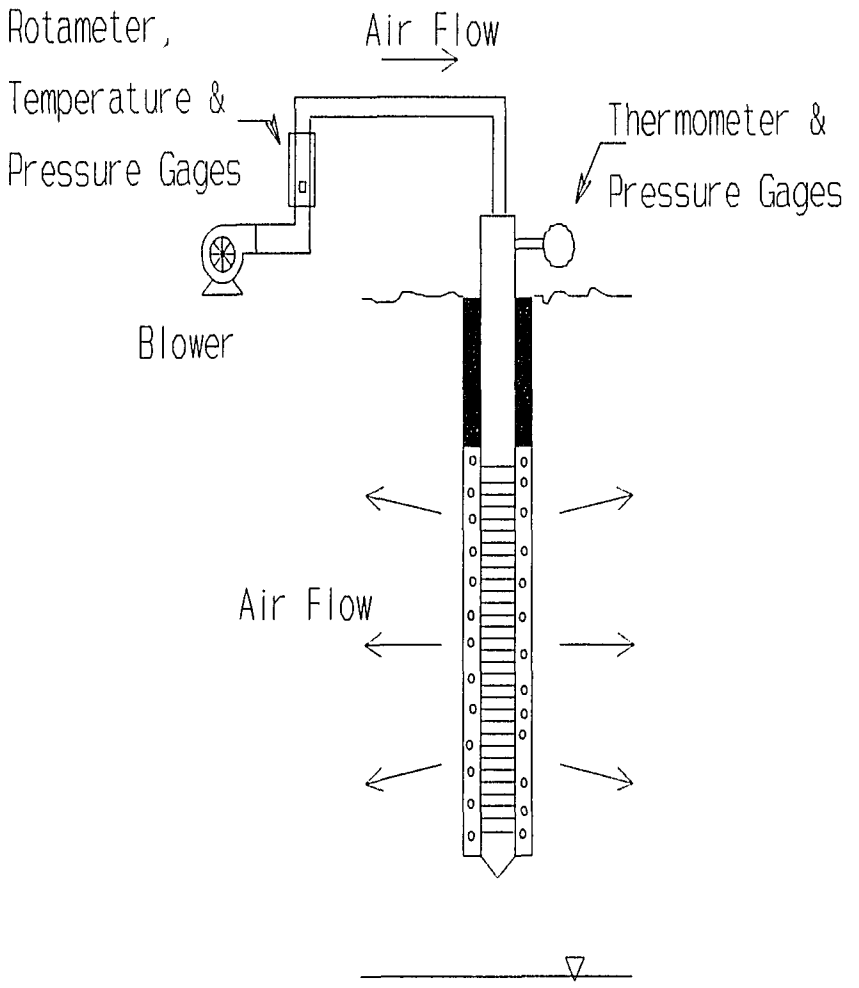

Figure 10. Air injection scenario; for extraction test, blower is turned around

drawn from comparing the model's predicted vacuum with data. A laboratory test was run to determine if losses were present. In the field, air was to be withdrawn from well W1 which is screened over a 76 cm (2.5 ft) long section of 5 cm (2 inch) diameter, 0.025 cm (0.01 inch) slotted schedule 40 PVC well screen at flowrates up to 4000 cm^3/sec. The screen was fitted with an end cap. A laboratory experiment was conducted in ambient air using an identical section of well screen. A flow meter was connected to the discharge side of the blower. Power to the blower was controlled by a variac as mentioned previously. With nothing attached to the inlet side of the blower, the flowrate was set to 5000 cm^3/sec by adjusting the variac. Then the 76 cm section of well screen (with an end cap) was attached to the blower inlet. The flow remained at 5000 cm^3/sec (the operator did not change the power to the blower). Had the screen caused significant pressure losses the flowrate would have decreased. The experiment was repeated for flowrates from 0 to 50,000 cm^3/sec with the same results. Thus, it was concluded that the well screen presented insignificant head losses.

MODEL

This chapter will present the reasoning behind choosing the radial and vertical steady, compressible flow model as the model that should best describe the field experiment. The DISCUSSION chapter will use the RESULTS to show that this model was an appropriate selection. A one-dimensional model was also used to determine air permeabilities. It will not be discussed in detail here, however, since it was already mentioned above - see equations (2) and (3).

Following the "Selection of Two-Dimensional Model" section of this chapter, the model will be derived and the boundary conditions appropriate to the field will be described. Then, the numerical solution method will be discussed followed by a description of how the data is used to determine air permeabilities.

Selection of Two-Dimensional Model

Observing the manometers during a test showed that steady state was reached in a matter of seconds (less than 5 seconds). This was something of a surprise. Since till is considered to have a low permeability, it was thought that steady state would take some time to achieve. That the flow field surface was open to the atmosphere beyond a 200 cm radius circle probably caused the rapid attainment of steady state.

A model representing the field conditions should incorporate radial and vertical flow since the wells are partially penetrating and air flow originates at the ground surface. The vacuum (or pressure) responses (see RESULTS) at the nested observation wells (W4 and W5) were fairly similar, indicating some degree of angular homogeneity since they are at nearly the same distance from the discharge well, W1. Thus, an axisymmetric model could be used. The model should also allow for compressibility of air. The model should be flexible enough to allow inhomogeneities and anisotropy.

Derivation

Baehr and Hult (1991) and Baehr et al. (1989) have excellent descriptions of the derivation of a radial and vertical axisymmetric flow equation including the assumptions and validity. The derivation can be summarized as follows.

Darcy's law in terms of the head (pressure) is:

$$\vec{q} = -\frac{\rho g \vec{k}}{\mu} \nabla \phi \tag{39}$$

where

$\vec{q}$ = specific discharge vector, cm/s

ρ = density of air, g/cm^3

g = acceleration due to gravity = 981 cm/s^2

μ = dynamic viscosity, g/cm-s

$\vec{k}$ = permeability vector, cm^2

∇ = gradient operator, cm^{-1}

ϕ = head, cm

The density is a function of the pressure and is given by the ideal gas law:

$$\rho = \frac{\omega P}{RT} \tag{40}$$

where

ω = average molecular weight of the air phase = 28.8 g/mol for humid air

R = universal gas constant = 8.3143x10^7 g-cm^2/s^2-mol-K

P = absolute pressure, g/cm-s^2

T = temperature of air, K

Then by substituting (40) into (39):

$$\vec{q} = -\left(\frac{\omega P}{RT}\right)\frac{g\vec{k}}{\mu}\nabla\phi \tag{41}$$

Since air is a compressible fluid, head is written as:

$$\phi = z + \frac{1}{g}\int_{P_o}^{P}\frac{dP}{\rho} \tag{42}$$

where

z = fixed datum, cm

P_O = reference air phase (absolute) pressure, g/cm-s^2

Substituting in the expression for density (40) and assuming that temperature and molecular weight are independent of pressure, equation (42) can be re-written as:

$$\phi = z + \frac{1}{g}\frac{RT}{\omega}\int_{P_o}^{P}\frac{dP}{P} \tag{43}$$

Performing the integration, one obtains:

$$\phi = z + \frac{RT}{\omega g}\ln\frac{P}{P_o} \tag{44}$$

To obtain $\nabla\phi$, it is recognized that z is constant; thus:

$$\nabla z = 0 \tag{45}$$

and,

$$\nabla\phi = \nabla\left(\frac{RT}{\omega g}\ln\frac{P}{P_o}\right) \tag{46}$$

If temperature and molecular weight are independent of position, then (46) can be

written as:

$$\nabla\phi = \frac{RT}{\omega g} \nabla \left(\ln \frac{P}{P_o} \right) \tag{47}$$

Since P_O is constant, (47) reduces to:

$$\nabla\phi = \frac{RT}{\omega g} \frac{\nabla P}{P} \tag{48}$$

Combining (41) and (48), one obtains:

$$\vec{q} = -\frac{\omega P g \vec{k}}{RT\mu} \frac{RT}{\omega g} \frac{\nabla P}{P} \tag{49}$$

which simplifies to:

$$\vec{q} = -\frac{\vec{k}}{\mu} \nabla P \tag{50}$$

For mass conservation under steady state conditions:

$$\nabla \cdot (\rho \vec{q}) = 0 \tag{51}$$

Substituting (40) into (51), one obtains:

$$\nabla \cdot \frac{\omega P}{RT} \vec{q} = 0 \tag{52}$$

Again assuming temperature and molecular weight are constant at all locations, (52) reduces to:

$$\nabla \cdot (P\vec{q}) = 0 \tag{53}$$

Then substituting $\vec{q}$ from (50),

$$\nabla \cdot \left(-P \frac{\vec{k}}{\mu} \nabla P \right) = 0 \tag{54}$$

If temperature is constant, then the dynamic viscosity is constant and (54) can be simplified to:

$$\nabla \cdot (\vec{k} \nabla P^2) = 0 \tag{55}$$

and letting $\Psi = P^2$, then:

$$\nabla \cdot (\vec{k} \nabla \psi) = 0 \tag{56}$$

In radial and vertical coordinates, (56) can be written as:

$$\frac{\partial}{\partial r}\left(k_r(r,z) \frac{\partial P^2}{\partial r} \right) + \frac{k_r(r,z)}{r} \frac{\partial P^2}{\partial r} + \frac{\partial}{\partial z}\left(k_z(r,z) \frac{\partial P^2}{\partial z} \right) = 0 \tag{57}$$

This is the governing equation for two dimensional axisymmetric compressible air flow under heterogeneous and anisotropic soil conditions. The boundary conditions will be discussed later.

There are some other phenomena and limitations that may be important that were not mentioned. The Reynolds number which is essentially a ratio of inertial to viscous forces, usually defines the validity of Darcy's law. In general, Darcy's law is valid if the Reynolds number is less than 1 or, possibly, 10 (Bear, 1979). From experiments using air in sand columns, Darcy's law was found to be valid if the Reynolds number was less than 6 (Yu, 1985).

The Klinkenberg effect (Klinkenberg, 1941) also known as Knudsen flow (Dullien, 1979) has been noted by Baehr and Hult (1991) and Massman (1989) as having a possible influence on air flow in soils. The effect causes increased air flow due to air molecules slipping on the boundaries of air filled pores. It is not much of a concern in water pumping tests because water is more viscous than air

and adheres more readily to soil surfaces. Water flow has a shorter mean free path between soil particles and has less "slippage," nullifying the effect. However, in air, it has been considered. The Klinkenberg effect on air flow increases as pore size decreases and vacuum or pressure increases relative to atmospheric pressure. As a worst case, Baehr and Hult (1991) concluded that even with a low permeability of 10^{-11} cm^2 and a vacuum of half an atmosphere, the most that the true permeability would differ is 30%. Massman (1989) neglected slip flow because data was taken in a sand and gravel formation. The field data that will be described in this report had a maximum vacuum of 0.1 atmosphere and a minimum permeability of 10^{-8} cm^2. Because of these and other uncertainties in modeling and the uncertainty in arriving at the proper factors to correct for slip flow, the effect will be neglected.

As a test to determine the applicability of using ground water models for air transport, an analysis can be made where the fluid (air) is assumed to be incompressible. For an incompressible fluid, the governing equation is written in terms of P rather than P^2. The derivation is similar except that ρ is held constant. Equation (53) simplifies to:

$$\nabla \cdot \vec{q} = 0 \tag{58}$$

and (42) is written as:

$$\phi = z + \frac{1}{\rho g}\int_{P_o}^{P} dP \tag{59}$$

Equation (50) is not affected by fluid compressibility. When (50) is substituted into (58), one obtains:

$$\nabla \cdot \left(-\frac{\vec{k}}{\mu} \nabla P \right) = 0 \tag{60}$$

which reduces to the following if the dynamic viscosity is constant in space:

$$\nabla \cdot (\vec{k} \nabla P) = 0 \tag{61}$$

The governing equation for two-dimensional incompressible flow under heterogeneous and anisotropic soil conditions is:

$$\frac{\partial}{\partial r}\left(k_r(r,z) \frac{\partial P}{\partial r} \right) + \frac{k_r(r,z)}{r} \frac{\partial P}{\partial r} + \frac{\partial}{\partial z}\left(k_z(r,z) \frac{\partial P}{\partial z} \right) = 0 \tag{62}$$

Equations (57) and (62) are solved by the same numerical solution since the governing equation can be written as:

$$\frac{\partial}{\partial r}\left(k_r(r,z) \frac{\partial \psi}{\partial r} \right) + \frac{k_r(r,z)}{r} \frac{\partial \psi}{\partial r} + \frac{\partial}{\partial z}\left(k_z(r,z) \frac{\partial \psi}{\partial z} \right) = 0 \tag{63}$$

If $\Psi = P^2$, then equation (57), which accounts for compressibility, is solved. If $\Psi = P$, then equation (62) which assumes the fluid is incompressible is solved. In the compressible case, the boundary conditions must be written in terms of P^2; in the incompressible case, the boundaries are in terms of P.

For air flow, the appropriate equation is (57) which, includes compressibility. For ground water flow, the incompressible equation (62) is used. However, since soil venting is used to remediate the zone above the water table, people who work with ground water often are the ones who are called on to remediate the vadose zone. Since ground water flow models are familiar to these scientists and analytical solutions have been developed for incompressible fluids (e.g. water), it would be useful to know if ground water flow models can

be used for estimating air transport.

Boundary Conditions

A key ingredient in modeling is the determination of the boundary conditions. The top boundary (z=300 cm) was an engineered zero flow boundary out to 200 cm as mentioned above. Beyond 200 cm, the boundary is atmospheric pressure. (In the compressible flow model, an atmospheric pressure boundary is entered into the model as atmospheric pressure squared.) For the bottom boundary, the water table is often considered to be the lower no flow boundary. Though this may be a reasonable choice in most circumstances, the data taken in this study indicate otherwise. As seen in RESULTS, there was no response at any of the wells screened below the discharge well for the initial test of October 7, 1991 and most subsequent tests. This could mean that the permeability is very high or that there was no flow in the region. Being close to the water table (water table at z=0 cm), there is considerable moisture in the soil pores restricting flow. Since the source of air is the ground surface (beyond r=200 cm), air does not have to migrate through the lower layer. The air opts for higher permeability paths. Bear (1972, Table 9.4.1) indicates that fine sand has a capillary rise of 35 to 70 cm, silt 70 to 150 cm, and clay over 200 cm. The till at the site is a loam, approximately 50% sand, 35% silt, and 15% clay. It is considered to have low permeability due to the soil structure despite a relatively high sand content. The capillary rises from Bear support the argument that the soil pores may be saturated to some height above the water table. Since there was no response in the lower two tiers of nested wells, the zero flow boundary was chosen as z=100 cm, raised above these wells but below all other wells.

At r=5 cm (the radius of the discharge well) and over the length of the

discharge well's screen, the boundary condition is the flowrate divided among the nodes. Above and below the screen are zero flow boundaries. The outer radial boundary is quite some distance from the discharge well. The actual position and type of boundary are not known. However, the boundary is far enough away that it makes no difference in the calculated pressure distribution whether it is a zero flow or an atmospheric pressure boundary. Sensitivity runs were made to verify this, and the boundary was placed at r=495 cm. The boundary conditions are shown in Fig. 11 and are summarized as follows for a grid defined between r=5 and 495 cm and z between 100 and 300 cm:

At z=100 cm and all r,

$$\frac{\partial \psi}{\partial z} = 0 \tag{64}$$

At z=300 cm and $5 \leq r \leq 200$ cm,

$$\frac{\partial \psi}{\partial z} = 0 \tag{65}$$

At z=300 cm and r>200 cm,

$$\psi = \psi_{atm} \tag{66}$$

At r=5 cm and $110 < z < 190$ cm,

$$\frac{\partial \psi}{\partial r} = Q' \tag{67}$$

where Q' = apparent flowrate.

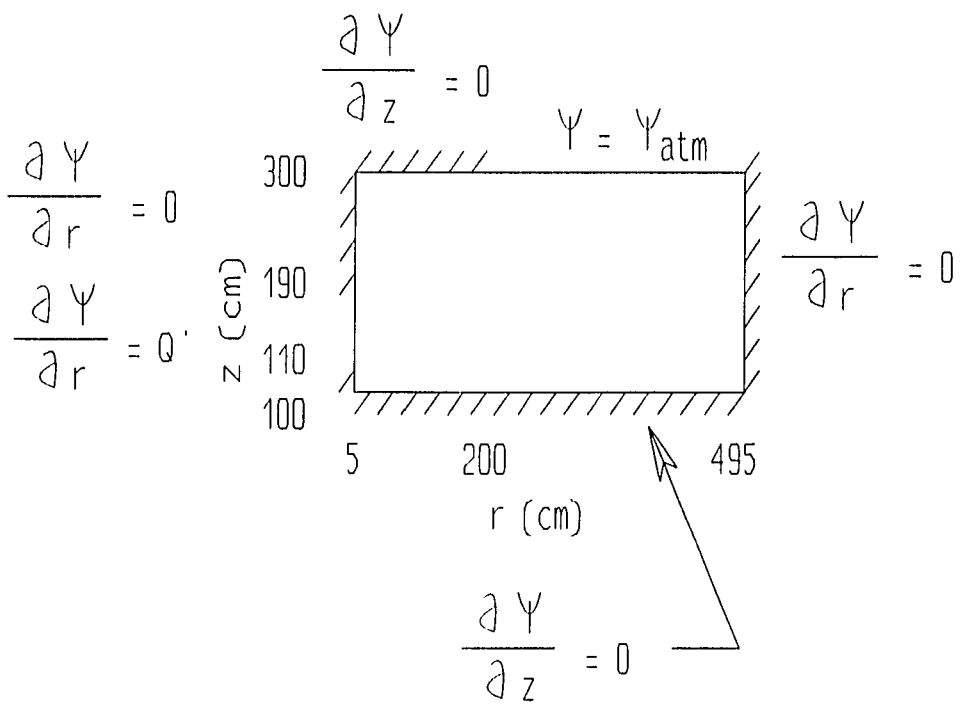

Figure 11. Boundary conditions

At r=5 cm and all other z,

$$\frac{\partial \Psi}{\partial r} = 0 \tag{68}$$

At r=495 cm,

$$\frac{\partial \Psi}{\partial r} = 0 \tag{69}$$

where $\Psi = P^2$ or $\Psi = P$ for the compressible and incompressible models, respectively. In determining the flowrate boundary at r=5 cm, the flowrate recorded by the rotameter was corrected for the temperature and pressure of the air flowing through the rotameter; this value is Q and is shown in Table 2 (see RESULTS) in units of cm^3/sec. When $\Psi = P^2$,

$$Q' = \frac{\mu P_w Q}{\pi k_r r_w L} \tag{70}$$

where

P_w = absolute pressure in extraction well W1, $g/cm\text{-}s^2$

r_w = radius of W1, cm

L = screen length of W1, cm

The flowrate was divided equally among the nodes representing the extraction well. Sensitivity runs revealed that non-uniform flow distributions made little difference in the best fit permeabilities.

Solution

The governing equation (63) was solved numerically for Ψ. A finite element computer program was written. The algorithm follows the Galerkin method and uses linear triangular basis functions. A grid generating (front end)

program was also written. Several grids were set up to see how they affected the results. The optimal grid is shown in Fig. 12. This grid has a geometric spacing of nodes in the radial direction and equal spacings in the vertical direction.

In the finite element program, a region number is assigned to each element. Each region is considered to be homogeneous but anisotropic. Details of the finite element programming are not discussed in this dissertation. However, Wang and Anderson (1982) and Bickford (1990) provide good discussions of the technique.

Optimization

The finite element program is used as a subroutine in a larger program which utilizes a least squares routine to determine the permeabilities which best fit the model to the data. The least squares routine is called DBCLSF and was published by the International Mathematical and Statistical Libraries (IMSL, Houston, Texas). It is based on the Levenberg-Marquardt algorithm (Marquardt, 1963). The objective function shown below minimizes the squared difference between the measured pressure at each well and the pressure calculated with the finite element program at each well. The values of k_r and k_z are varied until the minimum difference (Z) is found. The objective function is:

$$\min Z(k_{r1},k_{r2},..,k_{z1},k_{z2},..) = \tag{71}$$

$$\frac{1}{2}\sum_{i=1}^{n}[\psi_d(well\ i) - \psi_m(well\ i,k_{r1},k_{r2},..,k_{z1},k_{z2},..)]^2 \tag{72}$$

where

Z = the objective

n = number of data points (wells)

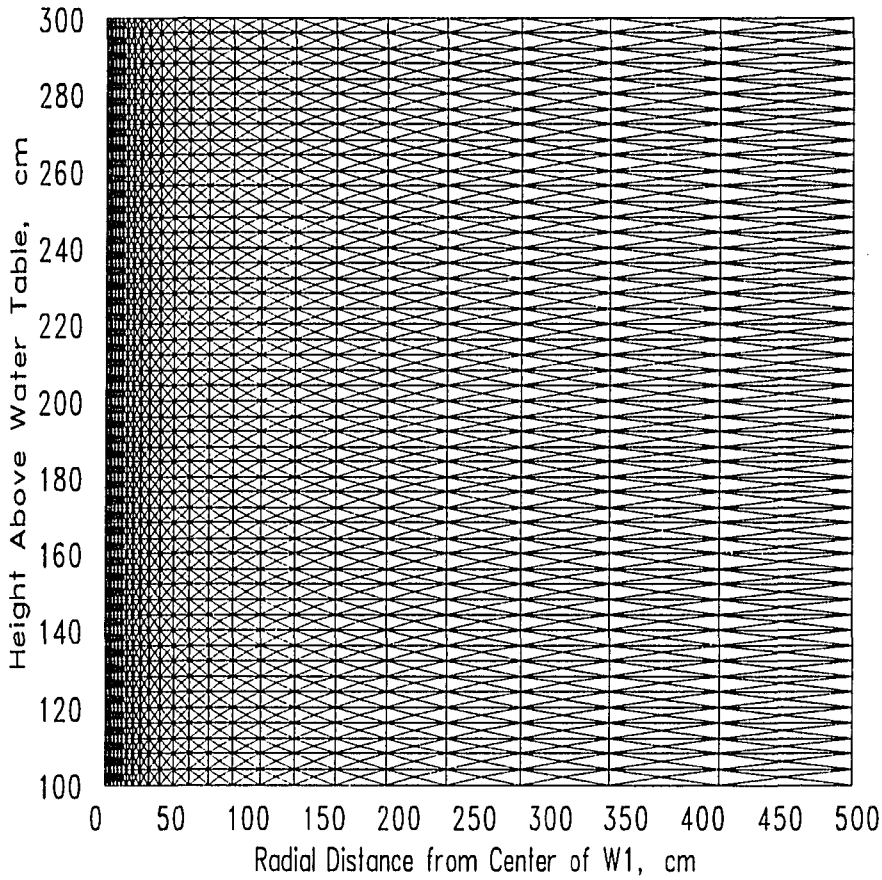

Figure 12. Finite element grid

Ψ_d = recorded data, either P or P^2, depending on whether (57) or (62) is being solved. P is absolute pressure, g/cm-s^2. P^2 is in g^2/cm^2-s^4.

Ψ_m = Ψ calculated by finite element model, same description as Ψ_d

k_{rj} = permeability of region j in radial direction, cm^2

k_{zj} = permeability of region j in vertical direction, cm^2

The data consists of pressures at wells. A well occupies a particular volume in the subsurface. In the modeling, this volume is represented by more than one node. To obtain a calculated pressure for comparison to the measured pressure in a well, the calculated pressures must be averaged over several nodes. An example of this averaging is shown in Fig. 13.

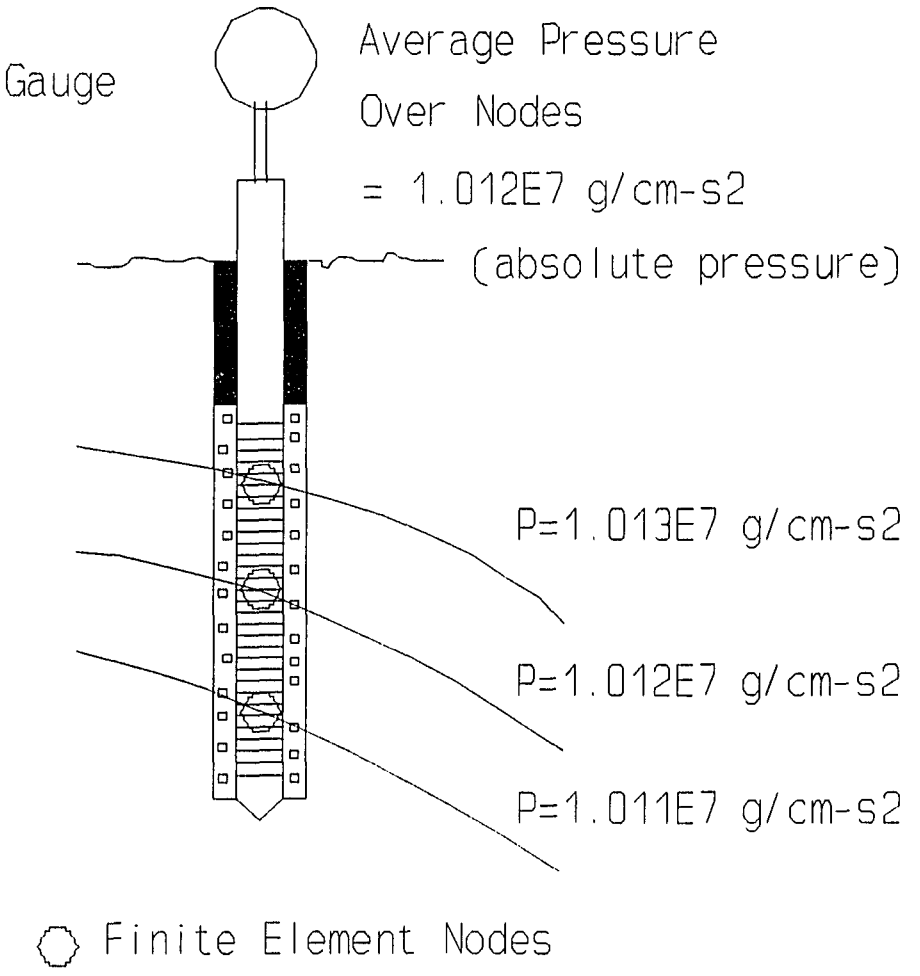

Figure 13. **Pressure averaging over several nodes**

RESULTS

Having described the field experiment and the models, this chapter will present the field data and the results of fitting the models to the data.

Field Data

After collecting the field data, the data were converted to consistent units for modeling. This section will show how the pressure and flowrate measurements were converted to appropriate units. This section will also show which data was selected for modeling. All of the data are shown in Appendix C, but the data selected for modeling are shown in Table 2.

Parameter conversions

Pressure unit conversion

Gage pressure was measured at wells at various horizontal distances from the pumping well as shown in Figs. 7 and 8. The pressure probes were U-Tube water-filled manometers or Magnehelic manometers. A Magnehelic manometer operates similar to a balance scale. Both types of gages indicated pressure (or vacuum) in inches of water. The U-tube manometers were calibrated in increments of 0.1 inch (0.25 cm) H_2O to a maximum of 8" H_2O. The Magnehelic manometers were calibrated in increments of 0.01 inch (0.025) cm H_2O to a maximum of 0.5 inch (1.3 cm) H_2O.

Since consistent units are required for the modeling described in the MODEL chapter, a demonstration of the required unit conversion will follow. The measured gage pressures for each test are shown in Table 2 and are in cm H_2O gage; these are converted to g/cm-s^2 absolute for the modeling. The conversion is:

Table 2. Data and best fit air permeabilities (k in cm^2x10^{-8}, +Q is extraction)

	Date	10/7/91	10/7/91	10/7/91	10/7/91
D	Barometer (inch Hg)	29.0	29.0	29.0	29.0
	Q (cm^3/sec)	-470	-710	-950	-1200
	W1 (cm H_2O)	28.2	35.1	42.2	56.1
	W2 (cm H_2O)	1.0	1.5	2.0	2.5
	W3 (cm H_2O)	0.8	1.0	1.3	1.5
A	W4A (cm H_2O)	0.0	0.0	0.0	0.0
	W4B (cm H_2O)	0.0	0.0	0.0	0.0
	W4C (cm H_2O)	0.1	0.3	0.4	0.5
	W4D (cm H_2O)	0.0	0.0	0.0	0.0
	W4E (cm H_2O)	0.0	0.0	0.0	0.0
T	W5A (cm H_2O)	0.0	0.0	0.0	0.0
	W5B (cm H_2O)	0.0	0.0	0.0	0.0
	W5C (cm H_2O)	0.2	0.3	0.4	0.5
	W5D (cm H_2O)	0.0	0.0	0.0	0.0
	W5E (cm H_2O)	0.0	0.0	0.0	0.0
A	W6 (cm H_2O)	0.3	0.3	0.3	0.5
	W7 (cm H_2O)	0.1	0.3	0.3	0.3
	Water Table (cm BGS)	300	300	300	300
	Days after heavy rain	3	3	3	3
2-D	k (Layer 4, 0-50cm BGS)	98.0	150.0	780.0	1800.0
M	k (Layer 3, 50-100cm BGS)	5.5	4.8	25.0	24.0
O	k (Layer 2, 100-150cm BGS)	770.0	1400.0	220.0	210.0
D	k (Layer 1, 150-200cm BGS)	2.7	2.7	3.4	3.5
E	Mean of Layers 1&2	45.6	61.5	27.3	27.1
L	Mean of Layers 1,2,3	22.5	26.3	26.5	26.0
1-D	k (100-200cm BGS)	2.0	2.4	2.7	2.5
Model	k (50-200cm BGS)	20.7	15.5	13.8	13.0

Table 2. (continued)

	Date	10/7/91	10/7/91	10/7/91	10/7/91	10/7/91
D	Barometer (inch Hg)	29.0	29.0	29.0	29.0	29.0
	Q (cm^3/sec)	2000	2800	3000	3300	3600
	W1 (cm H_2O)	-48.4	-58.7	-76.0	-96.7	-103.6
	W2 (cm H_2O)	-4.3	-4.6	-4.8	-6.1	-6.1
	W3 (cm H_2O)	-2.2	-2.3	-2.8	-2.8	-3.3
A	W4A (cm H_2O)	0.0	0.0	0.0	0.0	0.0
	W4B (cm H_2O)	0.0	0.0	0.0	0.0	0.0
	W4C (cm H_2O)	-0.6	-0.6	-0.8	-0.8	-0.8
	W4D (cm H_2O)	0.0	0.0	0.0	0.0	0.0
	W4E (cm H_2O)	0.0	0.0	0.0	0.0	0.0
T	W5A (cm H_2O)	0.0	0.0	0.0	0.0	0.0
	W5B (cm H_2O)	0.0	0.0	0.0	0.0	0.0
	W5C (cm H_2O)	-0.6	-0.8	-0.8	-0.8	-1.0
	W5D (cm H_2O)	0.0	0.0	0.0	0.0	0.0
	W5E (cm H_2O)	0.0	0.0	0.0	0.0	0.0
A	W6 (cm H_2O)	-0.7	-0.6	-0.5	-0.8	-0.9
	W7 (cm H_2O)	-0.3	-0.4	-0.4	-0.3	-0.3
	Water Table (cm BGS)	300	300	300	300	300
	Days after heavy rain	3	3	3	3	3
2-D	k (Layer 4, 0-50cm BGS)	1300.0	2300.0	930.0	1900.0	1000.0
M	k (Layer 3, 50-100cm BGS)	24.0	75.0	130.0	120.0	96.0
O	k (Layer 2, 100-150cm BGS)	370.0	270.0	180.0	260.0	220.0
D	k (Layer 1, 150-200cm BGS)	2.6	3.5	3.5	2.9	3.2
E	Mean of Layers 1&2	31.0	30.7	25.1	27.5	26.5
L	Mean of Layers 1,2,3	28.5	41.4	43.4	44.9	40.7
1-D	k (100-200cm BGS)	4.9	5.7	4.7	4.0	4.1
Model	k (50-200cm BGS)	10.3	13.6	16.4	11.1	14.3

Table 2. (continued)

	Date	10/17/91	10/17/91	6/17/92
D	Barometer (inch Hg)	29.4	29.4	29.4
	Q (cm^3/sec)	-685	-1190	4320
	W1 (cm H_2O)	35.1	56.2	-114.0
	W2 (cm H_2O)	1.3	2.5	-5.6
	W3 (cm H_2O)	0.8	1.3	-2.8
A	W4A (cm H_2O)	0.0	0.0	0.0
	W4B (cm H_2O)	0.0	0.0	0.0
	W4C (cm H_2O)	0.3	0.7	-1.3
	W4D (cm H_2O)	0.0	0.0	0.0
	W4E (cm H_2O)	0.3	0.4	0.0
T	W5A (cm H_2O)	0.0	0.0	0.0
	W5B (cm H_2O)	0.0	0.0	0.0
	W5C (cm H_2O)	0.3	0.5	-1.0
	W5D (cm H_2O)	0.0	0.0	0.0
	W5E (cm H_2O)	0.0	0.0	0.0
A	W6 (cm H_2O)	0.0	0.3	-0.3
	W7 (cm H_2O)	0.3	0.4	-0.3
	Water Table (cm BGS)	300	300	234
	Days after heavy rain	13	13	1
2-D	k (Layer 4, 0-50cm BGS)	1200.0	1400.0	7600.0
M	k (Layer 3, 50-100cm BGS)	120.0	140.0	370.0
O	k (Layer 2, 100-150cm BGS)	93.0	78.0	110.0
D	k (Layer 1, 150-200cm BGS)	3.9	3.7	4.6
E	Mean of Layers 1&2	19.0	17.0	22.5
L	Mean of Layers 1,2,3	35.2	34.3	57.2
1-D	k (100-200cm BGS)	2.3	2.5	4.4
Model	k (50-200cm BGS)	15.2	11.0	17.2

Table 2. (continued)

	Date	6/30/92	6/30/92	6/30/92	7/4/92	7/30/92
D	Barometer (inch Hg)	29.2	29.2	29.2	29.4	29.7
	Q (cm^3/sec)	2450	3670	3320	3240	2720
	W1 (cm H_2O)	-62.2	-148.5	-127.8	-131.3	-148.5
	W2 (cm H_2O)	-3.0	-4.8	-4.6	-5.1	-5.6
	W3 (cm H_2O)	-1.8	-2.8	-2.5	-2.8	-3.8
A	W4A (cm H_2O)	0.0	0.0	0.0	0.0	0.0
	W4B (cm H_2O)	0.0	0.0	0.0	0.0	0.0
	W4C (cm H_2O)	-1.0	-1.5	-1.4	-1.7	-2.3
	W4D (cm H_2O)	-0.1	-0.3	-0.3	-0.5	0.0
	W4E (cm H_2O)	0.0	0.0	0.0	0.0	0.0
T	W5A (cm H_2O)	0.0	-0.3	-0.3	-0.1	-1.0
	W5B (cm H_2O)	0.0	-0.3	0.0	-0.1	0.0
	W5C (cm H_2O)	-0.9	<-1.3	-1.3	<-1.3	<-1.3
	W5D (cm H_2O)	0.0	0.0	-0.1	-0.1	0.0
	W5E (cm H_2O)	0.0	0.0	0.0	-0.1	0.0
A	W6 (cm H_2O)	0.0	-0.1	-0.3	-0.3	-0.5
	W7 (cm H_2O)	-0.3	-0.5	-0.3	-0.6	-1.0
	Water Table (cm BGS)	267	267	267	271	254
	Days after heavy rain	14	14	14	2	1
2-D	k (Layer 4, 0-50cm BGS)	1800.0	720.0	660.0	800.0	1300.0
M	k (Layer 3, 50-100cm BGS)	170.0	340.0	850.0	320.0	200.0
O	k (Layer 2, 100-150cm BGS)	160.0	64.0	60.0	47.0	160.0
D	k (Layer 1, 150-200cm BGS)	4.9	5.2	4.9	4.6	3.3
E	Mean of Layers 1&2	28.0	18.2	17.1	14.7	23.0
L	Mean of Layers 1,2,3	51.1	48.4	63.0	41.1	47.3
1-D	k (100-200cm BGS)	4.6	2.9	3.0	2.9	2.1
Model	k (50-200cm BGS)	22.7	20.4	17.6	15.7	16.8

Let:

m = gage pressure (cm H_2O)

P_{gage} = gage pressure (g/cm-s^2)

P = absolute pressure (g/cm-s^2)

First, convert m to g/cm-s^2 gage:

$$P_{gage} = (m[cm\ H_2O])(980.6\ g/cm\text{-}s^2\text{-}cm\ H_2O) \tag{73}$$

Then, convert atmospheric pressure (inch Hg) to g/cm-s^2:

$$P_{atm} = (P_{atm}[inch\ Hg])(33860\ g/cm\text{-}s^2\text{-}inch\ Hg) \tag{74}$$

Then, add P_{gage} to P_{atm} (be sure P_{gage} is negative if it is a vacuum) to get the absolute pressure:

$$P = P_{atm} + P_{gage} \tag{75}$$

Therefore, if m=-1.5 cm H_2O and P_{atm}=29.5 inch Hg, then P=997,399 g/cm-s^2.

Flowrate conversion

Because the flowrate was recorded using a rotameter, calibrated at 20C and 1 atm, the recorded flowrate had to be corrected for the actual temperature and pressure according to Omega (1991):

$$Q = Q_{STP}\sqrt{\frac{T_{STP}P}{P_{STP}T}} \tag{76}$$

where

Q = actual flowrate, cfm (or cm^3/s)

Q_{STP} = flowrate shown on rotameter, cfm

T_{STP} = 293 K

P_{STP} = 29.92 inch Hg = 1.013E6 g/cm-s^2

T = air temperature flowing through rotameter, K

P = absolute pressure of air flowing through rotameter, g/cm-s^2

To convert cfm to cm^3/s, the following conversion is made:

$$Q[cm^3/s] = (Q[cfm])(471.9\ cm^3/s\text{-}cfm) \tag{77}$$

For a recorded flowrate of 3.5 cfm at a temperature of 30C, gage pressure of -1.5 cm H_2O, and atmospheric pressure of 29.5 inch Hg, the flowrate is 1610 cm^3/s. The flowrate values in Table 2 have been corrected for temperature and pressure according to (76) and (77) while the flowrates in Appendix C have not been corrected for temperature and pressure. In the Appendix, air was injected into or extracted from well, W1, in all tests except for some tests on 8/14/92. The injection or extraction well is the well having the greatest response or the well having "NoGage." If the injection/extraction well was not W1, a pressure gage was not fitted to the injection/extraction well. In all of the experiments on 8/14/92, soil moisture was so high that air flow could not leave or enter the extraction/injection well. This caused zero response at all monitoring wells.

In Appendix C, the heading "Rain" refers to the amount of rainfall that fell between the previous date and the current date. "Barom" is the barometric pressure provided by a gage at the site. It has not been corrected for the altitude of the site (to correct, subtract 0.9 from the value in Appendix C). "Power" in the appendix refers to the power setting on the variac which controlled the voltage to the blower. 100% power is 120 Volts; 50% power is 60 Volts. This allowed use of variable air extraction and injection rates. "Q(p=0)" is the flowrate if no load was applied to the blower; zero gage pressure at the blower.

To obtain this number, the blower was briefly disconnected from the well and sucked air directly from the atmosphere. This was useful in checking for leaks. "Q" was described above. "Tamb" is the temperature of the ambient (atmospheric) air. "Tfm" is the temperature at the flowmeter and was used to correct the recorded flowrate. The pressure at the flowmeter was also used to correct the flowrate. Pressure at the flowmeter was also required for correction of the flowrate; however, this is the same pressure as in well W1 since the flowmeter was positioned in line with the well. "T(W1)" is the temperature in Celcius of the air in W1. "Tens" refers to tensiometers 1, 2, or 3 (see Fig. 7). The reading is in centibars of soil matric suction (not total potential). A measurement of 10 cb means that there is 10 cb of soil suction at the position of the tensiometer's porous cup. A negative value would indicate that the porous cup was beneath the water table. "W1" through "W7" are pressures recorded at the wells. Negative values indicate vacuum which was the case for extraction tests. "N/M" or "N/A" indicates that a reading was not made (not measured/not available). The last row, "WT" is the depth from the ground surface to the water table. All of the experimental data listed in Appendix C are for short term (several minutes) tests unless the same flowrate is listed for subsequent columns. In such a case, the flowrate was held constant until a differenct flowrate is listed; such would be considered a long term test. An example of a long term test is one that began on 6/30/92 at 18:35 and ended 7/4/92 at 18:45. Between all tests, long or short, the blower was turned off. Pressures were observed to return to zero prior to beginning another test. The reader might also like to know that some of the data provided in Tables 2 and 3 are not given in Appendix C, as this would be a duplication. Depth to the water table is not provided for all tests. If the water table depth is provided for only one test on a particular day, then it is the same for other tests on the same day.

The following discussion is for those interested in using the two-dimensional (radial and vertical) steady state program listed in Appendix B. As mentioned earlier, the program solves (63). Due to the way the program was written, constant flowrate boundaries are expressed as:

$$Q_p = 2\pi k_r r_w L \frac{\partial \psi}{\partial r} \tag{78}$$

where

Q_p = boundary condition entered into the program in data file, QIN (units are g^2-cm/s^4 if $\Psi = P^2$); the other terms have been defined previously. According to Baehr and Hult (1991), the boundary condition for compressible flow ($\Psi = P^2$) is:

$$Q^* = \pi k_r r_w L \frac{\partial \psi}{\partial r} \tag{79}$$

where

Q^* = apparent flowrate (g^2-cm/s^4)

Observation of (78) and (79) shows that:

$$Q_p = 2\,Q^* \tag{80}$$

and from Baehr and Hult (1991):

$$Q^* = \mu_a P_{well} Q \tag{81}$$

where

P_{well} = absolute pressure in extraction well (g/cm-s^2)

Combining (80) and (81) gives the value that is entered into the input file QIN:

$$Q_p = 2\mu_a P_{well} Q \tag{82}$$

where Q_p is in g^2-cm/s^4.

To run the program in Appendix B treating air as incompressible ($\Psi = P$), the boundary condition entered into file QIN would be:

$$Q_p = \mu_a Q \tag{83}$$

where Q_p is in g-cm^2/s^2

Data reduction

Once the data were put in the proper consistent units by the methods described above, it was necessary to decide which tests should be modeled. All of the data for all of the tests are shown in Appendix C. The flowrates in Appendix C have been adjusted for temperature and pressure according to (76) and (77).

Some of the data in Appendix C are somewhat odd for various reasons. Such anomalies are not included in Table 2 which is a summary of the tests that were modeled. Appendix C is provided for future investigators should they wish more information on this study. Referring again to Appendix C, the tests on 7/17/91 were not included in the modeling since the nested wells had not yet been installed or flowrate data was not available. The test on 9/3/91 was not analyzed because the flowrate was not recorded. For these early tests, flowrate was not recorded because a large enough flowmeter had not been obtained. For the data of 6/30/92, all but the flowrate data are valid. Leaks in the system caused the flowrate reading to be too high; the leaks did not affect the pressure measurements which may be useful for future researchers. All of the data for the four day test beginning 6/30/92 are valid but only the first and last measurements were modeled. The four day test shows that steady state was reached by the first reading (seconds after the blower was turned on). The subsequent variations in flowrate and pressure are responses to weather changes. The manometers did not

all return to zero pressure after the blower was shut off on 7/4/92. This "trapped pressure" phenomenon will be addressed in the DISCUSSION chapter. The short test on 7/4/92 did not include measurements of monitoring well pressures but indicated how nature is sometimes difficult to understand; that is, why did the flowrate drop? Since the vacuum in the extraction well increased from 52 cm H_2O to 58 cm H_2O, the affect of turning the blower off after the long term test may somehow have caused the soil to be more restrictive. The two tests on 7/16/92 are not included in Table 2 since pressure data were not collected for all wells; the tests were run to get an idea of flowrate and vacuum at the extraction well.

Considerable rain fell in July, 1992. On 7/30/92, the water table was low enough so that pressures were recordable at the monitoring wells. However, the very next day, the water table finally responded to all of the rain and jumped from 250 to 225 cm below ground surface (BGS). The sudden response caused trapped pressure in the soil making the pressure measurements on 7/31/92 erratic. Throughout August, 1992, the water table was high enough to cause the moisture in the soil to be great enough to restrict all flow from nearly every well tested. Zero flow tests could not be modeled.

In Table 2, pressures of $<$-1.3 cm H_2O were found using a Magnehelic gage that has a maximum (or minimum) of 1.3 cm H_2O (1 inch H_2O).

Air Permeability from 1-D Model

For each pneumatic test shown in Table 2, a computer run was made which "best fit" the model to the pressures (or vacuums) at the observation wells by choice of the air permeabilities. In addition to the radial and vertical (2-D) modeling described in the MODEL chapter, simpler one-dimensional flow modeling was also performed. The one-dimensional (1-D) modeling, though not

as accurate as the two-dimensional modeling, is simpler. Comparing the 1-D to the 2-D modeling provides insight into the usefulness of simpler models. The one-dimensional model was described in the LITERATURE REVIEW. Knowing the extraction or injection rate and the pressure at two wells screened over the same interval, air permeability can be calculated using equation (3) above. k was found by using data at wells W1 and an average of W6 and W7 since they are at nearly the same distance from W1 (see Fig. 8). W1, W6, and W7 all have 76 cm screens and are screened over the same depth. k was also found using wells W2 and W3 which both have 152 cm screens and are screened over the same depth. Air permeabilities from the one-dimensional modeling are given with the data in Table 2.

Air Permeability from 2-D Model

The following discussion describes the 2-D modeling used to obtain the permeabilities listed in Table 2. Since the boundary conditions tell the model to ignore the region below $z=100$ cm, wells W4D, W4E, W5D, and W5E were excluded from the optimization. Further, since the least squares optimization routine treats each data point as being just as significant as all other data points, two of the nested wells (W4A and W4B) have also been excluded. This ensured that undue emphasis was not placed on obtaining zero response in the upper regions.

The finite element numerical solution to (63) is flexible enough that each element can be assigned a permeability in the r and z directions. However, due to the finite number of data points, it is not possible to have the model fit the data to such specific levels. It was expected that permeability would decrease with depth. The model was also used to determine the degree of anisotropy and heterogeneity in the field.

Prior to arriving at the most meaningful boundaries used for the modeling in Table 2, many scenarios were run. These scenarios are shown in Appendix D, refer to Fig. 14, and investigated:

1. Position of distant boundary (i.e. r_{max}).
2. Type of distant boundary, BC@r_{max} (atmospheric pressure or zero flow).
3. Position of the bottom zero flow boundary.
4. Extent of upper surface ground cover (i.e. r_B).
4. Soil heterogeneity.
5. Soil anisotropy.
6. Air compressibility versus incompressibility.
7. Number of data points.
8. Grid size
9. Spacing of nodes in r-direction.
10. Initial estimate of parameters/ability to converge.

Again, the scenarios are summarized in Appendix D where the terms r_B, r_{max} are shown in Fig. 14. In the appendix, Q is flowrate; if Q is positive, air is being extracted from W1. "O" is order and refers to whether air is being treated as compressible or incompressible; if compressible, the order is P^2 and if incompressible, the order is P. $BC@r_{max}$ refers to the boundary condition at r_{max}. r_{max} is very far from the most distant observation well. To tell if this boundary is far enough away, the results should be the same if the boundary is atmospheric pressure (P_{atm}) or zero flow (ZF). "Bottom" is the distance from the ground surface (BGS=below ground surface) to the bottom zero flow boundary. The bottom boundary position is physically the top of the capillary fringe where all pores are filled with water. In gravel, this is essentially the distance to the water table. In loam, the capillary fringe is difficult to determine. The "#Pts" column refers to the number of data points (wells) used in the fitting.

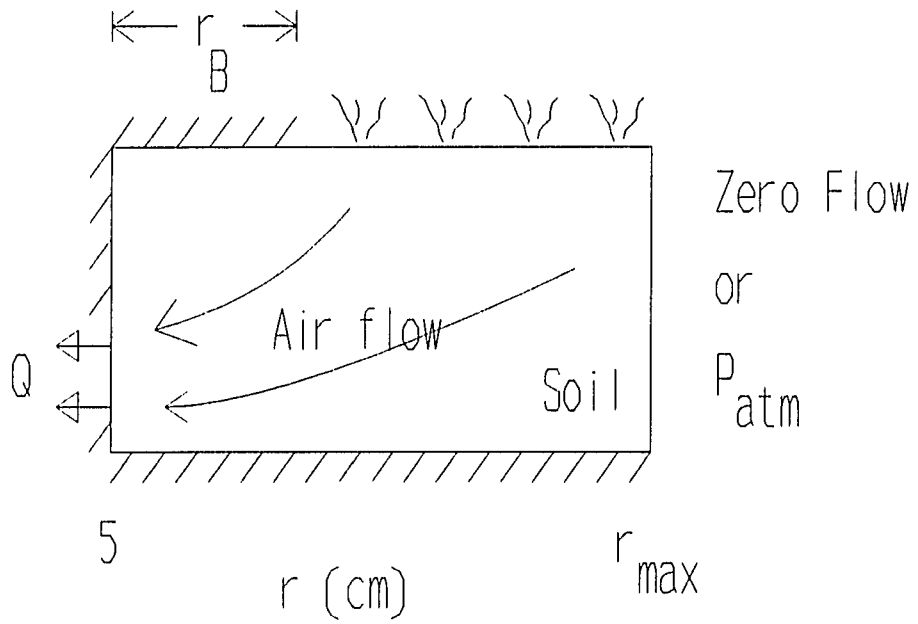

Figure 14. Boundary conditions used for modeling scenarios shown in Appendix D

The "Res" is residual and is the square root of the sum-squared difference between the data and model pressure at each well:

$$Res = \sqrt{(P_{gage,d}-P_{gage,m})_1^2 + (P_{gage,d}-P_{gage,m})_2^2 + (P_{gage,d}-P_{gage,m})_n^2} \quad (84)$$

where

$P_{gage,d}$ = gage pressure from data, cm H_2O

$P_{gage,m}$ = gage pressure calculated by model, cm H_2O

The air permeabilities in Appendix D indicate whether the soil was modeled as isotropic or anisotropic and heteogeneous or homogeneous. For example, k_r(100-200cmBGS) means that the soil in the region from 100 to 200 cm below ground surface was modeled as homogeneous but anisotropic. If there is no subscript on k, the soil is modeled as isotropic.

To summarize the scenarios, significant improvement in the residual, ability for the program to converge, and consistency of the best fit permeabilities occurred when three changes were made in the modeling. Most importantly, the nodes in the radial direction were changed from having an equal spacing to having a geometric spacing. For example if C=2 and node 1 is at r=5 cm, then node 2 is at r=5C=10cm, node 3 is at r=10C=20cm, etc. This node spacing allowed the nodes to be closer together at low radii where the pressure is changing most rapidly. The fits also significantly improved when the position of the bottom zero flow boundary was moved above the water table depth. This better represented the capillary fringe and also reflected what the data implied - the data showed no response in the wells below the extraction well. Most likely, k is low in those regions, so the flow opted for higher permeability paths. Thirdly, the soil was modeled as anisotropic and heterogeneous. In a homogeneous model, anisotropy improves the fit. However, when the soil is

modeled as having heterogeneous layers, the fit is vastly improved. When each layer is modeled as anisotropic, the fit does not improve by much, and k_r and k_z within a layer (for more than 2 layers) are not much different. Thus, the scenario that was physically reasonable and most consistent among different data sets was had zero flow at the distant boundary of r=500 cm, the bottom no flow boundary at 200 cm BGS (z=100 cm), and four isotropic soil layers each having a different k.

Fracturing in till may be a source of anisotropy over the thickness of the deposit whereas root channels, worm holes and the like may affect anisotropy in the upper horizon. Results of the modeling suggest that anisotropy is not as important as the variation of permeability with depth.

From the results shown in Table 2, the tests run after 10/7/91 produced k's that decreased with depth. The test on 10/7/91 had k for layer 2 greater than k for layer 3. This was not expected. However, an explanation for this "reversal" of k's is that the wetting front produced by the 1.3 inch (3.3 cm) rainfall 3 days prior to 10/7/91 had not gotten all the way to the water table and was actually occupying layer 3 and impeding air flow. There were other tests (e.g. 7/30/92), however, where there was 1.7 inch (4.3 cm) of rainfall one day before the test, but the reversal of k's was not evident.

The 1-D modeling can be compared with the 2-D modeling. Since the wells used in the 1-D modeling are screened over several layers of the 2-D 4-layer modeling, the 4-layer k's are geometrically averaged over the appropriate layers. The geometric means are shown in Table 2 and were calculated from:

$$\bar{k} = \exp\left(\frac{\ln(k_1)+\ln(k_2)+\ldots+\ln(k_n)}{n}\right) \tag{85}$$

where

n = number of air permeabilities to be averaged

$\overline{k}$ = geometric mean air permeability, cm^2

k_i = air permeability for layer i, cm^2

Domenico and Schwartz (1990) suggest that the geometric mean is the most suitable mean for permeability. Table 2 shows that k from W1 and W6/W7 is lower than k from W2 and W3 because the former are screened over deeper soil where k is lower.

To assess the 2-D model's ability to fit the data, Table 3 shows the recorded data and the model's pressure based on the best fit k's.

Table 3. Data and fitted pressures for four layer isotropic compressible fluid simulation. All units are cm H_2O except Q

Date Q(cm^3/s)	ID Res		W2	W3	W4C	W5C	W5B	W5A	W6	W7
10/7/91	CJ	Data	1.0	0.8	0.1	0.2	0.0	0.0	0.3	0.1
-470	0.4	Fit	1.1	0.4	0.2	0.2	0.1	0.0	0.2	0.2
10/7/91	CL	Data	1.5	1.0	0.3	0.3	0.0	0.0	0.3	0.3
-710	0.4	Fit	1.6	0.6	0.3	0.3	0.2	0.0	0.3	0.3
10/7/91	CM	Data	2.0	1.3	0.4	0.4	0.0	0.0	0.3	0.3
-950	0.5	Fit	2.2	0.8	0.4	0.4	0.2	0.0	0.3	0.2
10/7/91	CN	Data	2.5	1.5	0.5	0.5	0.0	0.0	0.5	0.3
-1200	0.6	Fit	2.7	1.0	0.6	0.6	0.3	0.0	0.4	0.3
10/7/91	BQ	Data	-4.3	-2.2	-0.6	-0.6	0.0	0.0	-0.7	-0.3
2000	0.7	Fit	-4.5	-1.6	-0.7	-0.7	-0.3	0.0	-0.5	-0.4
10/7/91	BT	Data	-4.6	-2.3	-0.6	-0.8	0.0	0.0	-0.6	-0.4
2800	0.7	Fit	-4.7	-1.7	-0.8	-0.8	-0.3	0.0	-0.5	-0.4
10/7/91	BR	Data	-4.8	-2.8	-0.8	-0.8	0.0	0.0	-0.5	-0.4
3000	1.1	Fit	-5.1	-1.8	-0.9	-0.9	-0.3	-0.1	-0.5	-0.4
10/7/91	BS	Data	-6.1	-2.8	-0.8	-0.8	0.0	0.0	-0.8	-0.3
3300	0.8	Fit	-6.3	-2.1	-0.9	-0.9	-0.3	0.0	-0.5	-0.4
10/7/91	BP	Data	-6.1	-3.3	-0.8	-1.0	0.0	0.0	-0.9	-0.3
3600	1.2	Fit	-6.4	-2.3	-1.1	-1.0	-0.4	-0.1	-0.6	-0.5
10/17/91	CE	Data	1.3	0.8	0.3	0.3	0.0	0.0	0.3	0.0
-690	0.4	Fit	1.4	0.5	0.4	0.3	0.1	0.0	0.1	0.1

Table 3. (continued)

Date	ID		W2	W3	W4C	W5C	W5B	W5A	W6	W7
$Q(cm^3/s)$	Res									
10/17/91	CF	Data	2.5	1.3	0.7	0.5	0.0	0.0	0.4	0.3
-1200	0.4	Fit	2.6	1.0	0.7	0.6	0.2	0.0	0.3	0.2
6/17/92	CB	Data	-5.6	-2.8	-1.3	-1.0	0.0	0.0	-0.3	-0.3
4300	0.9	Fit	-5.8	-2.1	-1.3	-1.2	-0.2	0.0	-0.5	-0.4
6/30/92	CC	Data	-3.0	-1.8	-1.0	-0.9	0.0	0.0	-0.3	-0.3
2500	0.8	Fit	-3.3	-1.2	-0.7	-0.7	-0.2	0.0	-0.3	-0.3
6/30/92	CH	Data	-4.6	-2.5	-1.4	-1.3	0.0	-0.2	-0.3	-0.3
3300	0.7	Fit	-4.8	-1.9	-1.5	-1.4	-0.2	-0.1	-0.5	-0.4
6/30/92	CG	Data	-4.8	-2.8	-1.5	-1.5	-0.2	-0.2	-0.5	-0.1
3700	0.9	Fit	-5.0	-2.0	-1.6	-1.5	-0.3	-0.1	-0.6	-0.5
7/4/92	CI	Data	-5.1	-2.8	-1.7	-1.7	-0.1	-0.1	-0.6	-0.3
3200	0.8	Fit	-5.3	-2.1	-1.9	-1.7	-0.3	-0.1	-0.6	-0.5
7/30/92	CD	Data	-5.6	-3.8	-2.3	-2.3	0.0	-0.5	-1.0	-0.5
2700	3.3	Fit	-4.6	-1.6	-0.8	-0.8	-0.2	-0.1	-0.4	-0.3

DISCUSSION

While the purpose of the RESULTS chapter was to simply present results, the present chapter aims to explain the results. The chapter will begin by comparing the results of the radial one-dimensional (1-D) model and radial and vertical two-dimensional (2-D) air flow model to assess whether the simpler 1-D model is adequate. It will then be shown that there are no correlations between the air permeabilities (k) found at the site and the physical characteristics of the field site. This was a disappointment. Originally, it was hoped that relations between air permeabilities and soil moisture, water table depth, or time after rainfall would be found.

Finding no correlations with physical characteristics allows a presentation of nominal k's for each soil layer. These design parameters can be used for larger extraction systems regardless of soil moisture or other physical parameters so long as the water table is at least 225 cm below ground surface (BGS). These nominal values were found when the water table was between 225 and 300 cm BGS. Thus, the nominal k's have questionable validity when the water table is greater than 300 cm BGS.

1-D Versus 2-D Modeling

The RESULTS chapter showed air permeabilities calculated using a one-dimensional analytical solution and a two-dimensional numerical solution fit to data. The one-dimensional model was only used for wells screened over the same depths. Flow was assumed to be radial. Since all of the wells are in the region covered by the impermeable surface, the flow between wells is more radial than it is at greater distances. The two-dimensional model incorporated flow at greater distances where there may be significant vertical flow. The main question to be answered in this section is: Is one-dimensional modeling adequate for

determining air permeabilites?

Table 2 shows that the 1-D modeling underpredicts the air permeabilities relative to the 2-D modeling. For the wells screened over layers one and two, k from the one-dimensional modeling is lower than k from the 2-D modeling by about 90% (an order of magnitude) for both the Oct. 7, 1991-only modeling and the "all but 10/7/91" modeling. The reason for distinguishing between the 10/7/91 tests and the others is that the 10/7/91 tests consistently gave a higher k for layer 2 than for layer 3. Recall from the RESULTS chapter that layer 1 occupies soil from z=100 to 150 cm, layer 2: 150 to 200 cm, layer 3: 200 to 250 cm, and layer 4: 250 cm to 300 cm (the ground surface).

For the wells screened over layers 1, 2, and 3, the percent difference (between the 1-D and 2-D k's) is not as great as that for the wells screened over layers 1 and 2 - about 50% rather than 90%. Accounting for errors in determining the one-dimensional air permeabilities for layers one and two are not great enough to raise the k's to the values found with the two-dimensional model. For instance, for a flowrate measurement of 8 cfm, the flow could actually lie between 7.7 and 8.3 cfm ($\pm$4%), a difference having little affect on k. The pressure difference between wells W1 and W6 or W7 is great enough that even a large error in W6 or W7 and a 20% error in the pressure at W1 would have little affect on k. However, the errors in the pressures used for calculating k based on W2 and W3 could be significant and could account for the difference in k for layers 1, 2, and 3, primarily for low flowrate tests since the measurement error is constant and not a percent. If each pressure was off by .05 inch H_2O (0.1 cm H_2O), the low flowrate test on 10/17/91 could have k varying from 1.1E-7 to 7.5E-7 cm^2. The reported value was 1.5E-7 cm^2. The effects on k of errors in the radial distances to the wells, the viscosity of air, and the screen length are insignificant.

To conclude this section, air permeabilities from one-dimensional modeling of the field data are not similar enough to the values determined with two-dimensional modeling to be useful in design. The comparison improves at shallower depths, however.

2-D Modeling

As it was determined to be the most accurate without having an excessive number of nodes, all of this discussion refers to modeling using the geometric spacing of nodes in the radial direction. It was of primary interest to be certain that air permeability does not vary with air flowrate. If k does vary with flowrate, then the air permeabilities obtained in this study with the method described herein would not be useful in designing large soil vapor extraction systems using higher flowrates.

Air permeabilities for several extraction tests are plotted in Fig. 15. The k's appear to vary randomly with flowrate and show a generally upward trent toward ground surface. Since there is not a trend with flowrate, the air permeabilities can probably be used for designing higher rate extraction systems.

Isobars are shown in Fig. 16 for a flowrate of 3600 cm^3/sec (7.6 cfm) and the four layer isotropic model. The figure demonstrates the variation of vacuum in r and z. Contours for vacuums greater than 0.2 cm H_2O are not shown since the contours get too close together to be distinguishable. The permeability of each layer is given in Table 2.

Anisotropy and compressibility

Other modeling scenarios, such as anisotropy and incompressibility, were considered. When the flow field was modeled as homogeneous but anisotropic, k_r=3.9x10^{-7} cm^2 and k_z=1.4x10^{-6} cm^2 (run BY). The ratio k_z/k_r=4 is not as

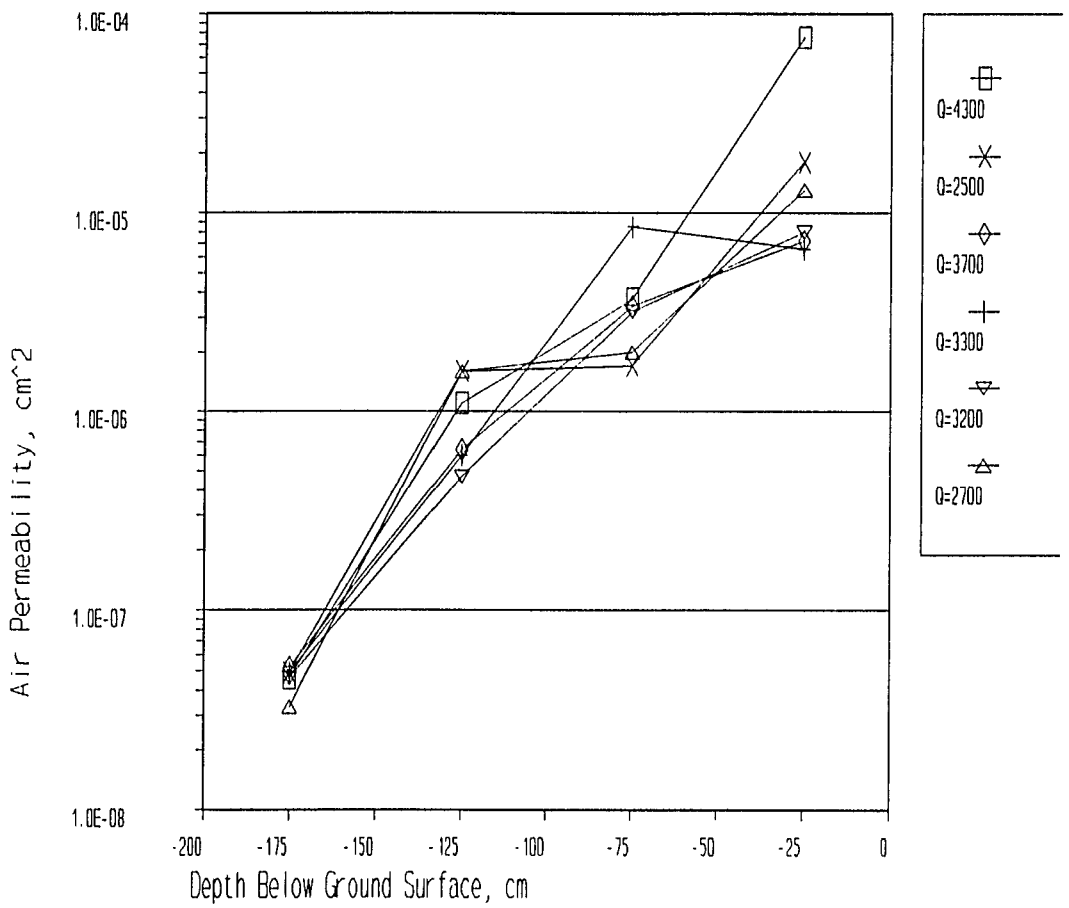

Figure 15. Effect of depth and extraction rate on k. Q in cm^3/s

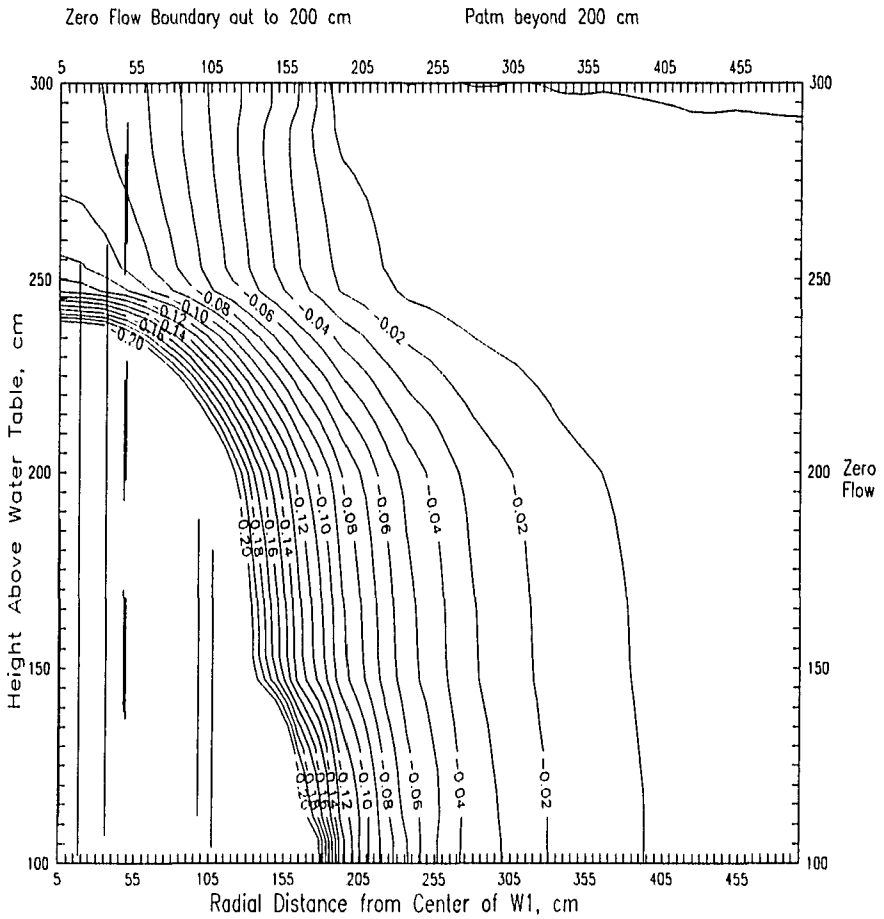

Figure 16. Vacuum contours from 0 to -0.2 cm of water by 0.01 increments for Q=3600 cm^3/s test on 10/7/91. Four layer compressible fluid model

great as the ratio of k between layers (from run BP) which is up to:

$$\frac{k(top\ layer)}{k(bottom\ layer)} = \frac{1x10^{-5}cm^2}{3x10^{-8}cm^2} = 330 \qquad (86)$$

This indicates that inhomogeneity is probably more important than anisotropy.

The importance of compressibility was also investigated. For an incompressible fluid, the governing equation is (62). The equation is solved using the same numerical solution as in the compressible fluid case. However, the boundary conditions are now stated in terms of P rather than P^2. While there has been much emphasis in the literature on the importance of compressibility of air in soil vapor extraction (Pedersen and Curtis, 1991; Shan et al., 1992; Baehr and Hult, 1991), it may not be that significant in practice. Running the finite element solution in compressible mode with four isotropic layers and at a flowrate of 3600 cm^3/sec gives air permeabilities that are nearly identical to those found in the compressible fluid case; the values are shown in Appendix D, run BX for the incompressible case and can be compared to run BP, the compressible case. The same is true when other flowrates are analyzed.

Correlations of k with Physical Characteristics

Throughout this research, there was a goal of trying to correlate air permeability with physical characteristics of nature. Possible physical characteristics of interest include soil moisture tension, water table depth, and rainfall.

Although it was hoped to find some correlations of k with soil moisture tension, water table depth, or rainfall, none were found. For the nine tests on 10/7/91, the k's varied as much as they varied on a variety of other days where the soil moisture conditions were different.

Despite the lack of definitive correlations, it should be noted that at water tables above 230 cm below the ground surface (BGS) no air could be injected into or withdrawn from any of the wells including the shallow ones, W4A and W5A (see data in Appendix C for 8/14/92). The water table from May to August, 1991, is shown in Fig. 17.

Despite the lack of trends of k with soil moisture, water table depth, or rainfall, some important conclusions can be drawn. For water tables above 230 cm BGS, soil venting is impossible presumably because of high moisture levels in the soil. For water tables below 230 cm BGS, a nominal k for each soil layer can be used for design. Breaking the subsurface into four isotropic layers of equal thickness provides a good representation of the strata. The k's are unaffected by rainfall or other weather conditions. The present study had no data for water tables greater than 300 cm BGS.

Nominal Air Permeabilities for Design in Loam Till

For design of large soil vapor extraction systems in loam till, the present research may be useful in providing air permeabilities. As mentioned in the previous section, so long as the water table is deeper than 230 cm BGS, one set of air permeabilities can be used for design without one worrying about how these values change with rainfall and soil moisture.

The nominal design values are given in Table 4. They are the geometric means of the k's determined from the present research. The means do not include the k's determined from the tests on 10/7/91 which provided k of layer 3 greater than k of layer 2. That day has been considered an anomaly and was thus omitted for determination of the nominal air permeabilities.

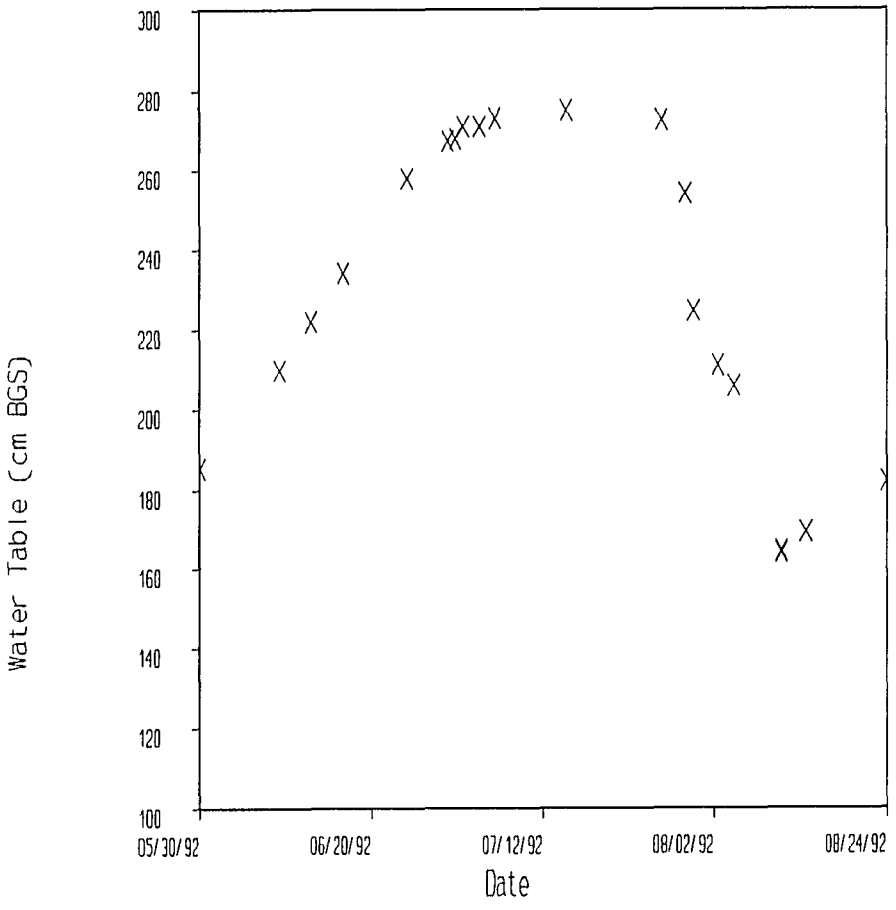

Figure 17. Depth to water table

Table 4. Nominal air permeabilities

Layer	Depth (cm BGS)	k (cm^2)
4	0-50	$1x10^{-5}$
3	50-100	$3x10^{-6}$
2	100-150	$9x10^{-7}$
1	150-200	$4x10^{-8}$

Long Term Tests

Until now, the discussion has focused entirely on short term tests, all of which reached steady state in seconds. But, what is steady state? Steady state is the state of no change. In outdoor systems, the weather is always changing. If nothing else, the barometric pressure is changing throughout a daily cycle as shown in the data in Fig. 18. This barometric pressure data was obtained using an absolute pressure transducer which recorded data every 30 minutes. The pressures have been corrected for the elevation of the site.

Changes in barometric pressure affect pressures in monitoring wells. Though the pressure gages on the monitoring wells provide gage pressure (pressure relative to atmospheric pressure), the pressure in a well does not change instantaneously with changes in atmospheric pressure. The data in Appendix C describes a long term test beginning on 6/30/92 at 18:35. When the blower was turned off on 7/4/92 at 18:57, not all of the manometers returned to zero vacuum (even after 30 minutes). When the well caps were removed, trapped pressure was released causing the manometers to return to zero. The trapped pressure could be due to infiltration or exfiltration which continued to cause a vacumm in the well even after the blower was turned off. This is a phenomena that makes modeling difficult. Assuming infiltration is the cause of the "trapped pressure,"

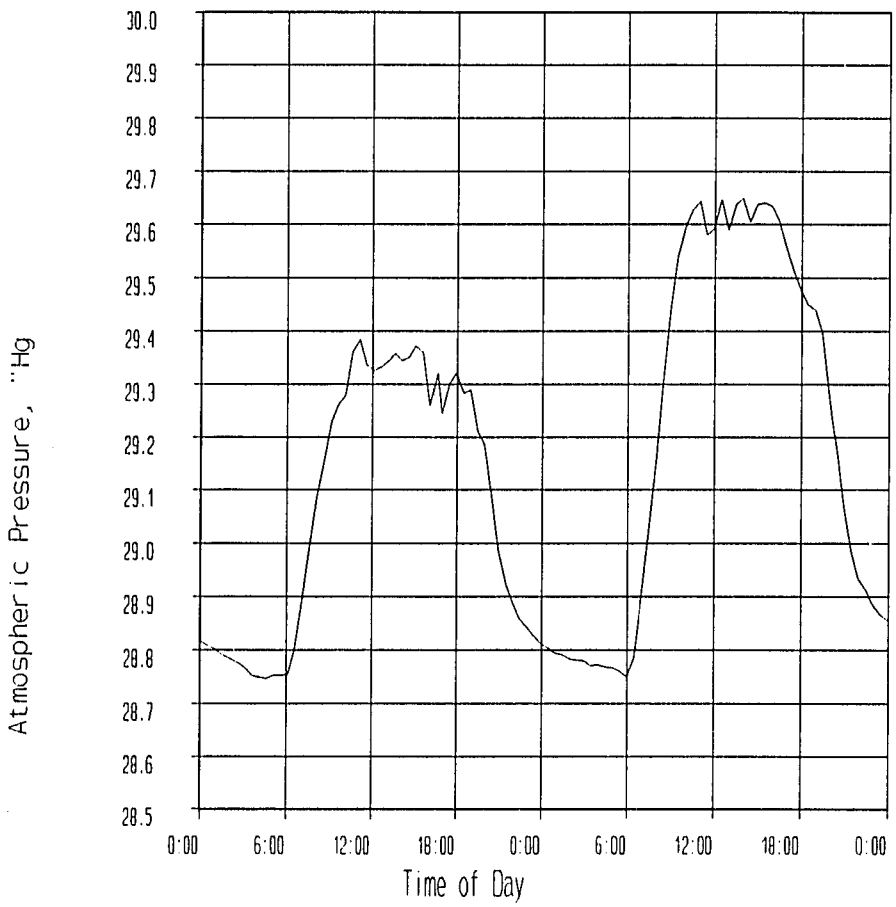

Figure 18. Atmospheric pressure on 7/17/92 through 7/19/92 (corrected for site elevation)

it could be accounted for in a more complex subsurface air flow model.

If the pressure in wells varied instantaneously with changes in atmospheric pressure, then the manometer readings would remain constant for steady air flow. This obviously not true since the manometer readings change with time. See, for example, the test described in the previous paragraph. To further complicate matters, a water manometer responds differently than a Magnehelic manometer to changes in atmospheric pressure. A Magnehelic manometer is similar to a balance scale.

A computer-monitored automatic data collection system was installed at the site in July, 1992. Some of the data for an extraction test beginning 7/30/92 and ending 8/3/92 are shown in Appendix C. The extraction rate was 4.4 cfm (2100 cm^3/s). Absolute pressure transducers were installed in the extraction well, W1, and monitoring well W3. A third transducer recorded barometric pressure. Tensiometers, T2 and T3, were also equipped with absolute pressure transducers. Data from the test is shown in Figs. 19 and 20. The figures show data only for the first day of the test. The computer was very sensitive to power surges, so data after 7/30/92 are not presented. The data presented show how the well pressures vary with barometric pressure. W1's initial drop and rapid rise to its intitial pressure was due to a short test just prior to the long term test. The long term test began at 15:00. Fig. 19 shows the data in terms of absolute pressure. In general, as barometric pressure decreases so does the pressure in the wells. This was found to be true for other data also. Fig. 20 shows the data in terms of gage pressure. The barometric gage pressure is constant since gage pressure is defined as absolute pressure minus barometric pressure. In Fig. 20, the well pressures are more constant than in Fig. 19 since barometric variations are removed.

There was 13 cm (5.2 inches) of rainfall spread throughout the week prior

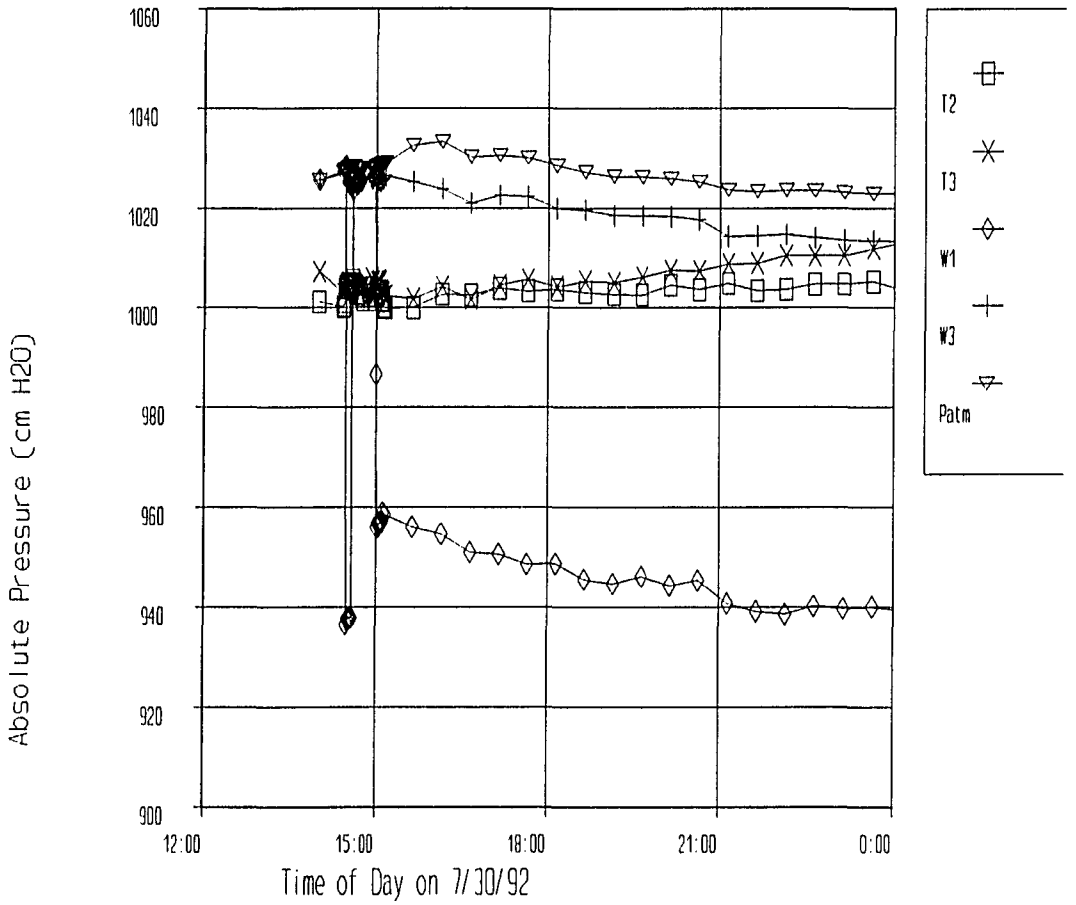

Figure 19. Absolute pressure variations with time. Initial extraction rate was 2100 cm^3/s

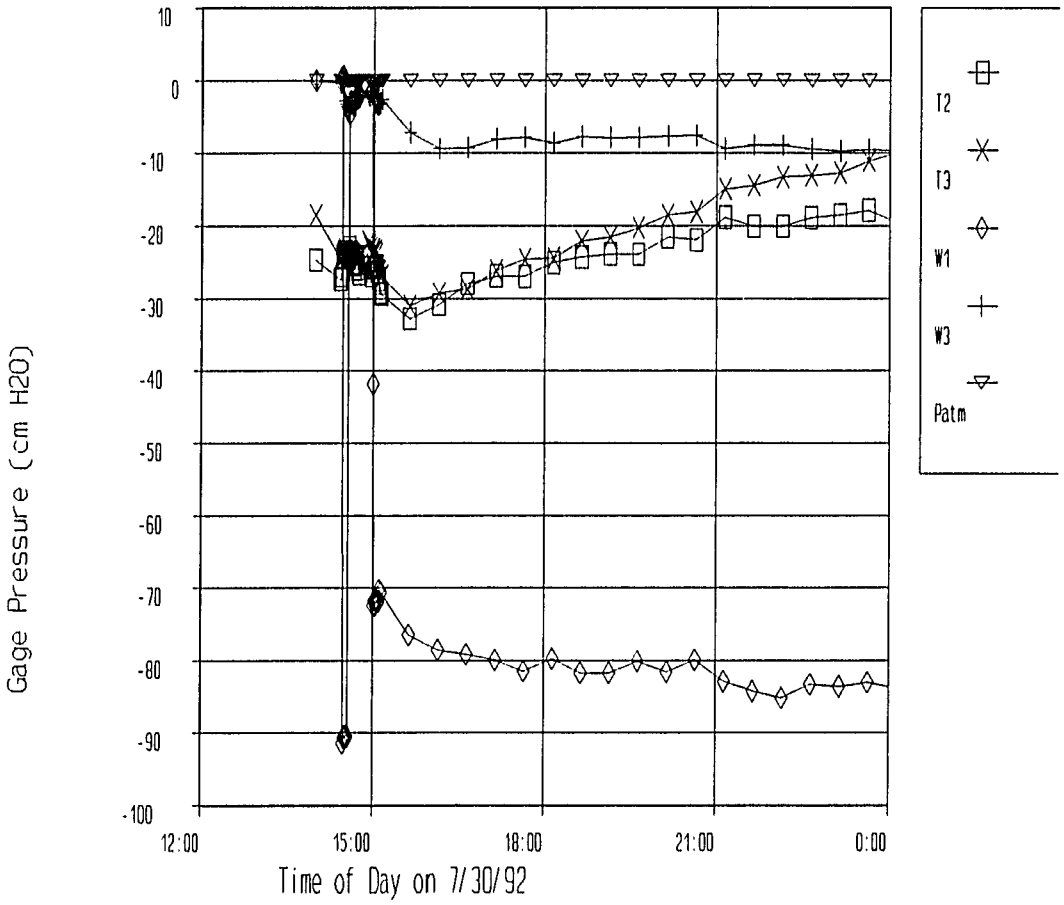

Figure 20. Gage pressure variations with time. Initial extraction rate was 2100 cm^3/s

to the test. The tensiometers in Figs. 19 and 20 indicate that soil matric pressure is increasing. Since the matric gage pressures in Fig. 20 are increasing, the soil is getting wetter with time. The infiltration front due to the rainfall is moving downward through the soil. The well responses in Fig. 20 slightly increase with time. The increased moisture in the soil causes larger vacuums near the extraction well. The extraction rate decreased with time (see Appendix C) since the blower had to operate against a larger pressure head in the extraction well. Other absolute pressure tensiometer transducer data during periods of little rainfall (not presented) showed a correlation between barometric pressure and tensiometer absolute pressure.

Currently there is no accepted way of handling atmospheric pressure changes in soil vapor extraction systems. Even though there is a correlation between well or tensiometer response and barometric pressure, the relationship varies with soil depth. A recent article by Massman and Farrier (1992) showed how changes in atmospheric pressure translate into the movement of surface air downward through soil. Based on advection and diffusion modeling of air transport in soil, they showed that the speed at which surface air moves into the soil is proportional to the thickness of the vadose zone. Since the vadose zone at the Iowa State University site is only 3 m thick (Massman and Farrier gave examples for vadose zones of 20 m and 100 m thick), one would expect pressure responses in the soil to vary slowly with changes in atmospheric pressure. Thus, since the atmospheric pressure is varying constantly in its diurnal cycle, correlating pressure changes in the soil with changes in atmospheric pressure is at best very difficult. The field data support this argument.

Air Permeability from Other Methods

As a comparison to the in-situ multiple well method, core samples from a

site two miles away and having similar soil characteristics were analyzed in a laboratory. The samples were taken from 15 and 30 cm depths and analyzed at soil tensions similar to those in the field tests found from tensiometers (i.e. 100 cm H_2O and 50 cm H_2O). The samples were obtained with Shelby tubes and tested using a gasometer such as that described by Evans (1965). The air permeabilities ranged from 10^{-9} to 10^{-7} cm^2 (IDNR, 1991). Comparison to the air permeabilities in Table 2 indicates that the field values are somewhat higher than the laboratory determined values. Many glacial till investigations have found scale effects of hydraulic conductivity. Pumping test values are consistently higher than laboratory values of hydraulic conductivity, for it is difficult to replicate fractures, sand seams, and other large scale phenomena with a core sample (Bradbury and Muldoon, 1989). The same may be true of air permeability.

In addition to comparing with laboratory studies, air permeability can be compared with the intrinsic permeability as calculated in equation (1) above. From pumping tests in oxidized till, Jones et al. (1992) and Edwards and Jones (in print) determined the hydraulic conductivity of a region extending from 100 to 500 cm below the ground surface at a similar site less than five miles away. The hydraulic conductivity was found to be approximately $5x10^{-4}$ cm/sec. The properties of water at 12°C are μ=0.012 g/cm-s and ρ=1.0 g/cm^3. Therefore, the intrinsic permeability from (1) is:

$$k = \frac{(0.012\,g/cm\text{-}s)(5x10^{-4}\,cm/s)}{(1\,g/cm^3)(981\,cm/s^2)} = 6.1x10^{-9}\,cm^2 \qquad (87)$$

This is lower than any of the field air permeabilities shown in Table 2. However, Reeve (1965) mentions that this is due to the effects of water on pore structure. For stable soils, a typical intrinsic to air permeability ratio is 2 to 3

while the ratio may be 50,000 for unstable soils.

Feasibility of SVE in Till

A comparison with other investigations of soil vapor extraction is useful for assessing the viability of soil vapor extraction (SVE) in till. Even though SVE is usually utilized to remediate sand or sand and gravel deposits rather than till, comparisons with such investigations may be helpful. Baehr and Hult (1991) reported air permeabilities around 10^{-7} cm^2 for a sand formation underneath a confining silt lens having $k=10^{-9}$ cm^2. In addition there was an upper sand layer (above the silt lens) exposed to the atmosphere. It had a permeability of 10^{-7} to 10^{-6} cm^2. In both layers, there was a 1 to 2 cm H_2O vacuum response 100 cm away from the extraction well. The extraction rate in the lower sand layer was 8000 cm^3/sec and was 24,000 cm^3/sec in the upper sand layer. The screened extraction intervals were 60 cm both above and below the silt lens. Since the vacuum response was about the same despite very different extraction rates, the boundary conditions and permeabilities had a profound effect. The vacuum at 100 cm in till from Table 2 at a flowrate of 3600 cm^3/sec is almost 1 cm H_2O indicating that SVE in till is feasible, but the radius of influence is smaller. In a controlled sand tank, Thornton and Wootan (1982) reported that the majority of vapor removal was accomplished in the first three days of extraction at 2000 cm^3/sec. The (intrinsic) permeability was $5x10^{-7}$ cm^2. At 20,000 cm^3/sec with an intrinsic permeability of 10^{-8} cm^2, again the majority of vapors were removed in the first three days of extraction from a sand and gravel formation.

To assess the viability of SVE in till without studying contaminant migration, a useful criteria is travel time - the time for an air particle to reach the extraction well from a given distance. Since the highest vapor concentrations will

most likely reside near the water table (Pedersen and Curtis, 1991), vapor particles originating 125 and 175 cm above the water table will be studied. Travel times are presented in Fig. 21. The travel times are for a flowrate of 3600 cm^3/sec to the vertical well W1 shown in Fig. 7 and were determined using the four layer isotropic model whose permeabilities are shown in Table 2. A vapor particle initially 200 cm from the extraction well at $z=175$ cm above the water table will be removed in three days of discharging at 3600 cm^3/sec. A particle at $z=125$ cm above the water table is in a layer of much lower permeability. Only particles within 100 cm at that height will be removed in three days. Therefore, at 3600 cm^3/sec, vapor particles between 100 and 200 cm from the extraction well will be removed in three days. For an SVE system to be effective in till with such a flowrate, discharge wells would have to be spaced at 400 cm intervals or use higher flowrates.

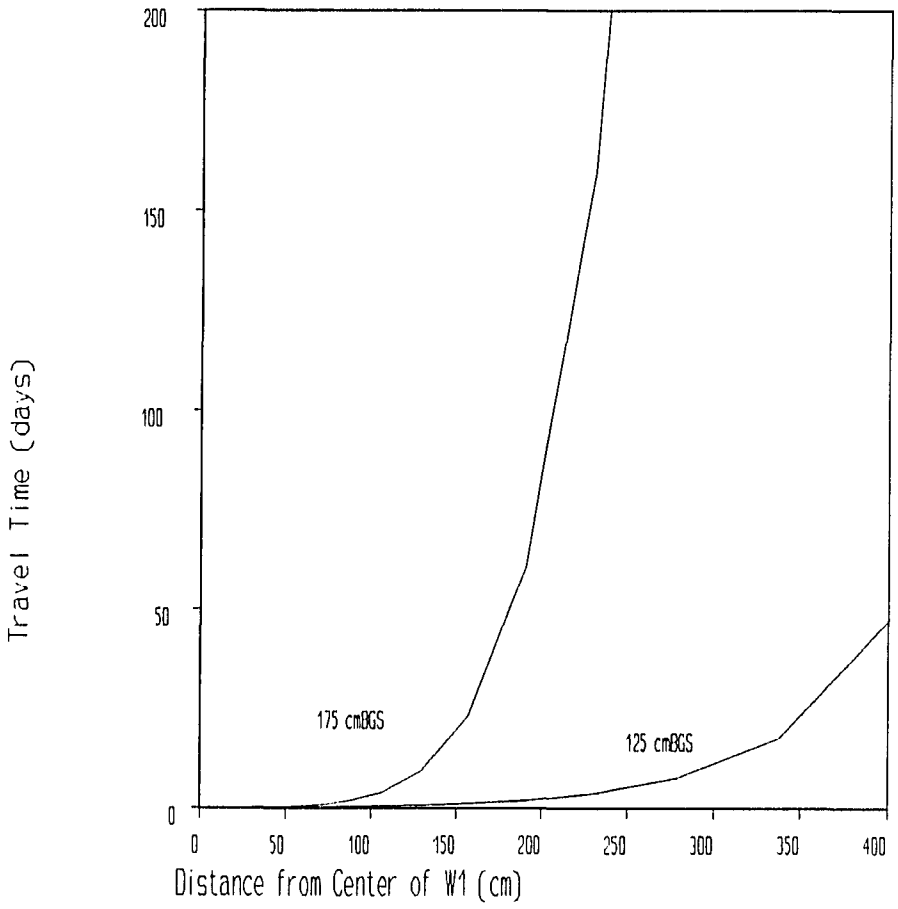

Figure 21. Travel times for an extraction rate of 3600 cm^3/s using the 10/7/92 permeabilities

CONCLUSION

Air permeability is a key parameter for designing soil vapor extraction systems. A field investigation was initiated to determine the air permeability of a glacial till soil in-situ. A number of vertical wells at various radial locations from a central discharge well and screened over various depths were installed in the loam till of central Iowa. An impermeable surface boundary was created out to a radial distance of 200 cm from the discharge well and monitoring wells were installed at various radial and vertical distances from the central well. Air was extracted or injected from the central well and air pressures were recorded at the monitoring wells.

The results of inverse modeling using a two-dimensional axisymmetric anisotropic, heterogeneous compressible flow model indicated that anisotropy was not as important as vertical heterogeneities. Further, the system could be modeled using ground water flow models (given appropriate boundary conditions) since incompressibility was also investigated and did not affect results. Modeling the soil as four layers of equal thickness (50 cm) with a no flow bottom boundary at 200 cm below the ground surface, air permeability varies from $4x10^{-8}$ cm^2 in the deepest region to $1x10^{-5}$ cm^2 in the shallowest layer. The variation with depth is attributable to increased water content with depth and higher bulk densities due to compaction.

When the air permeabilities determined from in-situ field tests are compared to laboratory tests and to an intrinsic permeability based on the hydraulic conductivity found from pumping tests, the in-situ air permeabilities are several orders of magnitude higher though the ratio varies with depth. Due to the increase in scale from the laboratory to the field, this is not uncommon. Large scale effects such as macropores, fractures, and sand seams are more likely encountered in the larger field scale.

The goals of this research were four-fold. (1) Provide multiple well field test data from air extraction tests in a low permeability soil since these soils have previously been considered "too tight" to remediate using soil vapor extraction. (2) Develop a model that represents air flow in the soil matrix and represents the field conditions. (3) Fit the model to field data to obtain air permeabilities. (4) Determine whether the model indeed does an adequate job of describing the field experiments.

Looking back at this research, two ideas for future work are apparent. (1) Future research should investigate gas tracer movement through the unsaturated soil matrix. This would give a better idea of travel times, effective porosity, and the sorption properties of the soil. (2) Near the vertical well site described in this dissertation, there are some horizontal wells. Use of horizontal wells for remediating the unsaturated zone where shallow water tables are present is becoming popular. Studies similar to those performed with vertical well could be done using horizontal wells. This would help development of models for air flow to horizontal wells. It might also shed some light on their economic feasibility.

REFERENCES

Abriola, L. M. 1984. Multiphase Migration of Organic Compounds in a Porous Medium. Springer-Verlag. New York, NY.

Abriola, L. M. and G. F. Pinder. 1985a. A multiphase approach to the modelling of porous media contamination by organic compounds, 1, Equation development. Water Resources Research. v. 21. pp. 11-18.

Abriola, L. M. and G. F. Pinder. 1985b. A multiphase approach to the modelling of porous media contamination by organic compounds, 2, Numerical simulation. Water Resources Research. v. 21. pp. 19-26.

Anderson, W. 1983. Geology of Iowa: Over Two Billion Years of Change. Iowa State University Press. Ames, IA. 268 pp.

Baehr, A. L. 1984. Immiscible contaminant transport in soils with an emphasis on gasoline hydrocarbons. Ph.D. dissertation. University of Delaware. Newark, Delaware.

Baehr, A. L. 1987. Selective transport of hydrocarbons in the unsaturated zone due to aqueous and vapor phase partitioning. Water Resources Research. v. 23. pp. 1926-1938.

Baehr, A. L. and M. Y. Corapcioglu. 1987. A compositional multiphase model for groundwater contamination by petroleum products, 2, Numerical simulation. Water Resources Research. v. 23. pp. 201-213.

Baehr, A. L., G. E. Hoag and M. C. Marley. 1989. Removing volatile contaminants from the unsaturated zone by inducing advective air-phase transport. Journal of Contaminant Hydrology. v. 4. pp. 1-26.

Baehr, A. L. and M. F. Hult. 1991. Evaluation of unsaturated zone air permeability through pneumatic tests. Water Resources Research. v. 27. pp. 2605-2617.

Bear, J. 1972. Dynamics of Fluids in Porous Media. American Elsevier Publishing. Co. New York, NY. 764 pp.

Bear, J. 1979. Hydraulics of Groundwater. McGraw-Hill Publishing Co. New York, NY. 569 pp.

Bickford, W. B. 1990. A First Course in the Finite Element Method. Richard D. Irwin, Inc. Homewood, IL. 649 pp.

Bradbury, K. R. and M. A. Muldoon. 1989. Hydraulic conductivity determinations in unlithified glacial and fluvial materials. Ground Water and Vadose Zone Monitoring. ASTM STP 1053, D. M. Nielsen and A. I. Johnson, Eds, American Society for Testing and Materials, Philadelphia, pp. 138-151.

Collins, R. E. 1961. Flow of Fluids Through Porous Media. Van Nostrand-Reinhold. Princeton, N.J.

Crow, W. L., E. P. Anderson, and E. M. Minugh. 1987. Subsurface venting of vapors emanating from hydrocarbon product on ground water. Ground Water Monitoring Review. v. 7. pp. 51-57.

Domenico, P. A. and F. W. Schwartz. 1990. Physical and Chemical Hydrogeology. John Wiley and Sons. New York, NY. 824 pp.

Dullien, F. A. L. 1979. Porous Media: Fluid Transport and Pore Structure. Academic Press. New York, NY. 396 pp.

Edwards, K. B. and L. C. Jones. Modeling pumping tests in oxidized till. Journal of Hydrology. (accepted for publication).

Evans, D. D. 1965. Gas movement. In Methods of Soil Analysis, American Society of Agronomy Monograph No. 9. pp. 319-324.

Falta, R. W., I. Javendel, K. Pruess, and P. A. Witherspoon. 1989. Density-driven flow of gas in the unsaturated zone due to the evaporation of volatile organic compounds. Water Resources Research. v. 25. pp. 2159-2169.

Freeze, R. A. and J. A. Cherry. 1979. Groundwater. Prentice-Hall. Englewood Cliffs, NJ. 604 pp.

Hutzler, N. J., B. E. Murphy, and J. S. Gierke. 1988. State of Technology Review: Soil Vapor Extraction Systems. U.S. EPA, CR-814319-01-1.

IDNR (Iowa Department of Natural Resources). 1991. Aquitard hydrology project, Ames research site. Annual progress report. Geological Survey Bureau. Iowa City, IA.

Johnson, P. C., M. W. Kemblowski, and J. D. Colthart. 1990a. Quantitative analysis for the cleanup of hydrocarbon-contaminated soils by in-situ soil venting. Ground Water. v. 28. pp. 413-429.

Johnson, P. C., C. C. Stanley, M. W. Kemblowski, D. L. Byers, and J. D. Colthart. 1990b. A practical approach to the design, operation, and monitoring of in situ soil-venting systems. Ground Water Monitoring Review. v. 10. pp. 159-178.

Jones, L. C, T. Lemar, and C. Tsai. 1992. Results of two pumping tests in Wisconsin age weathered till in Iowa. Ground Water. v. 30. pp. 529-538.

Jury, W. A., W. F. Spencer, and W. J. Farmer. 1983. Behavior assessment model for trace organics in soil, I, Model description. Journal of Environmental Quality. v. 12, pp. 558-564.

Kidder, R. E. 1957. Unsteady flow of gas through a semi-infinite porous medium. Journal of Applied Mechanics, ASME Transactions. v. 24. pp. 329-332.

Kirkham, D. 1946. Field method for determination of air permeability of soil in its undisturbed state. Soil Science Society of America. v. 11. pp. 93-99.

Klinkenberg, L. J. 1941. The permeability of porous media to liquids and gases, in Drilling and Production Practice. American Petroleum Institute. pp. 200-213.

Kuo, J-F., E. M. Ajeta, and P-H. Yang. 1990. A two-dimensional model for estimating radius of influence of a soil venting process. Proceedings of HAZMACON 90. April 17-19. Anaheim, California. Association of Bay Area Governments.

Marquardt, D. 1963. An algorithm for least-squares estimation of nonlinear parameters. Journal of the Society of Industrial and Applied Mathematics. v. 11, no. 2, pp. 431-441.

Massman, J. W. 1989. Applying groundwater flow models in vapor extraction system design. Journal of Environmental Engineering. v. 115, pp. 129-149.

Massman, J. and D. F. Farrier. 1992. Effects of atmospheric pressures on gas transport in the vadose zone. Water Resources Research. v. 28. pp. 777-791.

McWhorter, D. B. 1990. Unsteady radial flow of gas in the vadose zone. Journal of Contaminant Hydrology. v. 5. pp. 297-314.

Muskat, M. and H. G. Botset. 1931. Flow of gas through porous materials. Physics. v. 1. pp. 27-47.

Omega Engineering, Inc. 1991. Complete Flow and Level Measurement Handbook and Encyclopedia. Omega Engineering, Inc. Stamford, CT.

Pedersen, T. A. and J. T. Curtis. 1991. Soil Vapor Extraction Technology Reference Handbook. PB91-168476, EPA/540/2-91/003. February. 316 pp.

Poulovassilis, A. 1970. The effect of the entrapped air on the hysteresis curves of a porous body and on its hydraulic conductivity. Soil Science. v. 109. pp. 154-162.

Press, F. and R. Siever. 1986. Earth. W. H. Freeman and Company. New York, NY. 656pp.

Reeve, R. C. 1965. Air-to-water permeability ratio. In Methods of Soil Analysis. American Society of Agronomy. Monograph No. 9. pp. 520-528.

Ressler, D. 1992. Personal communication. Graduate student in Agronomy at Iowa State University. (515) 294-6517.

Savage, K. M. 1992. Personal commmunication. University of Cincinnati. (513) 569-7865.

Schwille, F. 1984. Migration of organic fluids immiscible with water, in Pollutants in Porous Media, Ecological Studies no. 47, pp. 27-48. Springer-Verlag. New York, NY.

Shan, C., R. W. Falta, and I. Javandel. 1992. Analytical solutions for steady state gas flow to a soil vapor extraction well. Water Resources Research. v. 28. pp. 1105-1120.

Silka, L. R. 1988. Simulation of vapor transport through the unsaturated zone-Interpretation of soil-gas surveys. Ground Water Monitoring Review. v. 8. pp. 115-123.

Sleep, B. E. and J. F. Sykes. 1989. Modeling the transport of volatile organics in variably saturated media. Water Resources Research. v. 25, pp. 81-92.

Smith, G. 1992. Personal communication. Burns and McDonnell Consultants. Kansas City, MO. (816) 333-4375.

Stonestrom, D. A. and J. Rubin. 1989. Air permeability and trapped-air content in two soils. Water Resources Research. v. 25. pp. 1959-1969.

Swallow, J. A. and P. M. Gschwend. 1983. Volatilization of organic compounds from unconfined aquifers. Third National Symposium on Aquifer Restoration and Ground Water Monitoring. National Water Well Association. Columbus, Ohio.

Theis, C. V. 1935. The relation between lowering of the piezometric surface and the rate and duration of discharge of a well using ground water storage. Transactions, American Geophysical Union, 16th Annual Meeting, Part 2. Washington D.C. pp. 519-524.

Thornton, J. S. and W. L. Wootan. 1982. Venting for the removal of hydrocarbon vapors from gasoline contaminated soil. Journal of Environmental Science and Health. v. A17(1). pp. 31-44.

USDA (United States Department of Agriculture). 1984. Soil Survey of Story County, Iowa. Soil Conservation Service. Ames, IA.

Wang, H. 1990. In situ lateral earth pressure and its effect on vertical hydraulic conductivity in a glacial till deposit. Ph.D. dissertation. Iowa State University, Ames, IA. 133 pp.

Wang, H. F. and M. P. Anderson. 1982. Introduction to Groundwater Modeling. W. H. Freeman and Co. New York, NY. 237 pp.

Weeks, E. P. 1978. Field determination of vertical permeability to air in the unsaturated zone. Geological Survey Professional Paper 1051. 41 pp.

Wilson, D. E., R. E. Montgomery, and M. R. Sheller. 1987. A mathematical model for removing volatile subsurface hydrocarbons by miscible displacement. Water, Air, and Soil Pollution. v. 33. pp. 231-255.

Yu, L. L. 1985. Study of air flow through porous media. M. S. Thesis. University of Connecticut. Storrs, CT.

ACKNOWLEDGMENTS

Financial support for this research was provided by the United States Department of Agriculture National Needs Graduate Fellowship Program. I would like to thank my major professor, Dr. LaDon Jones, for his many helpful insights during the progression of this research. Thanks are also expressed to my Ph.D. committee members, Dr. T. Al Austin (co-major professor), Dr. James Baker, Dr. Robert Horton, and Dr. Richard Dague. Finally, I would like to thank my wife, Debbie, for her love and friendship.

APPENDIX A: CONVERSION FACTORS

Distance:

$$1 = \frac{2.54 \text{ cm}}{1 \text{ inch}} = \frac{30.48 \text{ cm}}{1 \text{ foot}}$$

Pressure:

$$1 = \frac{980.6 \text{ g/cm-s}^2}{1 \text{ cm } H_2O \text{ (4°C)}} = \frac{33860 \text{ g/cm-s}^2}{1 \text{ inch Hg (0°C)}}$$

$$1 = \frac{29.92 \text{ "Hg (0°C)}}{1 \text{ atm}} = \frac{1020 \text{ cm } H_2O \text{ (4°C)}}{1 \text{ bar}} = \frac{10.20 \text{ cm } H_2O \text{ (4°C)}}{1 \text{ cb}}$$

$$1 = \frac{70.28 \text{ cm } H_2O \text{ (4°C)}}{1 \text{ psi}} = \frac{27.67 \text{ "}H_2O \text{ (4°C)}}{1 \text{ psi}} = \frac{2.035 \text{ "Hg (0°C)}}{1 \text{ psi}}$$

Flowrate:

$$1 = \frac{471.9 \text{ cm}^3/\text{s}}{1 \text{ cfm}}$$

APPENDIX B: COMPUTER PROGRAM FOR MODELING AIR TRANSPORT

```
//PARESTSC JOB
//STEP EXEC FORTVCLG,FVPOPT=2,TIME.GO=(16,30)
//FORT.SYSIN DD *
@PROCESS  DC(PASS1)
C*************************************************************
C  PROGRAM NAME: PAREST-SC
C
C  WRITTEN BY:
C               DR. LADON C. JONES
C               ASSOCIATE PROFESSOR OF CIVIL ENGINEERING
C               375 TOWN ENGINEERING BLDG.
C               IOWA STATE UNIVERSITY
C               AMES, IOWA  50011
C               (515) 294-6848
C  AND MODIFIED BY:
C               KEN EDWARDS, GRADUATE STUDENT
C
C  LEAST SQUARES PARAMETER ESTIMATION
C  FINITE ELEMENT MODEL FOR STEADY RADIAL AND VERTICAL
C  COMPRESSIBLE GAS (AIR) FLOW TO A WELL
C  ANISOTROPIC AND INHOMOGENOUS
C  linear triangular elements
C  LU decomposition, band storage mode
C  Written for the HDS mainframe computer FORTRAN 77
C*************************************************************
      INTEGER BDCK,FEMAX
      PARAMETER(NNODE=2475,NELEM=4800,NNBN=06,BDCK=1)
      PARAMETER(NWELL=19,NSAMP=1)
      PARAMETER(NMW=08,FEMAX=38,NPC=1)
      PARAMETER(NLCA=49,NUCA=49)
      PARAMETER(NTCA=NLCA+NUCA+1)
      PARAMETER(NTNODE=NTCA*NNODE)
      PARAMETER(NTT=(2*NLCA+NUCA+1)*NNODE)
      PARAMETER(NVAR=4,NF=NMW,NTZONE=4)
      PARAMETER(ISW=2)
C
      CHARACTER*80 TITLE
C
      REAL*8 RLOC(NNODE),ZLOC(NNODE),BHEAD(NNBN)
      REAL*8 KRC(NELEM,3,3),KZC(NELEM,3,3)
      REAL*8 FVALUE(NF),HEAD(NNODE)
      REAL*8 DRAWD(NSAMP,NMW,ISW)
      REAL*8 QP(NPC,NWELL)
      REAL*8 XGUESS(NVAR)
      REAL*8 HKH,HKV,TOTAL,CC,PATM
      REAL*8 XLB(NVAR),XUB(NVAR),XSCALE(NVAR),X(NVAR)
      REAL*8 FSCALE(NF),RPARAM(7),FJAC(NF,NVAR)
      REAL RWKSP(6168)
C
      INTEGER NODEI(NELEM),NODEJ(NELEM),NODEK(NELEM),NLAY(NELEM)
      INTEGER NBNODE(NNBN),NWLOC(NPC,NWELL)
      INTEGER MWINFO(NMW,FEMAX+1)
      INTEGER IBAND
      INTEGER IPARAM(6)
```

```
      EXTERNAL GWSIM
C
      COMMON/PASS1/KRC,KZC,QP,BHEAD,RLOC,ZLOC,DRAWD,TOTAL,HEAD
     $,CC,PATM
      COMMON/PASS2/NBNODE,IBAND,NWLOC,MWINFO,NODEI,NODEJ,NODEK,NLAY
      COMMON/WORKSP/ RWKSP
C
      DATA XSCALE/NVAR*1.0D0/,FSCALE/NF*1.0D0/
C
C  IN XGUESS, ENTER ALL KR'S FIRST, THEN KZ'S
      DATA XGUESS/.326D-07,.155D-05,.204D-5,.128D-04/
      DATA XLB/.1D-15,.1D-15,.1D-15,.1D-15/
      DATA XUB/4*.1D-1/
C
      TOTAL=1.0D60
C
      CALL SPINIT
      CALL XUFLOW(0)
      CALL IWKIN(6168)
C*************************************************
C READ IN THE TITLE CARD OF THE INPUT FILE
C*************************************************
C
       READ(9,22)TITLE
       WRITE(10,22)TITLE
C
C
C CALL SUBROUTINE GRIDIN TO READ IN
C THE ELEMENT AND NODE INFORMATION
C
C
      CALL GRIDIN(NNODE,NELEM,NODEI,NODEJ,NODEK,RLOC,ZLOC,NLAY)
C
C
C CALL SUBROUTINE BANDWID TO DETERMINE THE BANDWIDTH
C
C
      CALL BANDWID(NELEM,IBAND,NODEI,NODEJ,NODEK)
C
C
C CHECK CALCULATED BANDWIDTH AGAINST DIMENSION
C
      IF (IBAND.NE.NLCA) THEN
      WRITE(6,*)'  ERROR IN BANDWIDTH DIMENSION'
      WRITE(6,*)' DIMENSION OF LOWER DIAGONALS (NLCA) ',NLCA
      WRITE(6,*)' COMPUTED NLCA (IBAND) ',IBAND
      STOP
      END IF
C
C CALL SUBROUTINE
C GLOBCON TO COMPUTE ELEMENT CONSTANTS
C
C SUBROUTINE GLOBCON(NN,NE,NCA,NJ,NK,IB,DT,RL,ZL,AKR,AKZ,ASO)
C
      CALL GLOBCON(NNODE,NELEM,NTCA,NODEI,NODEJ,NODEK,IBAND,
     &RLOC,ZLOC,KRC,KZC)
C
```

```
C
C*****************************************
C READ IN THE SAMPLE NUMBER AND SAMPLE TIME
C*****************************************
C
        READ(19,22)TITLE
        WRITE(20,22)TITLE
        READ(19,22)TITLE
        WRITE(20,22)TITLE
        READ(19,*)PATM,CC
        WRITE(20,17)PATM,CC
C
      DO 123 I=1,NSAMP
        READ(19,22)TITLE
        WRITE(20,22)TITLE
      DO 123 J=1,NMW
      READ(19,*)DRAWD(I,J,1),DRAWD(I,J,2)
      WRITE(20,17)DRAWD(I,J,1),DRAWD(I,J,2)
123   CONTINUE
C
C*****************************************
C  READ IN THE MONITORING WELL INFORMATION
C  FOR EACH WELL THE NUMBER OF FINITE ELEMENT
C  NODES AND THE NODES ARE INPUT
C*****************************************
C
      DO 391 I=1,NMW
C
       READ(17,22)TITLE
       WRITE(18,22)TITLE
       READ(17,22)TITLE
       WRITE(18,22)TITLE
      READ(17,*)MWINFO(I,1)
      WRITE(18,29)MWINFO(I,1)
       READ(17,22)TITLE
       WRITE(18,22)TITLE
      DO 394 J=1,MWINFO(I,1)
      READ(17,*)MWINFO(I,J+1)
      WRITE(18,29)MWINFO(I,J+1)
394   CONTINUE
391   CONTINUE
C*************************************
C READ IN THE WELL LOCATION AND PUMPING RATE
C FROM QIN
C*************************************
      READ(16,22)TITLE
      WRITE(10,22)TITLE
      READ(16,22)TITLE
      WRITE(10,22)TITLE
C
      DO 731 I=1,NPC
C
      READ(16,*)(NWLOC(I,J),QP(I,J),J=1,NWELL)
      WRITE(10,28)(NWLOC(I,J),QP(I,J),J=1,NWELL)
C
731   CONTINUE
C
```

```
C************************************************
C READ IN THE TRANSMISSIVITY AND STORAGE COEFFICIENT
C************************************************
C
       READ(9,22)TITLE
       WRITE(10,22)TITLE
C
C      READ(9,*)(K,KRV(K),KZV(K),SOV(K),I=1,NELEM)
C      WRITE(10,11)(I,KRV(I),KZV(I),SOV(I),I=1,NELEM)
C
      READ(9,*)HKH,HKV
      WRITE(10,*)HKH,HKV
C
C      DO 928 I=1,NELEM
C      KRV(I)=HKH
C      KZV(I)=HKV
C928   CONTINUE
C
C************************************************
C READ IN THE KNOWN BOUNDARY HEADS
C************************************************
C
       READ(9,22)TITLE
       WRITE(10,22)TITLE
       READ(9,22)TITLE
       WRITE(10,22)TITLE
      IF(BDCK.GT.0) THEN
       READ(9,*)(NBNODE(I),BHEAD(I),I=1,NNBN)
       WRITE(10,12)(NBNODE(I),BHEAD(I),I=1,NNBN)
      END IF
C
C CALL GWSIM
C      CALL GWSIM(NF,NVAR,XGUESS,FVALUE)
C
C CALL THE LEAST SQUARES ROUTINE
C
      IBTYPE=0
C
      LDFJAC=NF
C
C
C
      CALL DBCLSF(GWSIM,NF,NVAR,XGUESS,IBTYPE,XLB,XUB,XSCALE,FSCALE,
     &IPARAM,RPARAM,X,FVALUE,FJAC,LDFJAC)
C
      WRITE(21,*)' '
      WRITE(21,*)'NUMBER OF ITERATIONS',IPARAM(3)
      WRITE(21,*)'NUMBER OF FUNCTION CALLS',IPARAM(4)
      WRITE(21,*)'LOWER AND UPPER BOUNDS'
      DO 448 I=1,NVAR
       WRITE(21,*)XLB(I),XUB(I)
448   CONTINUE
      WRITE(21,*)
      WRITE(21,*)'CALCULATED HEADS'
      WRITE(21,*)'NODE, R, Z, HEAD'
C OUTPUT IN PABS (G/CM-S2) AND GAGE (CM H2O)
      DO 600 I=1,NNODE
```

```
        WRITE(21,18)I,RLOC(I),ZLOC(I),DSQRT(HEAD(I)),
     $ (DSQRT(HEAD(I))-PATM)/CC
600    CONTINUE
C
C*****************************************************************
C FORMAT CARDS FOR MAIN PROGRAM
C*****************************************************************
10     FORMAT(4I5)
11     FORMAT(I5,F5.1,F5.1)
C 12   FORMAT(I5,F12.1)
13     FORMAT(F10.2,F10.3,F10.3,F10.3,F10.3)
15     FORMAT(4I5)
16     FORMAT(2F20.5)
C 17   FORMAT(3F10.2)
C 18   FORMAT(I5,F10.2,F10.2,F15.5)
22     FORMAT(A80)
28     FORMAT(I5,F20.5)
29     FORMAT(I5)
12     FORMAT(I5,1PE16.5)
17     FORMAT(3(1PE16.5))
18     FORMAT(I5,F10.3,F10.3,2(1PE16.5))
C
C*****************************
C END OF PROGRAM
C*****************************
       STOP
       END
C*****************************************
C SUBROUTINE BANDWID, COMPUTES THE BANDWIDTH
C*****************************************
       SUBROUTINE BANDWID(NE,IB,NI,NJ,NK)
C
       INTEGER NE,IB,I
       INTEGER NI(NE),NJ(NE),NK(NE)
       INTEGER IMAX,ISUM1,ISUM2,ISUM3
C
C
C COMPUTE THE BANDWIDTH
C
C
        IB = 0
C
       DO 100 I=1,NE
C
C
C SET MAXIMUM DIFFERENCE IN NODE NUMBERS TO ZERO
C
C
       IMAX=0
C
C************************************
C CHECK FOR MAXIMUM NODE DIFFERENCE
C************************************
C
       ISUM1 = ABS(NI(I) - NJ(I))
       ISUM2 = ABS(NI(I) - NK(I))
       ISUM3 = ABS(NJ(I) - NK(I))
```

```
       IMAX=ISUM1
        IF (ISUM2.GT.IMAX) THEN
        IMAX = ISUM2
        END IF
        IF (ISUM3.GT.IMAX) THEN
          IMAX = ISUM3
        END IF
        IF (IMAX.GT.IB) THEN
        IB = IMAX
        END IF
C
100      CONTINUE
C
C
C*********************************************
C PRINT OUT THE BANDWIDTH
C*********************************************
C
       WRITE(10,*)'NUMBER OF LOWER DIAGONALS= ',IB
      WRITE(10,*)'TOTAL BANDWIDTH= ',2*IB+1
C
      RETURN
      END
C
C SUBROUTINE GLOBAL
C ASSEMBLES THE COEFFICIENT MATRIX FOR
C THE LEFT HAND SIDE AND RIGHT HAND SIDE
C
C

C*****************************************
      SUBROUTINE GRIDIN(NN,NE,NI,NJ,NK,RL,ZL,NL)
C
C SUBROUTINE TO READ IN THE FINITE ELEMENT
C ELEMENT AND NODE INFORMATION
C
C
      INTEGER NN,NE,K,I
      INTEGER NI(NE),NJ(NE),NK(NE),NL(NE)
      REAL*8 RL(NN),ZL(NN)
      CHARACTER*80 TITLE
C
C
C READ IN THE TITLE CARD OF THE FILE
C
C
      READ(14,22)TITLE
      WRITE(15,22)TITLE
C
C*****************************************
C READ IN THE ELEMENT DATA
C*****************************************
       READ(14,22)TITLE
       WRITE(15,22)TITLE
      READ(14,*)(K,NI(K),NJ(K),NK(K),NL(K),I=1,NE)
      WRITE(15,10)(I,NI(I),NJ(I),NK(I),NL(I),I=1,NE)
C
```

```
C
C*****************************************
C READ IN THE NODE DATA
C*****************************************
       READ(14,22)TITLE
       WRITE(15,22)TITLE
       READ(14,*)(K,RL(K),ZL(K),I=1,NN)
       WRITE(15,11)(I,RL(I),ZL(I),I=1,NN)
C
C
C FORMAT CARDS FOR SUBROUTINE
C
10     FORMAT(5I5)
11     FORMAT(I5,F5.1,F5.1)
22     FORMAT(A80)
C
       RETURN
       END
@PROCESS DC(PASS1,PASS3)
C**************************
C SUBROUTINE TO SIMULATE THE HEADS
C FOR A GIVEN VALUE OF KR, KZ, AND SO
C**************************
       SUBROUTINE GWSIM(NF,NX,X,FVAL)
       INTEGER NF,NX,FEMAX1
       REAL*8 X(NX),FVAL(NF)
       INTEGER NNODE1,NELEM1,NLCA1,NUCA1,NTCA1,BDCK1
       INTEGER IBAND,I,KK,MM,K
       PARAMETER(NNODE1=2475,NELEM1=4800,NNBN1=06,BDCK1=1)
       PARAMETER(NLCA1=49,NUCA1=49)
       PARAMETER(NTCA1=NLCA1+NUCA1+1)
       PARAMETER(NTT1=(2*NLCA1+NUCA1+1)*NNODE1)
       PARAMETER(NTNN1=NTCA1*NNODE1)
       PARAMETER(NPC1=1,NWELL1=19,NSAMP1=1)
       PARAMETER(NMW1=08,FEMAX1=38,ISW1=2,NTZON1=4)
C
       INTEGER NBNODE(NNBN1),IPVT(NNODE1),MWINFO(NMW1,FEMAX1+1)
       INTEGER LDA,LDFAC,JL,JU,J,IPUMP,IPATH,KU1,KTEMP
       INTEGER NODEI(NELEM1),NODEJ(NELEM1),NODEK(NELEM1),NLAY(NELEM1)
       INTEGER NWLOC(NPC1,NWELL1),WLOC(NWELL1)
C
       REAL*8 KRC(NELEM1,3,3),KZC(NELEM1,3,3)
       REAL*8 ALM(NTCA1,NNODE1),ARM(NTCA1,NNODE1)
       REAL*8 SUM1,KRR,KZZ,KR(NTZON1),KZ(NTZON1)
       REAL*8 HEAD(NNODE1)
       REAL*8 FAC(2*NLCA1+NUCA1+1,NNODE1)
       REAL*8 RHS(NNODE1),QP(NPC1,NWELL1)
       REAL*8 Q(NWELL1),BHEAD(NNBN1)
       REAL*8 RLOC(NNODE1),ZLOC(NNODE1)
       REAL*8 CTOTAL,TOTAL,SAMPT(NSAMP1+1),SUM,CC,PATM
       REAL*8 DRAWD(NSAMP1,NMW1,ISW1)
C
       COMMON/PASS1/KRC,KZC,QP,BHEAD,RLOC,ZLOC,DRAWD,TOTAL,HEAD
      $,CC,PATM
       COMMON/PASS2/NBNODE,IBAND,NWLOC,MWINFO,NODEI,NODEJ,NODEK,NLAY
       COMMON/PASS3/ALM,ARM,FAC,RHS
       COMMON/WORKSP/RWKSP
```

```
C
C       DATA FAC/NTT1*0.0D0/
        DATA Q/NWELL1*0.0D0/
        DATA WLOC/NWELL1*1/
C
        CALL DCOPY (NTT1,0.0D0,0,FAC,1)
        CALL DCOPY (NNODE1,0.0D0,0,RHS,1)
        CALL DCOPY (NTNN1,0.0D0,0,ALM,1)
C
        CTOTAL=0.0D0
C
C COMPUTE THE COEFFICIENT MATRICES
C
        DO 446 I=1,NTZON1
          IF(NX.GT.NTZON1)THEN
C     ANISOTROPIC
           KR(I)=X(I)
           KZ(I)=X(I+NTZON1)
           WRITE(*,*)'I,KR,KZ',I,KR(I),KZ(I)
          ELSE
C     ISOTROPIC
           KR(I)=X(I)
           WRITE(*,*)'I,K ISOTROPIC',I,KR(I)
          ENDIF
446     CONTINUE
C
C*****************************************************
C COMPUTE AND ASSEMBLE THE NODE DATA
C ELEMENT BY ELEMENT
C*****************************************************
C
C************************************************
C ASSEMBLE THE MATRIX COEFFICIENTS FOR ELEMENT M
C************************************************
C
C*********************************************
C STORAGE IN BAND STORAGE MODE
C A(I,J) GOES IN A(IB+1+I-J,J)
C*********************************************
C
        KU1=IBAND+1
        DO 444 M=1,NELEM1
          I=NODEI(M)
          J=NODEJ(M)
          K=NODEK(M)
          KRR=KR(NLAY(M))
          KZZ=KR(NLAY(M))
          IF(NX.GT.NTZON1)KZZ=KZ(NLAY(M))
C
C  ASSEMBLE DIAGONAL TERMS
C
C
C I,I TERM
C
        ALM(KU1,I)=ALM(KU1,I)+KRC(M,1,1)*KRR+KZC(M,1,1)*KZZ
C
C AL(J,J) = AL(J,J) + SUM1
```

```
C
      ALM(KU1,J)=ALM(KU1,J)+KRC(M,2,2)*KRR+KZC(M,2,2)*KZZ
C
C AL(K,K) = AL(K,K) + SUM1
C
      ALM(KU1,K)=ALM(KU1,K)+KRC(M,3,3)*KRR+KZC(M,3,3)*KZZ
C
C AL(I,J) = AL(I,J) + SUM1
C
      KTEMP = KU1 + I - J
C
      ALM(KTEMP,J)=ALM(KTEMP,J)+KRC(M,1,2)*KRR+KZC(M,1,2)*KZZ
C
C AL(J,I)=AL(J,I) + SUM1
C
      KTEMP = KU1 + J - I
C
      ALM(KTEMP,I)=ALM(KTEMP,I)+KRC(M,2,1)*KRR+KZC(M,2,1)*KZZ
C
C AL(I,K)=AL(I,K)+SUM1
C
      KTEMP = KU1 + I - K
C
      ALM(KTEMP,K)=ALM(KTEMP,K)+KRC(M,1,3)*KRR+KZC(M,1,3)*KZZ
C
C AL(K,I)=AL(K,I) + SUM1
C
      KTEMP = KU1 + K - I
C
      ALM(KTEMP,I)=ALM(KTEMP,I)+KRC(M,3,1)*KRR+KZC(M,3,1)*KZZ
C
C AL(J,K)=AL(J,K) + SUM1
C
      KTEMP = KU1 + J - K
C
      ALM(KTEMP,K)=ALM(KTEMP,K)+KRC(M,2,3)*KRR+KZC(M,2,3)*KZZ
C
C AL(K,J)=AL(K,J) + SUM1
C
      KTEMP=KU1+K-J
C
      ALM(KTEMP,J)=ALM(KTEMP,J)+KRC(M,3,2)*KRR+KZC(M,3,2)*KZZ
C
444   CONTINUE
C
C*************************************************
C ADJUST THE LHS FOR THE KNOWN HEAD
C BOUNDARY CONDITIONS
C*************************************************
      IF (BDCK1.GT.0) THEN
      DO 120 I=1,NNBN1
      KK=MAX(1,NBNODE(I)-NUCA1)
      MM=MIN(NNODE1,NBNODE(I)+NLCA1)
      DO 130 J=KK,MM
      K=NBNODE(I)-J+IBAND+1
      ALM(K,J)=0.0D0
130   CONTINUE
```

```
      ALM(IBAND+1,NBNODE(I))=1.0D0
120   CONTINUE
      END IF
C*************************************************
C DO THE LU DECOMPOSITION OF THE LHS
C IMSL ROUTINE: DLFTRB
C USES BAND STORAGE MODE
C*************************************************
      LDA=NTCA1
      LDFAC=2*NLCA1+NUCA1+1
C*************************************************
C LU FACTORIZATION
C*************************************************
      CALL DLFTRB(NNODE1,ALM,LDA,NLCA1,NUCA1,FAC,LDFAC,IPVT)
C
      INF=0
      ISAMP=1
C
       DO 560 I=1,NWELL1
       Q(I)=QP(1,I)
       RHS(NWLOC(1,I))=-Q(I)
560    CONTINUE
C
C
C*********************************************
C ADJUST RHS FOR KNOWN BOUNDARY NODES
C*********************************************
      IF(BDCK1.GT.0) THEN
       DO 570 I=1,NNBN1
       RHS(NBNODE(I))=BHEAD(I)
570    CONTINUE
      END IF
C
C
C*********************************************
C CALL THE IMSL ROUTINE TO SOLVE THE LINEAR SYSTEM
C*************************************************
C*********************************************
C SOLVE THE SYSTEM
C*********************************************
      IPATH=1
      CALL DLFSRB(NNODE1,FAC,LDFAC,NLCA1,NUCA1,IPVT,RHS,IPATH,HEAD)
C
C*****************************************************
C CHECK FOR HEAD PRINTOUT
C*****************************************************
C
      DO 385 J=1,NMW1
      IF(DRAWD(ISAMP,J,1).GT.0.5) THEN
      INF=INF+1
      SUM=0.0D0
      DO 386 K=1,MWINFO(J,1)
      IF(HEAD(MWINFO(J,K+1)).LT.0.0)THEN
       WRITE(*,*)'NODE,HEAD',MWINFO(J,K+1),HEAD(MWINFO(J,K+1))
       SUM=SUM-DSQRT(DABS(HEAD(MWINFO(J,K+1))))
      ELSE
       SUM=SUM+DSQRT(HEAD(MWINFO(J,K+1)))
```

```
      ENDIF
386   CONTINUE
      SUM=SUM/MWINFO(J,1)
      FVAL(INF)=(DRAWD(ISAMP,J,2)-PATM)/CC-(SUM-PATM)/CC
      CTOTAL=CTOTAL+FVAL(INF)*FVAL(INF)
      END IF
385   CONTINUE
C
C  CHECK FOR PRINT OUT BEST SOLUTION
      IF(CTOTAL.LT.TOTAL) THEN
C      REWIND 21
      WRITE(21,*)'BEST CURRENT SOLUTION. REGIONS & VARS:',NTZON1,NX
      WRITE(21,*)'SUM OF SQUARED ERROR'
      WRITE(21,14)CTOTAL
      WRITE(21,*)'VARIABLE VALUES.  IF ISOTROPIC, K=KR'
      WRITE(21,*)'KR(ZONE 1),KR(ZONE 2)..,KZ(ZONE 1),KZ(ZONE 2)..'
      WRITE(*,*)'BEST CURRENT SOLUTION. REGIONS & VARS:',NTZON1,NX
      WRITE(*,*)'SUM OF SQUARED ERROR'
      WRITE(*,14)CTOTAL
      WRITE(*,*)'VARIABLE VALUES. ALL RADIAL THEN VERT UNLESS ISO'
      DO 872 I=1,NX
      WRITE(21,*)X(I)
      WRITE(*,*)X(I)
872   CONTINUE
      WRITE(21,*)'FUNCTION VALUE, MEASURED P, MODEL P'
      WRITE(*,*)'FUNCTION VALUE, MEASURED P, MODEL P'
      DO 873 I=1,NF
        SUM=(DRAWD(ISAMP,I,2)-PATM)/CC-FVAL(I)
        WRITE(21,*)FVAL(I),(DRAWD(ISAMP,I,2)-PATM)/CC,
     $  SUM
        WRITE(*,*)FVAL(I),(DRAWD(ISAMP,I,2)-PATM)/CC,
     $  SUM
873   CONTINUE
      TOTAL=CTOTAL
      END IF
C
13    FORMAT(F10.2,F10.3,F10.3,F10.3,F10.3)
14    FORMAT(1PE16.5)
      RETURN
      END
C
C*********************************************
C SUBROUTINE TO COMPUTE ELEMENT CONSTANTS
C ELEMENT CONSTANTS ARE A FUNCTION ONLY OF
C THE GRID AND NOT FUNCTIONS OF KR, KZ OR SO
C*********************************************
      SUBROUTINE GLOBCON(NN,NE,NCA,NI,NJ,NK,IB,RL,ZL,KRC,KZC)
C
      INTEGER NN,NE,NCA,IB,I,J,K,KTEMP,KU1,M
      INTEGER NI(NE),NJ(NE),NK(NE)
      REAL*8 RL(NN),ZL(NN)
      REAL*8 KRC(NE,3,3),KZC(NE,3,3)
      REAL*8 RI,RJ,RK,ZI,ZJ,ZK
      REAL*8 SUM1,SUM2,SUM3,AREA
      REAL*8 PIE,CONST1,CONST2
      REAL*8 BI,BJ,BK,CI,CJ,CK
C
```

```
      PIE=3.141592654D0
C
      CONST1=2.0D0*PIE/60.0D0
      CONST2=2.0D0*PIE/12.0D0
C
      DO 100 M=1,NE
C
      RI=RL(NI(M))
      RJ=RL(NJ(M))
      RK=RL(NK(M))
      ZI=ZL(NI(M))
      ZJ=ZL(NJ(M))
      ZK=ZL(NK(M))
C
C DETERMINE THE AREA OF THE ELEMENT
C
      SUM1=RI*ZJ-RJ*ZI
      SUM2=RK*ZI-RI*ZK
      SUM3=RJ*ZK-RK*ZJ
C
      AREA=(SUM1+SUM2+SUM3)/2.0D0
C
C
C TERMS FROM SPATIAL INTEGRATION INVOLVING
C  KR AND KZ
C
      BI=ZJ-ZK
      BJ=ZK-ZI
      BK=ZI-ZJ
      CI=RK-RJ
      CJ=RI-RK
      CK=RJ-RI
C
      SUM2=CONST2*(RI+RJ+RK)/AREA
C
      KRC(M,1,1)=SUM2*(BI*BI)
      KZC(M,1,1)=SUM2*(CI*CI)
C
      KRC(M,1,2)=SUM2*(BI*BJ)
      KZC(M,1,2)=SUM2*(CI*CJ)
C
      KRC(M,1,3)=SUM2*(BI*BK)
      KZC(M,1,3)=SUM2*(CI*CK)
C
      KRC(M,2,1)=KRC(M,1,2)
      KZC(M,2,1)=KZC(M,1,2)
C
      KRC(M,2,2)=SUM2*(BJ*BJ)
      KZC(M,2,2)=SUM2*(CJ*CJ)
C
      KRC(M,2,3)=SUM2*(BJ*BK)
      KZC(M,2,3)=SUM2*(CJ*CK)
C
      KRC(M,3,1)=KRC(M,1,3)
      KZC(M,3,1)=KZC(M,1,3)
C
      KRC(M,3,2)=KRC(M,2,3)
```

```
      KZC(M,3,2)=KZC(M,2,3)
C
      KRC(M,3,3)=SUM2*(BK*BK)
      KZC(M,3,3)=SUM2*(CK*CK)
C
100   CONTINUE
C
C//GO.FT12F001 DD DSN=N1$KBE.D2.HEAD,DISP=(NEW,CATLG),
C// UNIT=DISK,SPACE=(6204,(50,50),RLSE),
C// DCB=(RECFM=FB,LRECL=132,BLKSIZE=6204)
      RETURN
      END
C
//GO.FT09F001 DD DSN=N1$KBE.D2.FEIN1BN,DISP=SHR
//GO.FT10F001 DD DSN=N1$KBE.D2.FEINCK,DISP=SHR
//GO.FT11F001 DD DSN=N1$KBE.D2.HSAMP,DISP=SHR
//GO.FT12F001 DD DSN=N1$KBE.D2.HEAD,DISP=SHR
//GO.FT13F001 DD DSN=N1$KBE.D2.FEHI,DISP=SHR
//GO.FT14F001 DD DSN=N1$KBE.D2.FEGRIDBN,DISP=SHR
//GO.FT15F001 DD DSN=N1$KBE.D2.GRIDEC,DISP=SHR
//GO.FT16F001 DD DSN=N1$KBE.D2.QINBN,DISP=SHR
//GO.FT17F001 DD DSN=N1$KBE.D2.WINFOBP,DISP=SHR
//GO.FT18F001 DD DSN=N1$KBE.D2.WINFOCK,DISP=SHR
//GO.FT19F001 DD DSN=N1$KBE.D2.DRAWDBP,DISP=SHR
//GO.FT20F001 DD DSN=N1$KBE.D2.DRAWDCK,DISP=SHR
//GO.FT21F001 DD DSN=N1$KBE.D2.BFIT,DISP=SHR
//
```

APPENDIX C: FIELD DATA

APPENDIX C. FIELD DATA

Date	07/17/91	07/17/91	09/03/91	09/17/91	10/07/91	10/17/91
Rain (inch)				2	-0	-0
Time	16:30	16:44	16:44	16:30		13:32
Barom ("Hg)						
Power (%)						44
Q(p=0) (cfm)						
Q (cfm)	2.1	N/A	N/A			1.5
Tamb (C)						26
Tfm (C)						29.6
T(W1) (C)			21.7			29.6
Tens1 (cb)				9		
Tens2 (cb)				4		
Tens3 (cb)				5		
The following are pressures (negative indicates vacuum)						
W1 (cmH2O)	-103.63	-207.26	-224.54			35.14
W2 (cmH2O)	-2.03	-3.56	-6.10			1.27
W3 (cmH2O)	-1.52	-2.79	-3.05			0.76
W4A (cmH2O)						0.00
W4B (cmH2O)						0.00
W4C (cmH2O)						0.25
W4D (cmH2O)						0.00
W4E (cmH2O)						0.25
W5A (cmH2O)						0.00
W5B (cmH2O)						0.00
W5C (cmH2O)						0.25
W5D (cmH2O)						0.00
W5E (cmH2O)						0.00
W6 (cmH2O)	-0.25	-0.76	-0.25			0.00
W7 (cmH2O)	-0.25	-0.25	-1.02			0.25
WT (cm BGS)						

Date	10/17/91	05/30/92	06/09/92	06/13/92	06/17/92	06/25/92
Rain (inch)	-0	1	0.25	-0	0.5	-0
Time	13:37					
Barom ("Hg)						
Power (%)	88				67	
Q(p=0) (cfm)					9.7	
Q (cfm)	2.5				9.7	
Tamb (C)	26				23.5	
Tfm (C)	31.8					
T(W1) (C)	31.8				19.9	
Tens1 (cb)				9	10	10
Tens2 (cb)				6	4	5
Tens3 (cb)				6	7	8
The following are pressures (negative indicates vacuum)						
W1 (cmH2O)	56.23				-114.00	
W2 (cmH2O)	2.54				-5.59	
W3 (cmH2O)	1.27				-2.79	
W4A (cmH2O)	0.00				0.00	
W4B (cmH2O)	0.00				0.00	
W4C (cmH2O)	0.71				-1.27	
W4D (cmH2O)	0.00				0.00	
W4E (cmH2O)	0.38				0.00	
W5A (cmH2O)	0.00				0.00	
W5B (cmH2O)	0.00				0.00	
W5C (cmH2O)	0.51				-1.02	
W5D (cmH2O)	0.00				0.00	
W5E (cmH2O)	0.00				0.00	
W6 (cmH2O)	0.25				-0.25	
W7 (cmH2O)	0.38				-0.25	
WT (cm BGS)		185.34	209.72	221.92	234.11	257.88

Date	06/30/92	06/30/92	06/30/92	06/30/92	06/30/92	06/30/92
Rain (inch)	-0	-0	-0	-0	-0	-0
Time	11:30	13:12	13:30	13:40	14:19	17:50
Barom ("Hg)	29.51	29.43	29.42	29.42	29.42	29.17
Power (%)		48	75	48	48	48
Q(p=0) (cfm)						
Q (cfm)		7.5	10.6	7.6	7.5	7.5
Tamb (C)	31	35	37	37	37	39
Tfm (C)		48	58	57	54	55
T(W1) (C)		20.6	20	20	19.9	19.4
Tens1 (cb)	11	12	12	12	12	12
Tens2 (cb)	6	7	8	8	8	7
Tens3 (cb)	9	10	10	10	10	10
The following are pressures (negative indicates vacuum)						
W1 (cmH2O)		-55.27	-124.36	-62.18	-62.18	-62.18
W2 (cmH2O)		-3.05	-4.32	-3.05	-3.05	-3.05
W3 (cmH2O)		-1.78	-2.54	-1.78	-1.78	-1.78
W4A (cmH2O)		0.00	0.00	0.00	0.00	0.00
W4B (cmH2O)		0.00	0.00	0.00	0.00	0.00
W4C (cmH2O)		-1.02	-1.52	-1.02	-1.02	-1.02
W4D (cmH2O)		-0.25	-0.25	0.00	0.00	-0.13
W4E (cmH2O)		0.00	0.00	0.00	0.00	0.00
W5A (cmH2O)		-0.03	0.00	-0.03	-0.25	-0.03
W5B (cmH2O)		0.00	0.00	0.00	0.00	0.00
W5C (cmH2O)		-0.88	-1.22	-0.91	-0.90	-0.93
W5D (cmH2O)		0.00	0.00	0.00	0.00	-0.04
W5E (cmH2O)		-0.03	0.00	0.00	0.00	0.00
W6 (cmH2O)		0.00	0.00	0.00	0.00	0.00
W7 (cmH2O)		-0.25	-0.64	-0.25	-0.25	-0.25
WT (cm BGS)	267.33	267.03	267.03	267.03	267.03	267.33

Date	06/30/92	06/30/92	06/30/92	06/30/92	06/30/92	06/30/92
Rain (inch)	-0	-0	-0	-0	-0	-0
Time	18:22	18:27	18:29	18:31	18:35	18:54
Barom ("Hg)					29.2	29.2
Power (%)	48	60	80	90	76	76
Q(p=0) (cfm)						
Q (cfm)	5.4	6.5	7.8	8.4	7.5	7.5
Tamb (C)	38				35	35
Tfm (C)	24.3			19.6	19.1	18.3
T(W1) (C)	24.3			19.6	19.1	18.3
Tens1 (cb)					11	11
Tens2 (cb)					7	7
Tens3 (cb)					10	10
The following are pressures (negative indicates vacuum)						
W1 (cmH2O)	-62.18	-89.81		-148.54	-127.81	-127.81
W2 (cmH2O)	-3.05	-3.81	-4.57	-4.83	-4.57	-4.57
W3 (cmH2O)				-2.79	-2.54	-2.54
W4A (cmH2O)				0.00	0.00	0.00
W4B (cmH2O)				0.00	0.00	0.00
W4C (cmH2O)				-1.52	-1.40	-1.52
W4D (cmH2O)				-0.25	-0.25	-0.25
W4E (cmH2O)				N/M	N/M	N/M
W5A (cmH2O)				-0.25	-0.25	-0.03
W5B (cmH2O)				-0.25	0.00	-0.13
W5C (cmH2O)				<-1.3	-1.30	-1.31
W5D (cmH2O)				0.00	-0.13	-0.17
W5E (cmH2O)				0.00	0.00	-0.13
W6 (cmH2O)				-0.13	-0.25	-0.25
W7 (cmH2O)				-0.51	-0.30	-0.30
WT (cm BGS)					267.33	

Date	07/01/92	07/01/92	07/02/92	07/04/92	07/04/92	07/04/92
Rain (inch)	-0	-0	1	-0	-0	-0
Time	10:04	16:40	16:16	18:45	18:57	19:35
Barom ("Hg)	29.45	28.95	29.45	29.4	29.4	
Power (%)	76	76	76	76	-0	76
Q(p=0) (cfm)						19
Q (cfm)	7.4	7.1	7.4	7.3	-0	6.2
Tamb (C)	26	34	22	27	27	
Tfm (C)	17.1	19.3	15	15.5		
T(W1) (C)	17.1	19.3	15	15.5		
Tens1 (cb)	10	12	10	10	10	
Tens2 (cb)	6	7	2	4	4	
Tens3 (cb)	10	10	9	10	10	
The following are pressures (negative indicates vacuum)						
W1 (cmH2O)	-127.81	-117.45	-131.27	-131.27	0.00	-148.54
W2 (cmH2O)	-4.45	-4.32	-5.46	-5.08	0.00	
W3 (cmH2O)	-2.54	-2.54	-2.79	-2.79	0.00	
W4A (cmH2O)	0.00	0.00	0.00	0.00	0.00	
W4B (cmH2O)	0.00	0.00	-0.13	0.00	0.00	
W4C (cmH2O)	-1.42	-1.52	-2.03	-1.65	0.00	
W4D (cmH2O)	-0.38	-0.46	-3.56	-0.51	0.00	
W4E (cmH2O)	N/M	N/M	N/M	N/M	N/M	
W5A (cmH2O)	-0.13	-0.04	-0.05	-0.05	0.00	
W5B (cmH2O)	-0.13	-0.03	-0.43	-0.14	-0.14	
W5C (cmH2O)	-1.23	-1.26	<-1.3	<-1.3	-0.04	
W5D (cmH2O)	-0.10	0.00	-0.61	-0.13	-0.10	
W5E (cmH2O)	-0.13	0.00	-0.13	-0.13	-0.13	
W6 (cmH2O)	-0.05	-0.25	-0.25	-0.25	0.00	
W7 (cmH2O)	-0.38	-0.51	-0.76	-0.64	0.00	
WT (cm BGS)	267.94	267.94	270.99	270.99	270.99	

Date	07/06/92	07/08/92	07/14/92	07/16/92	07/16/92	07/17/92
Rain (inch)	-0	0.25	1.6	1.6	-0	-0
Time	20:30			16:44	16:47	15:56
Barom ("Hg)	29.65			29.65	29.65	
Power (%)	-0			50	80	
Q(p=0) (cfm)						
Q (cfm)				5.2	7.5	
Tamb (C)						
Tfm (C)						
T(W1) (C)						
Tens1 (cb)						5
Tens2 (cb)						
Tens3 (cb)						
The following are pressures (negative indicates vacuum)						
W1 (cmH2O)				-62.18	-148.54	
W2 (cmH2O)						
W3 (cmH2O)				-2.41	-3.56	
W4A (cmH2O)						
W4B (cmH2O)						
W4C (cmH2O)						
W4D (cmH2O)						
W4E (cmH2O)						
W5A (cmH2O)						
W5B (cmH2O)						
W5C (cmH2O)						
W5D (cmH2O)						
W5E (cmH2O)						
W6 (cmH2O)						
W7 (cmH2O)						
WT (cm BGS)	273.12					

Date	07/24/92	07/25/92	07/27/92	07/28/92	07/30/92	07/30/92
Rain (inch)	0.8	2	0.25	0.4	1.7	-0
Time	12:33		16:23	15:12	14:27	15:00
Barom ("Hg)	30.1		29.62	29.58	29.7	29.7
Power (%)					76	60
Q(p=0) (cfm)						
Q (cfm)					6.2	4.4
Tamb (C)	19				20	20
Tfm (C)					18	19
T(W1) (C)					18	19
Tens1 (cb)	5		7		2	2
Tens2 (cb)					0.2	0.3
Tens3 (cb)					0.2	0.2
The following are pressures (negative indicates vacuum)						
W1 (cmH2O)					-148.54	-110.54
W2 (cmH2O)					-5.59	-4.32
W3 (cmH2O)					-3.81	-2.54
W4A (cmH2O)					0.00	0.00
W4B (cmH2O)					0.00	0.00
W4C (cmH2O)					-2.29	-1.27
W4D (cmH2O)					0.00	0.00
W4E (cmH2O)					0.00	0.00
W5A (cmH2O)					-0.99	-0.79
W5B (cmH2O)					0.00	-0.04
W5C (cmH2O)					<-1.3	<-1.3
W5D (cmH2O)					0.00	0.00
W5E (cmH2O)					0.00	0.25
W6 (cmH2O)					-0.51	-0.25
W7 (cmH2O)					-1.02	-0.76
WT (cm BGS)			272.51		253.92	253.01

Date	07/31/92	07/31/92	08/03/92	08/03/92	08/05/92	08/11/92
Rain (inch)	0.2	-0	0.3	-0	-0	2
Time	15:43	16:07	3:00	8:57	17:04	16:15
Barom ("Hg)	29.5	29.5		29.8	30.2	29.68
Power (%)	60	60	60	60	-0	-0
Q(p=0) (cfm)	15.4					
Q (cfm)	-0		0-3unsteady	-0		
Tamb (C)	29	29		20		
Tfm (C)	20	20		20		
T(W1) (C)	20	20		20		
Tens1 (cb)	5	5		4		
Tens2 (cb)	0.9	1.5		1.4	2	
Tens3 (cb)	1.4	1.5		1.1	2.2	
The following are pressures (negative indicates vacuum)						
W1 (cmH2O)	-124.36	-124.36		-131.27		
W2 (cmH2O)	-0.51	-1.02		-0.25		
W3 (cmH2O)	-0.38	-0.76		-0.13		
W4A (cmH2O)	0.00	0.00		0.00		
W4B (cmH2O)	0.00	0.00		0.00		
W4C (cmH2O)	0.00	0.00		0.00		
W4D (cmH2O)	0.00	0.00		0.00		
W4E (cmH2O)	0.00	0.00		0.00		
W5A (cmH2O)	-0.13	-0.23		-0.03		
W5B (cmH2O)	0.00	-0.10		0.00		
W5C (cmH2O)	-0.25	-0.48		-0.08		
W5D (cmH2O)	0.00	0.05		0.00		
W5E (cmH2O)	0.00	0.00		0.00		
W6 (cmH2O)	0.00	0.00		0.00		
W7 (cmH2O)	0.00	0.00		0.00		
WT (cm BGS)	224.66	224.66		210.94	205.76	164.00

Date	08/11/92	08/13/92	08/14/92	08/14/92	08/14/92	08/14/92
Rain (inch)	-0	1	-0	-0	-0	-0
Time	16:45		17:00	17:05	17:10	17:25
Barom ("Hg)	29.68		30.2	30.2	30.2	30.2
Power (%)	70		50	50	50	50
Q(p=0) (cfm)			14.5	14.5	14.5	14.5
Q (cfm)	1.8		2.4	-0	-0	-0
Tamb (C)	28					
Tfm (C)	28					
T(W1) (C)	28					
Tens1 (cb)			5			
Tens2 (cb)	1.3		1			
Tens3 (cb)	1.4		1			
The following are pressures (negative indicates vacuum)						
W1 (cmH2O)	-165.81		182.75	0.00	0.00	0.00
W2 (cmH2O)	-0.76		N/M	0.00	0.00	0.00
W3 (cmH2O)	-0.76		N/M	0.00	0.00	0.00
W4A (cmH2O)	0.00		N/M	0.00	0.00	0.00
W4B (cmH2O)	0.00		N/M	0.00	0.00	0.00
W4C (cmH2O)	-0.38		N/M	0.00	0.00	NoGage
W4D (cmH2O)	0.00		N/M	0.00	0.00	0.00
W4E (cmH2O)	0.00		N/M	0.00	0.00	0.00
W5A (cmH2O)	-0.15		N/M	0.00	0.00	0.00
W5B (cmH2O)	-0.03		N/M	0.00	0.00	0.00
W5C (cmH2O)	-0.61		N/M	0.00	0.00	0.00
W5D (cmH2O)	0.00		N/M	0.00	0.00	0.00
W5E (cmH2O)	0.00		N/M	0.00	0.00	0.00
W6 (cmH2O)	0.00		N/M	NoGage	0.00	0.00
W7 (cmH2O)	-1.02		N/M	0.00	NoGage	0.00
WT (cm BGS)	164.31		167.05			169.19

Date	08/14/92	08/14/92	08/14/92	08/14/92	08/24/92	08/24/92
Rain (inch)	-0	-0	-0	-0	-0	-0
Time	17:15	17:20	17:30	17:35	9:15	9:23
Barom ("Hg)	30.2	30.2	30.2	30.2	29.7	29.7
Power (%)	50	50	50	50	45	45
Q(p=0) (cfm)	14.5	14.5	13	13	12.1	12.3
Q (cfm)	-0	3	-0	-0	-0	1.8
Tamb (C)					25	25
Tfm (C)						
T(W1) (C)					25	25
Tens1 (cb)					6	6
Tens2 (cb)					2.1	2.1
Tens3 (cb)					0.9	0.9
The following are pressures (negative indicates vacuum)						
W1 (cmH2O)	0.00	0.00	0.00	210.87	168.69	147.61
W2 (cmH2O)	0.00	0.00	0.00	0.00	1.91	1.91
W3 (cmH2O)	0.00	0.00	0.00	0.00	0.76	0.76
W4A (cmH2O)	0.00	NoGage	0.00	0.00	0.00	0.00
W4B (cmH2O)	NoGage	0.00	0.00	0.00	0.00	0.00
W4C (cmH2O)	0.00	0.00	0.00	0.00	0.00	0.38
W4D (cmH2O)	0.00	0.00	0.00	0.00	0.00	0.00
W4E (cmH2O)	0.00	0.00	0.00	0.00	0.00	0.00
W5A (cmH2O)	0.00	0.00	0.00	0.00	0.00	0.00
W5B (cmH2O)	0.00	0.00	NoGage	0.00	0.03	0.03
W5C (cmH2O)	0.00	0.00	0.00	0.00	0.79	0.79
W5D (cmH2O)	0.00	0.00	0.00	0.00	0.00	0.00
W5E (cmH2O)	0.00	0.00	0.00	0.00	0.00	0.00
W6 (cmH2O)	0.00	0.00	0.00	0.00	0.00	0.25
W7 (cmH2O)	0.00	0.00	0.00	0.00	0.13	0.25
WT (cm BGS)		168.58			181.99	

Date	08/24/92	08/24/92	08/24/92	08/24/92	08/24/92	08/24/92
Rain (inch)	-0	-0	-0	-0	-0	-0
Time	9:33	9:45	9:52	9:57	9:59	10:06
Barom ("Hg)	29.7	29.7	29.7	29.7	29.7	29.7
Power (%)	45	45	45	45	45	45
Q(p=0) (cfm)	12.1	12.1	12.1	12.1	12.1	12.1
Q (cfm)	-0	unsteady	unsteady	-0	unsteady	3.2
Tamb (C)	25	25	25	25	25	25
Tfm (C)						
T(W1) (C)	25	25	25	25	25	25
Tens1 (cb)	6		6	6		
Tens2 (cb)	2.1		2.1	2.1		
Tens3 (cb)	0.9		0.9	0.9		
The following are pressures (negative indicates vacuum)						
W1 (cmH2O)	0.00	11.43	9.91	0.51	N/M	0.76
W2 (cmH2O)	0.00	N/A	N/A	0.00	N/M	0.25
W3 (cmH2O)	0.00	0.25	0.25	0.00	N/M	NoGage
W4A (cmH2O)	0.00	0.00	0.00	0.00	0.00	0.00
W4B (cmH2O)	0.00	0.00	0.00	0.00	0.00	0.00
W4C (cmH2O)	0.00	0.25	0.25	0.00	0.00	0.51
W4D (cmH2O)	0.00	0.00	0.00	0.00	N/M	0.00
W4E (cmH2O)	0.00	0.00	0.00	0.00	N/M	0.00
W5A (cmH2O)	0.00	0.00	0.00	0.00	N/M	0.00
W5B (cmH2O)	0.00	0.00	0.00	0.00	N/M	0.00
W5C (cmH2O)	0.00	0.79	0.79	0.00	N/M	0.76
W5D (cmH2O)	0.00	0.00	0.00	0.00	N/M	0.00
W5E (cmH2O)	0.00	0.00	0.00	0.00	N/M	0.00
W6 (cmH2O)	NoGage	NoGage	NoGage	0.00	N/M	NoGage
W7 (cmH2O)	0.00	0.00	0.00	0.00	N/M	0.25
WT (cm BGS)						

Date	08/24/92	08/24/92	08/24/92	08/24/92
Rain (inch)	-0	-0	-0	-0
Time	10:15	10:23	10:25	10:26
Barom ("Hg)	29.7	29.7	29.7	29.7
Power (%)	45	45	45	45
Q(p=0) (cfm)	12.1	12.1	12.1	12.1
Q (cfm)	3.3	-0	unstable	3.2
Tamb (C)	25	25	25	25
Tfm (C)				
T(W1) (C)	25	25		25
Tens1 (cb)				6
Tens2 (cb)				2.1
Tens3 (cb)				0.9
The following are pressures (negative indicates vacuum)				
W1 (cmH2O)				0.51
W2 (cmH2O)				0.25
W3 (cmH2O)		0.00		0.00
W4A (cmH2O)				0.00
W4B (cmH2O)				0.00
W4C (cmH2O)				0.51
W4D (cmH2O)				0.00
W4E (cmH2O)				0.00
W5A (cmH2O)				0.00
W5B (cmH2O)				0.00
W5C (cmH2O)				0.76
W5D (cmH2O)				0.00
W5E (cmH2O)				0.00
W6 (cmH2O)				0.00
W7 (cmH2O)				0.25
WT (cm BGS)				

APPENDIX D: MODELING SCENARIOS FOR DATA TAKEN 10/7/91

APPENDIX D. MODELING SCENARIOS FOR DATA TAKEN 10/7/91.

Purpose	ID	Q cm^3/s	O	r_B cm	r_{max} cm	BC @r_{max}	Bottom cmBGS	Δr	#Pts	Res cmH_2O		k cm^2
All wells fitted	B	2000	P	0	495	ZF	300	equal	14	1.6	k_r(0-300cmBGS)	5e-05
											k_z(0-300cmBGS)	1e-02
Isotropic	C	2000	P	0	495	ZF	300	equal	14	3.1	k(0-300cmBGS)	3e-03
BC@r_{max}	D	2000	P	0	495	P_{atm}	300	equal	14	1.6	k_r(0-300cmBGS)	5e-05
											k_z(0-300cmBGS)	1e-02
r_B	E	2000	P	205	495	P_{atm}	300	equal	14	3.1	k_r(0-300cmBGS)	4e-03
											k_z(0-300cmBGS)	1e-03
Same as B but P^2	F	2000	P^2	0	495	ZF	300	equal	14	1.5	k_r(0-300cmBGS)	8e-09
											k_z(0-300cmBGS)	2e-06
Same as F but isotropic	G	2000	P^2	0	495	ZF	300	equal	14	3.1	k(0-300cmBGS)	4e-07
BC@r_{max}	H	2000	P^2	0	495	P_{atm}	300	equal	14	1.5	k_r(0-300cmBGS)	8e-09
											k_z(0-300cmBGS)	2e-06

r_B	I	2000	P^2	205	495	P_{atm}	300	equal	14	3.1	k_r(0-300cmBGS)	6e-07
											k_z(0-300cmBGS)	2e-07
r_{max}	J	2000	P^2	0	195	ZF	300	equal	14	1.6	k_r(0-300cmBGS)	1e-08
											k_z(0-300cmBGS)	3e-06
BC@r_{max}	K	2000	P^2	0	195	P_{atm}	300	equal	14	1.6	k_r(0-300cmBGS)	1e-08
											k_z(0-300cmBGS)	3e-06
r_B	L	2000	P^2	195	195	P_{atm}	300	equal	14	NoCon	k_r(0-300cmBGS)	
											k_z(0-300cmBGS)	
Same as F	M	2000	P^2	0	495	ZF	300	equal	14	1.8	k_r(0-300cmBGS)	9e-09
but more exact Q										0.0	k_z(0-300cmBGS)	2e-06
										0.0		
Q	O	-470	P^2	0	495	ZF	300	equal	14	0.7	k_r(0-300cmBGS)	1e-08
											k_z(0-300cmBGS)	2e-06
Q	Q	-710	P^2	0	495	ZF	300	equal	14	0.9	k_r(0-300cmBGS)	1e-08
											k_z(0-300cmBGS)	2e-06

Q	S	-950	P^2	0	495	ZF	300	equal	14	1.1	k_r(0-300cmBGS)	1e-08
											k_z(0-300cmBGS)	2e-06
Q	T	-1200	P^2	0	495	ZF	300	equal	14	1.4	k_r(0-300cmBGS)	1e-08
											k_z(0-300cmBGS)	2e-06
W	W	2800	P^2	0	495	ZF	300	equal	14	1.9	k_r(0-300cmBGS)	1e-08
											k_z(0-300cmBGS)	3e-06
Q	Z	3000	P^2	0	495	ZF	300	equal	14	2.3	k_r(0-300cmBGS)	8e-09
											k_z(0-300cmBGS)	2e-06
Q	AA	3300	P^2	0	495	ZF	300	equal	14	2.3	k_r(0-300cmBGS)	9e-09
											k_z(0-300cmBGS)	3e-06
Q	V	3600	P^2	0	495	ZF	300	equal	14	2.8	k_r(0-300cmBGS)	1e-08
											k_z(0-300cmBGS)	3e-06
non-uniform Q	P	2000	P^2	0	495	ZF	300	equal	14	2.0	k_r(0-300cmBGS)	9e-09
											k_z(0-300cmBGS)	2e-06

Like M but W2,W3 only	N	2000	P^2	0	495	ZF	300	equal	2	0.0	k_r(0-300cmBGS) k_z(0-300cmBGS)	7e-08 1e-06
r_B	R	2000	P^2	35	495	ZF	300	equal	14	1.3	k_r(0-300cmBGS) k_z(0-300cmBGS)	4e-08 7e-05
Q	U	-1200	P^2	35	495	ZF	300	equal	14	NoCon	k_r(0-300cmBGS) k_z(0-300cmBGS)	
Q	X	3600	P^2	35	495	ZF	300	equal	14	1.9	k_r(0-300cmBGS) k_z(0-300cmBGS)	6e-08 9e-05
r_B	Y	2000	P^2	95	495	ZF	300	equal	14	NoCon	k_r(0-300cmBGS) k_z(0-300cmBGS)	
Same as V but more exact Q	AF	3600	P^2	0	495	ZF	300	equal	14	2.8	k_r(0-300cmBGS) k_z(0-300cmBGS)	9e-09 2e-06
#layers	AL	3600	P^2	0	495	ZF	300	equal	14	3.8	k(0-100cmBGS) k(100-200cmBGS) k(200-300cmBGS)	1e-06 1e-07 2e-01

Fit only W4A-C,W5A-C	AR	3600	P^2	0	495	ZF	300	equal	6	0.9	k(0-100cmBGS)	1e-05
											k(100-200cmBGS)	2e-06
											k(200-300cmBGS)	1e-07
Anisotropic	AS	3600	P^2	0	495	ZF	300	equal	6	0.5	k_r(0-100cmBGS)	1e-05
											k_z(0-100cmBGS)	1e-05
											k_r(100-200cmBGS)	2e-06
											k_z(100-200cmBGS)	3e-07
											k_r(200-300cmBGS)	1e-07
											k_z(200-300cmBGS)	1e-13
All wells	AT	3600	P^2	0	495	ZF	300	equal	14	2.2	k_r(0-100cmBGS)	1e-05
											k_z(0-100cmBGS)	1e-05
											k_r(100-200cmBGS)	1e-08
											k_z(100-200cmBGS)	4e-07
											k_r(200-300cmBGS)	2e-07
											k_z(200-300cmBGS)	1e-13

Better layer cutoffs than AT	AX	3600	P^2	0	495	ZF	300	equal	14	2.1	k_r(0-100cmBGS)	1e-05
											k_z(0-100cmBGS)	1e-05
											k_r(100-200cmBGS)	3e-08
											k_z(100-200cmBGS)	5e-07
											k_r(200-300cmBGS)	4e-09
											k_z(200-300cmBGS)	1e-13
Different bounds	AY	3600	P^2	0	495	ZF	300	equal	14	2.1	k_r(0-100cmBGS)	1e-06
											k_z(0-100cmBGS)	7e-06
											k_r(100-200cmBGS)	3e-08
											k_z(100-200cmBGS)	5e-07
											k_r(200-300cmBGS)	4e-09
											k_z(200-300cmBGS)	1e-13
Q	BA	2000	P^2	0	495	ZF	300	equal	14	1.4	k_r(0-100cmBGS)	1e-06
											k_z(0-100cmBGS)	4e-06
											k_r(100-200cmBGS)	2e-08
											k_z(100-200cmBGS)	5e-07
											k_r(200-300cmBGS)	5e-09
											k_z(200-300cmBGS)	1e-13

BC@r_{max}	AU	3600	P^2	205	495	P_{atm}	300	equal	14	2.2	k_r(0-100cmBGS)	1e-05
											k_z(0-100cmBGS)	1e-05
											k_r(100-200cmBGS)	1e-08
											k_z(100-200cmBGS)	4e-07
											k_r(200-300cmBGS)	2e-07
											k_z(200-300cmBGS)	1e-13
Better layer cutoffs	AZ	3600	P^2	205	495	P_{atm}	300	equal	14	2.1	k_r(0-100cmBGS)	1e-05
											k_z(0-100cmBGS)	7e-06
											k_r(100-200cmBGS)	3e-08
											k_z(100-200cmBGS)	5e-07
											k_r(200-300cmBGS)	4e-09
											k_z(200-300cmBGS)	1e-13
BC@r_{max}	BB	3600	P^2	205	495	ZF	300	equal	14	2.1	k_r(0-100cmBGS)	9e-06
											k_z(0-100cmBGS)	3e-06
											k_r(100-200cmBGS)	3e-08
											k_z(100-200cmBGS)	5e-07
											k_r(200-300cmBGS)	4e-09
											k_z(200-300cmBGS)	1e-13

Q	BC	2000	P^2	205	495	ZF	300	equal	14	1.4	k_r(0-100cmBGS)	9e-06
											k_z(0-100cmBGS)	1e-06
											k_r(100-200cmBGS)	1e-08
											k_z(100-200cmBGS)	4e-07
											k_r(200-300cmBGS)	7e-08
											k_z(200-300cmBGS)	1e-13
Q	BD	-470	P^2	205	495	ZF	300	equal	14	N/A	k_r(0-100cmBGS)	2e-01
											k_z(0-100cmBGS)	1e-06
											k_r(100-200cmBGS)	1e-08
											k_z(100-200cmBGS)	2e-06
											k_r(200-300cmBGS)	1e-13
											k_z(200-300cmBGS)	1e-07
Q	BE	-1200	P^2	205	495	ZF	300	equal	14		k_r(0-100cmBGS)	
											k_z(0-100cmBGS)	
											k_r(100-200cmBGS)	
											k_z(100-200cmBGS)	
											k_r(200-300cmBGS)	
											k_z(200-300cmBGS)	

Bottom, omit wells below W1	BF	3600	P^2	205	495	ZF	200	equal	10	1.9	k_r(0-100cmBGS)	7e-01
											k_z(0-100cmBGS)	9e-01
											k_r(100-200cmBGS)	3e-08
											k_z(100-200cmBGS)	4e-07
2 layer,isotropic	BH	3600	P^2	205	495	ZF	200	equal	10	4.0	k(0-100cmBGS)	1e+1
											k(100-200cmBGS)	2e-07
1 layer	BG	3600	P^2	205	495	ZF	200	equal	10	5.1	k_r(0-200cmBGS)	5e-01
											k_z(0-200cmBGS)	4e-07
4 layer,isotropic	BI	3600	P^2	205	495	ZF	200	equal	10	4.4	k(0-50cmBGS)	3e-01
											k(50-100cmBGS)	5e-03
											k(100-150cmBGS)	1e-06
											k(150-200cmBGS)	1e-07
4 layer,	BK	3600	P^2	205	495	ZF	200	equal	10	4.4	k_r(0-50cmBGS)	2e-01

Anisotropic											k_z(0-50cmBGS)	3e-02
											k_r(50-100cmBGS)	9e-04
											k_z(50-100cmBGS)	4e-03
											k_r(100-150cmBGS)	1e-06
											k_z(100-150cmBGS)	1e-06
											k_r(150-200cmBGS)	1e-07
											k_z(150-200cmBGS)	1e-07
Q	BM	2000	P^2	0	495	ZF	200	equal	10	4.9	k(0-50cmBGS)	3e-01
											k(50-100cmBGS)	5e-03
											k(100-150cmBGS)	2e-09
											k(150-200cmBGS)	1e-16
r_B	BJ	3600	P^2	0	495	ZF	200	equal	10	4.4	k_r(0-100cmBGS)	1e-07
											k_z(0-100cmBGS)	1e-04
											k_r(100-200cmBGS)	1e-07
											k_z(100-200cmBGS)	1e-06
Geom spacing of radial nodes	BN	3600	P^2	205	495	ZF	200	geom	10	1.3	k(0-50cmBGS)	1e-01
											k(50-100cmBGS)	3e-06
											k(100-150cmBGS)	1e-06
											k(150-200cmBGS)	3e-08

	BY	3600	P^2	205	495	ZF	200	geom	10	4.1	k_r(0-200cmBGS)	4e-07
											k_z(0-200cmBGS)	1e-06
omit W4D,E	BP	3600	P^2	205	495	ZF	200	geom	8	1.3	k(0-50cmBGS)	1e-05
											k(50-100cmBGS)	1e-06
											k(100-150cmBGS)	2e-06
											k(150-200cmBGS)	3e-08
BC@r_{max}	BW	3600	P^2	205	495	P_{atm}	200	geom	8	1.2	k(0-50cmBGS)	1e-05
											k(50-100cmBGS)	9e-07
											k(100-150cmBGS)	2e-06
											k(150-200cmBGS)	3e-08
Order	BX	3600	P	205	495	ZF	200	geom	8	1.2	k(0-50cmBGS)	1e-05
											k(50-100cmBGS)	1e-06
											k(100-150cmBGS)	3e-06
											k(150-200cmBGS)	4e-08

Q	BV	3600	P^2	205	495	ZF	200	geom	8	2.2	k_r(0-100cmBGS)	5e-03
											k_z(0-100cmBGS)	5e-03
											k_r(100-200cmBGS)	5e-08
											k_z(100-200cmBGS)	5e-07
Q	BQ	2000	P^2	205	495	ZF	200	geom	8	0.7	k(0-50cmBGS)	1e-05
											k(50-100cmBGS)	2e-07
											k(100-150cmBGS)	4e-06
											k(150-200cmBGS)	3e-08
Q	BT	2800	P^2	205	495	ZF	200	geom	8	0.7	k(0-50cmBGS)	2e-05
											k(50-100cmBGS)	8e-07
											k(100-150cmBGS)	3e-06
											k(150-200cmBGS)	4e-08
Q	BR	3000	P^2	205	495	ZF	200	geom	8	1.1	k(0-50cmBGS)	9e-06
											k(50-100cmBGS)	1e-06
											k(100-150cmBGS)	2e-06
											k(150-200cmBGS)	4e-08

Q	BS	3300	P^2	205	495	ZF	200	geom	8	0.8	k(0-50cmBGS)	2e-05
											k(50-100cmBGS)	1e-06
											k(100-150cmBGS)	3e-06
											k(150-200cmBGS)	3e-08
other tests; see Table 2		CB,CC,...	P^2	205	495	ZF	200	geom	8		k(0-50cmBGS)	
											k(50-100cmBGS)	
											k(100-150cmBGS)	
											k(150-200cmBGS)	